Unravelling the mechanism of summer monsoon rainfall modes over the West Coast of India using model simulations

Article

Accepted Version

Quarterly Journal of the Royal Meteorological Society
A journal of the atmospheric sciences and physical oceanography
RMetS

Unravelling the Mechanism of Summer Monsoon Rainfall Modes over the West Coast of India using Model Simulations

Journal:	*QJRMS*
Manuscript ID	QJ-22-0313.R1
Wiley - Manuscript type:	Research Article
Date Submitted by the Author:	15-May-2023
Complete List of Authors:	Phadtare, Jayesh; University of Leeds, School of Earth and Environment Fletcher, Jennifer; University of Leeds, ICAS Ross, Andrew; University of Leeds, Earth and Environment Turner, Andrew; University of Reading, Meteorology Schiemann, Reinhard; NCAS Climate, University of Reading Burns, Helen; University of Leeds
Keywords:	Dynamic/Processes < 1. Tools and methods, Numerical methods and NWP < 1. Tools and methods, Mesoscale < 2. Scale, Local or boundary layer scale < 2. Scale, Synoptic < 2. Scale, Convection < 3. Physical phenomenon, Dynamics < 3. Physical phenomenon, Floods < 3. Physical phenomenon
Country Keywords:	India

ORIGINAL ARTICLE

Unravelling the Mechanism of Summer Monsoon Rainfall Modes over the West Coast of India using Model Simulations

Jayesh A. Phadtare[1,2*] | Jennifer K. Fletcher[1,2] | Andrew N. Ross[1] | Andrew G. Turner[3,4] | Reinhard K. H. Schiemann[4] | Helen L. Burns[5]

[1]School of Earth and Environment, University of Leeds, UK

[2]National Centre for Atmospheric Science, University of Leeds, UK

[3]Department of Meteorology, University of Reading, UK

[4]National Centre for Atmospheric Science, University of Reading, UK

[5]Centre for Environmental Modelling And Computation, University of Leeds, UK

Correspondence
Jayesh Phadtare, Department of Civil and Environmental Engineering and Earth Sciences, University of Notre Dame, Notre Dame, IN 46556
Email: jayesh.phadtare@gmail.com

Present address
*Department of Civil and Environmental Engineering and Earth Sciences, University of Notre Dame, Notre Dame, IN 46556

Funding information
Weather and Climate Science for Service Partnership (WCSSP) India, a collaborative initiative between the Met Office, supported by the UK Government's Newton Fund, and the Indian Ministry of Earth Sciences (MoES).

A transition from a predominantly offshore to an onshore rainfall phase over the west coast of India was simulated using three one-way nested domains with 12-, 4-, and 1.33-km horizontal grid spacing in the Weather Research and Forecasting model. The mechanism of offshore-onshore rainfall oscillation and the orographic effects of the Western Ghats are studied. A convective parameterization scheme was employed only in the 12-km domain. A trough extending offshore from the west coast facilitates offshore rainfall. This trough is absent during the onshore phase, and rainfall occurs over the coast mainly via orographic uplift by the Western Ghats. The model overestimates rainfall over the Western Ghats at all resolutions as it consistently underestimates the boundary layer stratification along the coast. Weaker stratification weakens the blocking effect of the Western Ghats, resulting in anomalous deep convection and rainfall over its windward slopes. The 4- and 1.33-km domains simulate the offshore-to-onshore transition of rainfall but fail to capture a sufficient contrast in rainfall between land and sea compared to observations. The 12-km domain produces light rainfall, anchored along the coast, throughout the simulation period, and hence gravely underestimates the offshore rainfall. The offshore rainfall persisted in the 4- and 1.33-

km domains in a sensitivity experiment in which the Western Ghats were flattened. This suggests that orographic effects do not significantly influence offshore rainfall. In another experiment, the convective parameterization scheme in the 12-km domain was turned off. This experiment simulated the offshore and onshore rainfall phases correctly to some extent but the rainfall intensity was unrealistically high. Thus, a model with a horizontal grid spacing of O(∼ 1 km), in which convection evolves explicitly, is desired for simulating the west coast rainfall variations. However, improvements in the representation of boundary layer processes are needed to capture the land-sea contrast.

KEYWORDS
Orographic effects, Indian Summer monsoon, Coastal rainfall

1 | INTRODUCTION

The west coast of the Indian peninsula is one of the rainiest places on our planet and a host to rainforests with a high level of biodiversity, thanks to the Western Ghats mountain range. This region is prone to flash floods and landslides during the summer monsoon season (Francis and Gadgil, 2006; Kumar et al., 2008; Hunt and Menon, 2020; Mohandas et al., 2020). In June 2016, the Interaction of Convective Organization and Monsoon Precipitation, Atmosphere, Surface and Sea (INCOMPASS) field campaign took place over the Indian region in order to understand the interaction between the convective and large-scale weather systems in the summer monsoon (Turner et al., 2020). One of its southern legs involved aircraft and ground-based observations over the west coast of India and the adjacent Arabian Sea during 21-26 June (henceforth referred to as the 'INCOMPASS IOP'). Heavy rainfall shifted from the offshore region (henceforth referred to as the 'offshore mode') to the onshore region (henceforth referred to as the 'onshore mode') during this period. It was speculated that the interactions between the monsoonal westerly jet, a mid-tropospheric dry air intrusion, and convection lead to the offshore and onshore rainfall modes (Fletcher et al., 2020). A climatological study by Hunt et al. (2021) supports this hypothesis. Grossman and Durran (1984), with the help of field observations and a simple 2D model of flow over an orographic barrier, suggest that the offshore rainfall over the Arabian Sea may result from upstream blocking and uplift of the monsoonal jet by the Western Ghats. On the other hand, a study involving WRF model simulations by Zhang and Smith (2018) suggests that the offshore rainfall results from large-scale instabilities, and that the Western Ghats merely serve as the eastern boundary for it. Shige et al. (2017) and Hunt et al. (2021) showed that the offshore-onshore oscillation of rainfall over the Indian west coast is associated with large-scale forcing from the Boreal Summer Intraseasonal Oscillation (BSISO) phases.

Current operational numerical weather models still have issues in realistically simulating rainfall over this coastal hilly region. A 10-day weather forecasting exercise in support of the INCOMPASS field campaign showed that the operational Met Office Unified Model (MetUM) at a horizontal resolution of N768 (17 km) with a convection scheme, as well as its limited-area model (LAM) version at 4.4 km using explicit convection, overestimate the onshore rainfall and underestimate the offshore rainfall over the west coast (figure 10 in Martin et al. (2020)); this could be a direct consequence of poor representation of the offshore-onshore rainfall modes. Mohandas et al. (2020) reported that medium-range forecasts from the global National Centre for Medium-Range Weather Forecasting (NCMRWF) Unified Model (NCUM), a version of MetUM, simulate the observed

circulation patterns over the west coast but do not get the rainfall distribution right. Rajendran et al. (2012) argues that capturing the convective-regional-global scale interaction is necessary in order to simulate the observed long-term rainfall trends over this region in the models. Thus, a realistic simulation of offshore-onshore rainfall modes over the west coast and their relationship with large-scale weather systems is imperative for regional and global models in order to produce useful short-term and long-term forecasts of rainfall.

Smith et al. (2015) show that the MetUM simulates the observed rainfall intensity over the hills on the west coast of the UK at 1.5 km resolution; rainfall intensity reduces when the resolution is decreased. They suggest that the sensitivity of the orographic rainfall to the horizontal grid spacing is different for different mountain ranges and it is mainly governed by the geometry of the orographic features. In general, the horizontal grid spacing that is adequate to faithfully represent the effects of orography on simulated rainfall appears to be a few to 10 km (see Smith et al. (2015) and references therein). Some of the latest operational numerical weather prediction (NWP) models employ grid spacing of O($\sim$ 1 km). The fundamental assumption in the convective parameterization is that the convective cells are much smaller than the model grid box and remain unresolved. At O($\sim$ 1 km) resolution, convective cells are partially resolved. Thus, the usage of a convective parameterization scheme at this resolution is questionable as individual convective cells can occupy more than one grid box. This scale is generally referred to as the 'grey zone' of convective parameterization (Gerard et al., 2009; Kirshbaum, 2020). Peatman et al. (2014) showed that the models which rely on convective parameterization fail to simulate the observed interaction between convection and sea breeze over the islands of the Maritime Continent. High-resolution convection-permitting simulations produced a much improved diurnal cycle of circulation and rainfall (Birch et al., 2015, 2016). Nevertheless, there are many studies where the usage of a convective parameterization scheme within and near the grey zone of convection has improved the overall model simulation of a meteorological event (e.g., Zheng et al. (2016); Mahoney (2016); Phadtare (2018)). This can be due to the prescribed CAPE consumption and entrainment-detrainment rates for shallow and deep convection in the scheme. Recently, convective schemes are being improved by including a scale-dependency in these factors (e.g. Zheng et al. (2016)).

The grid spacing of a few km, however, is inadequate to resolve the eddies within the planetary boundary layer (PBL). Thus, a PBL scheme is needed to represent the boundary layer processes (Wyngaard, 2004; Honnert, 2016; Kirshbaum, 2020). The boundary layer processes determine the orographic influence by controlling the near-surface stratification of the atmosphere. One of the key parameters controlling the orographic effects is the Froude Number (F) of the impinging flow:

$$F = \frac{U}{NH} \tag{1}$$

where U is the mean wind speed upstream of the orographic barrier, N is the mean Brunt-Väisälä frequency of the atmosphere, and H is the height of the orography (Sheppard, 1956; Smith, 1979; Kirshbaum et al., 2018). When F < 1, flow is blocked by the orographic barrier, whereas when F > 1, the flow has sufficient kinetic energy to overcome the orographic barrier and move to the lee side. Several idealized simulation experiments (Chu and Lin, 2000; Chen and Lin, 2005b,a; Jiang, 2003; Reeves and Lin, 2007; Miglietta and Rotunno, 2009) have shown that in the blocked case, precipitating systems remain upstream of the orography, and in the unblocked case, precipitation occurs over the orographic slopes (heavy) and the lee region (light to moderate). A recent study by Phadtare et al. (2022) showed that when the incident low-level flow over the west coast of India is classified according to F, the classification leads to the offshore-onshore rainfall pattern – the low F values are associated with the offshore mode, and high F values with the onshore mode. Further, they show that the offshore mode is characterised by strong land-sea breeze variations and greater control of the local diurnal cycle over the west coast rainfall. Conversely, the onshore mode has suppressed land-sea breeze and the rainfall has a weak diurnal cycle. Thus, the mechanisms by which the release of convective instability takes place in the two modes are different. Mechanical uplifting is dominant during the onshore mode, whereas during the offshore mode, it is mainly facilitated by daytime heating. Therefore, even though the majority of the literature suggests that

the offshore-onshore modes are caused by the large-scale variability of the atmosphere, the blocking/uplifting from the Western Ghats, as well as its thermal forcing, seem to play an important role. Thus, a pertinent question that needs to be answered is: are the representation of orographic effects and the diurnal cycle of rainfall in the present-day models adequate for simulating the offshore-onshore rainfall modes?

The purpose of this study is to understand the impacts of horizontal grid resolution and the presence of a convective parameterization scheme on the model simulation of the offshore-onshore rainfall modes over the west coast of India and understand the role of the Western Ghats in these modes. The INCOMPASS IOP is chosen as a case study. Section 2 of this article describes the datasets used and model setup, section 3 shows how model domains at different horizontal resolutions perform at simulating the observed offshore-onshore rainfall transition and the evolution of dynamics, section 4 presents the results of model sensitivity experiments relating to the convective parameterization and the presence of the Western Ghats. Section 5 presents the main conclusions and discussion on the future avenues for research.

2 | DATA AND MODEL SETUP

2.1 | IMERG rainfall

The Integrated Multi-satellitE Retrievals for GPM (IMERG) product, version 06B (Huffman et al., 2015), is used for describing the patterns of rainfall over the Indian west coast during the offshore-onshore modes. IMERG provides global surface rainfall on a 0.1° spatial grid at 30-minute intervals. The dataset is provided by the National Aeronautics and Space Administration (NASA). IMERG is produced by merging passive microwave and infrared rainfall estimates which are further calibrated with the rain gauges on a monthly basis. Satellite-based rainfall estimates over the west coast of India are known to have biases. The Tropical Rainfall Measuring Mission (TRMM) 3B42 product gives the maximum rainfall off the coast instead of the Western Ghats slopes. This is because the coastal clouds are deeper than those over the Western Ghats (Shrestha et al., 2015; Kumar and Bhat, 2017), and hence the infrared rainfall estimates undervalue the orographic rainfall. The latest IMERG product places the maximum rainfall correctly over the Western Ghats slopes (e.g., Prakash and Srinivasan (2021); Phadtare et al. (2022)), but still underestimates the intensity of heavy rainfall episodes (> 25 mm h^{-1}) compared to the rain gauges (Murali Krishna et al., 2017). Rojas et al. (2021) concluded that IMERG underestimated the overall rainfall over the mountainous region of Chile by 16% and warm rain events by 50%. Thus, it is possible that the IMERG underestimates the actual rainfall over the orography of the Western Ghats by about 16-50%.

2.2 | Rain gauges

To validate the IMERG rainfall, we have used rainfall data from the rain gauge network of the India Meteorological Department (IMD). The network comprises automatic weather stations (AWS) and automatic rain gauges (ARG) (Saha et al., 2021). These automatic stations use tipping-bucket rain gauges. The dataset was obtained from IMD in support of the Indo-UK joint INCOMPASS project. A total of 44 rain gauges were selected along the west coast. Rain gauges with more than 10% missing data were excluded from the analysis.

2.3 | Radiosondes

We use the upper-air radiosonde observations from Mangalore (74.83°E, 12.95°N and 31 m elevation) and Amini Divi (72.73°E, 11.12°N and 4 m elevation) stations in order to evaluate the model simulation for the near-surface stratification and winds. This data was obtained from the Atmospheric Soundings web portal of the University of Wyoming (`weather.uwyo.edu/upperair/`

sounding.html). Mangalore is located over the west coast, whereas Amini Divi is an island in the Arabian Sea. Radiosonde observations are ideal for determining the near-surface stratification as they provide high-resolution in situ observations. The near-surface atmospheric stratification directly influences the orographic blocking as well as the sub-grid orographic drag parameterization (Stensrud, 2009).

2.4 | Reanalysis

The fifth-generation European Centre for Medium-Range Weather Forecasts Reanalysis (ERA5) dataset is used for evaluating the model simulated large-scale fields. ERA5 is available at hourly intervals on a 0.25° horizontal grid and 137 vertical levels starting from the surface and up to a height of 80 km (Hersbach et al., 2018).

2.5 | WRF model

The Advanced Research version of the Weather Research and Forecasting (WRF 4.1.3) model (Skamarock et al., 2008) is used to simulate the INCOMPASS IOP. Three one-way nested grids, all centred over the Indian west coast, were employed for the simulations (Fig. 1). The outermost grid will be referred to as D12, the intermediate as D4, and the innermost as D1 as the grid spacings of these domains are 12, 4, and 1.33 km, respectively. D12 is large enough to include the entire Arabian Sea to the west, the Bay of Bengal to the east and the Himalayas to the north. D1 is large enough to include the entire Western Ghats over the Indian peninsula and the mesoscale systems over the offshore region of the Arabian Sea. The physics schemes recommended in the tropical suite of the WRF model are used. The modified Tiedtke convective parameterization scheme (Tiedtke, 1989; Zhang et al., 2011) is used only in D12. This scheme accounts for deep, middle, and shallow convection. The domains D4 and D1 allow convection to develop explicitly. More details on the grids used and other physics schemes are given in Table 1. 35 vertical eta levels are used with a lid at 50 hPa; the lowest level is at 20 m elevation above the surface and there are 10 levels below 1500 m. Note that one-way nesting was used here in order to understand the differences in the simulation of each domain. In two-way nesting, the inner/finer domain gets the boundary conditions from the outer/coarser domain, and the output of the inner domain is fed back to the outer grid to improve the overall simulation; in one-way nesting, only the former part is true. The initial and lateral boundary conditions to D12 are taken from ERA5.

Each mode of the offshore-onshore rainfall oscillation can last for about 4-7 days (Fletcher et al., 2020; Hunt et al., 2021). Thus, in order to allow sufficient time for such variability to develop in the model simulation, we start the simulation at 0000 UTC 13 June 2016 and end it on 0000 UTC 28 June 2016; only the simulation between 0000 UTC 20 June - 0000 UTC 28 June, a period which coincides with the INCOMPASS IOP, is analyzed.

3 | CONTROL SIMULATION

The purpose of the control simulation is to simulate the event as realistically as possible using actual topographical and meteorological conditions as input. Model biases in the simulated rainfall and other meteorological parameters are identified for all domains in this run. The sensitivity simulations described in section 4 will be compared with the control run in order to understand the effect of the modified topography and convection representation in the model.

Domains	D12	D4	D1
Grid cells	356×348	649×601	889×985
Grid spacing	12 km	4 km	1.33 km
Boundary conditions	ERA5	D12	D4
Convection	New Tiedke (Tiedtke, 1989; Zhang et al., 2011)	-	-
Microphysics	WRF Single-moment 6-class (Hong and Lim, 2006)		
Planetary boundary layer	Yonsei University (Hong et al., 2006)		
Surface layer	MM5 (Zhang and Anthes, 1982)		
Land surface	Noah (Chen and Dudhia, 2001)		
Radiation	RRTMG (Iacono et al., 2008)		

TABLE 1 Details of the WRF domains shown in Figure 1 and the physics schemes used.

3.1 | Rainfall

First, we identify the offshore and onshore modes of rainfall, if they exist, in different domains of the model. The model evaluation can then be done on the basis of the time periods of these modes, and the overall distribution and the diurnal cycle of rainfall in each mode.

3.1.1 | Offshore and onshore modes

Figure 2 shows Hovmöller diagrams of 12-14°N mean rainfall during 20-27 June from the IMERG rainfall product and the three WRF domains. The latitudinal band of 12-14°N is chosen as this was the region where the INCOMPASS IOP was conducted and the transition of rainfall from offshore-to-onshore region was seen (Fletcher et al., 2020). Rainfall occurs over the offshore region during 20-24 June ('Offshore' mode), and over the onshore region ('Onshore' mode) during 26-27 June; the offshore region gets little rainfall during the onshore mode (Fig. 2a). Domains D4 and D1 simulate the offshore and onshore modes of rainfall somewhat similar to the observed modes (Fig. 2c,d). Distinct offshore and onshore modes are not seen in domain D12, which employs a convection scheme (Fig. 2b). According to the IMERG observations, the offshore mode is characterized by rainfall episodes occurring in the early morning hours over the sea, and the onshore mode by a stationary system over the coast and the Western Ghats. Domains D4 and D1 qualitatively simulate these characteristics of offshore and onshore modes. However, note that during the offshore mode, the intensity of rainfall over the coast in these domains is much greater than observed.

3.1.2 | Mean rainfall

In IMERG, two prominent offshore rainfall zones are seen during the offshore mode, a northwest-southeast oriented rain band over the Arabian Sea and an off-the-coast rain band (Figure 3). Heavy rainfall (> 30 mm/day) is widespread over the sea while rainfall is mostly light over the coast. During the onshore mode, rainfall around Mangalore increases (>50 mm/day), with the slopes of the Western Ghats at 14°N receiving the heaviest rainfall (> 80 mm/day). Note that the onshore mode is seen only to the south of 15°N in this case. An Offshore rainband is seen north of 15°N. A clear land-sea contrast in rainfall is quite evident during both modes in the 12-14°N belt. In domain D12, rainfall is located along the coast during both modes. Domains D4 and D1 do get the offshore and onshore modes right to some extent. Although there is heavy rainfall over the sea during the

offshore mode in these domains, it is not located as far offshore as in the IMERG field. In addition, there is heavy rainfall (> 80 mm/day) over the coast during the offshore mode and the observed land-sea contrast in rainfall is missing in D4 and D1. During the onshore mode, heavy rainfall in domains D4 and D1 is mainly over the Western Ghats slopes. In these domains, the coastal region receives only light rainfall during this mode. In reality, a broad patch of heavy rainfall accumulation, extending from the Western Ghats slopes to the coastal zone, is seen in the IMERG field during the onshore mode. Thus, although the convection-permitting domains simulate the offshore and onshore rainfall during the respective modes, it is erroneously shifted eastwards, i.e., towards the orography. This discrepancy is further emphasized in the next figure.

Figure 4 shows rainfall anomalies in the WRF domains with respect to the IMERG rainfall. The rainfall fields in these domains are regridded to the IMERG resolution for ease of comparison. The anomalous rainfall intensity over the west coast during the offshore mode is between 50-100 mm day^{-1} which is far higher than the reported underestimation of orographic rainfall by the IMERG product (16-50%). During the onshore mode, D12 gravely underestimates the west coast rainfall. The D4 and D1 overestimate rainfall over the Western Ghats slopes by 50-100 mm day^{-1} at most places and slightly underestimate rainfall along the coast south of 15°N where the onshore mode is seen.

3.1.3 | Diurnal cycle

Phadtare et al. (2022) showed that the rainfall during the offshore regime is controlled by a strong diurnal cycle, whereas that during the onshore regime has a weak diurnal cycle. Therefore, here we analyze if the model can simulate the observed diurnal cycle of rainfall during the offshore mode. Figure 5 shows the diurnal variation of mean rainfall over a latitudinal band of 12-14°N during the offshore mode of this case study from IMERG and model simulations. Just off the coast, the IMERG rainfall increases in the early morning period of 0000-0300 UTC (0530-0830 IST), and during 0300-0600 UTC rainfall increases further offshore. The D4 and D1 domains simulate the near-coast heavy rainfall mode during 0000-0300 UTC correctly but miss the enhancement further offshore during 0300-0600 UTC. Notice that the early morning rainfall in IMERG stays strictly off the coast (Fig. 5a), whereas the simulated offshore rainfall in D4 and D1 intrudes over the land. These domains also simulate onshore rainfall maxima during 0600-1200 UTC. Onshore daytime rainfall is not seen at all in the IMERG dataset. Thus, anomalous morning, as well as daytime rainfall over land in D4 and D1, lead to anomalous rainfall over the coast during the offshore mode. In domain D12, offshore rainfall increases during 0000-0600 UTC but the intensity remains less than half of the observed intensity. Rainfall over the coast increases around 0400 UTC and remains high throughout the day.

To summarize, the west coast rainfall modes are entirely absent in D12; the rainfall is anchored along the coast almost all the time and offshore rainfall is very weak in this domain. The D4 and D1 domains do simulate the offshore-onshore modes, but they fail to capture the land-sea contrast and the diurnal cycle of rainfall along the coast during the offshore phase. Both domains produce daytime maximum rainfall over land which is not seen in the observations.

3.2 | Dynamics and thermodynamics

This section evaluates the model simulation for its dynamic (synoptic, mesoscale) and thermodynamic (humidity, convection) fields. In the process, explanations for the discrepancies in the simulated rainfall fields reported in section 3.1 are given.

3.2.1 | Large-scale dynamics

During the offshore mode, there was a northwest-southeast oriented trough over the region extending from the northern Arabian Sea to the southern Bay of Bengal. Note that the rainfall over the Arabian Sea occurs over the trough region with its limits being a ridge to the west and the Western Ghats to the east (Figures 2a, 3a). During the onshore mode, the trough over the Bay of

Bengal moved northeastwards and transformed into a well-developed cyclonic circulation. The western end over the northern Arabian Sea also intensified and developed into a closed cyclonic circulation. A ridge sits over the west coast during this mode which provides an unfavourable environment for the organised large-scale rainfall. However, the westerly jet is stronger during this mode and rainfall over the west coast mainly results from the orographic lifting (Phadtare et al., 2022). Note that the offshore mode is not the same as the break phase (Krishnan et al., 2000) of the summer monsoon. Organized rainbands are absent over the Indian region during the break phase, but they do appear over the eastern Arabian Sea during the offshore phase. However, the offshore-onshore mode oscillation is likely to happen during the break-to-active transition as organized rainbands propagate northward (Shige et al., 2017; Hunt et al., 2021). The model simulates the main features of the offshore and onshore modes correctly (Figure 6b,d), but overestimates the wind speed, especially downstream of the Western Ghats, i.e. over the Indian peninsula and the Bay of Bengal, during the onshore mode. This wind bias is also seen in the D4 and D1 domains (not shown).

The offshore rainfall not only cools the boundary layer over the sea, but the cold pools also present a substantial barrier to the low-level monsoonal flow. Figure 7 shows 950 hPa virtual potential temperature perturbation and winds during the simulated rainfall events in the offshore and onshore modes from domain D1. During the offshore event (Fig. 7a) the rainfall has a squall-line-like north-south organization. This system was propagating westward (Fig. 2d) and it leaves a trail of cold air behind it. The low-level monsoonal flow is obstructed by this cold pool, and the outflow itself is directed southward. As a consequence, the flow along the coast is cooler and has a northwesterly direction leading to suppression of rainfall over the coast. On the other hand, during the onshore mode (Fig. 7b), the flow is westerly and almost perpendicular to the Western Ghats. The air parcels reaching the coast during the onshore event are warmer than those during the offshore events by about 2-3 K. As a result, rainfall is enhanced over the Western Ghats. These simulated features of offshore and onshore rainfall events are in accordance with the observations of Fletcher et al. (2020). The onshore mode is also characterized by a drier mid-troposphere and moister lower-troposphere over the Arabian Sea (Fletcher et al., 2020; Hunt et al., 2021). The simulated humidity fields in the three domains are analyzed next.

3.2.2 | Mid-tropospheric humidity

Figure 8 shows the difference in the vertical cross-section of specific humidity averaged over the 12-14°N band during the onshore and offshore modes in the three model domains. All domains simulate a drier mid-troposphere and moister lower-troposphere during the onshore mode. The westerlies are also stronger during the onshore mode. However, note that in domain D12, the onshore winds do not strengthen and the Western Ghats slopes are drier during the onshore mode compared to the offshore mode. This is contrary to the observations of the case study (Fletcher et al., 2020) and this is the reason that the Western Ghats receive less rainfall during the onshore mode than the offshore mode in D12 (Figure 4). In domains D4 and D1, the low-level wind and moisture anomalies during the onshore mode are strongest over the west coast. This leads to rainfall enhancement over the Western Ghats slopes during the onshore mode.

3.2.3 | Convection

Figure 9 shows the vertical cross-sections of the temporal fraction for which the simulated radar reflectivity was at least 20 dBZ in any grid-box in the 12-14°N latitudinal band in the D4 and D1 model domains. The 20 dBZ threshold is typically used to identify precipitation features in a radar dataset, e.g., Xu and Rutledge (2015). In D12 domain, the convective rain is a subgrid entity produced by the convective parameterization scheme, and it is not reflected in the grid-resolved hydrometeor fields (Chen et al., 2021). Therefore, simulated radar reflectivity from domain D12 is not shown. In domains D4 and D1, there is a frequent widespread deep convection over the Arabian Sea and the west coast during the offshore mode. During the onshore mode, convection is less frequent and remains below 2.5 km altitude over the Arabian Sea. During this mode, deep convection is

confined to the coast. The simulated transformation in the deep convective activity in D4 and D1 is similar to that reported by Fletcher et al. (2020) and Hunt et al. (2021). The only difference is that the model domains simulate deep convection over the coast and orography even during the offshore mode, whereas in the observations it occurred only over the sea. This suggests that there is an anomalous supply of conditional instability to the coast during the offshore mode in D4 and D1. Notice that the dry air intrusion spans the entire region during the onshore mode and not just the offshore part (Fig. 8). Nevertheless, deep convection develops over the coast. This suggests that if the low-level supply of conditional instability and an uplifting mechanism (orography in this case) are present, deep convection can develop despite a dry mid-troposphere.

3.2.4 | Orographic blocking

The model simulates warmer and weakly stratified PBL over the coast during both modes compared to the radiosonde observations (Figure 10a,e). The nighttime temperature anomaly at the surface is around 4 K during the onshore mode. The anomaly reduces in the daytime to around 2 K. Thus, the model severely underestimates the nocturnal cooling of the surface and PBL. The zonal wind speed profiles from the radiosondes (Figure 10b,f) show a stronger monsoonal jet during the onshore mode than the offshore mode. The model captures this variation, however, it overestimates wind speed below 800 hPa at both times. The 0000 UTC equivalent potential temperatures (θ_e) are also higher (by 7-10 K) in the PBL, suggesting that the model transports more instability towards the Western Ghats during nighttime (Figure 10c). During the daytime, the PBL warms up; the simulated θ_e values are closer to the observations at 1200 UTC (Figure 10g). Due to the warmer temperatures, the relative humidity in the PBL is also lower in the simulation compared to the observations (Figures 10d,h). Profiles from the D12 and D4 domains also exhibit similar PBL biases over but they are not shown for the sake of brevity.

The radiosonde profile during the onshore mode shows a well-mixed PBL over the Arabian Sea, whereas the offshore mode has a stratified PBL (Figure 10i). The PBL stratification may be due to the evaporative cold pools produced by the rainfall. Since rainfall is absent over the offshore region during the onshore mode, the offshore PBL is well mixed. The model consistently produces a well-mixed PBL irrespective of the rainfall mode. It simulates the wind speed within the PBL correctly but overestimates the jet speed at 800 hPa by about 4-5 m s^{-1}.

As a result of the bias towards stronger wind and weaker PBL stratification, the orographic blocking is weak in the model. Figure 11a-c shows U, N, and F values, respectively, averaged over 50-1000 m altitude above the surface (refer to equation 1) from the 0000 and 1200 UTC Mangalore radiosondes and the corresponding values of these parameters from the hourly output of the WRF simulation. The simulated soundings are averaged over a 12 km horizontal box centred over the radiosonde location. The mean height of the Western Ghats within the 12-14°N band is considered for H, which is about 1000 m. The Western Ghats range is roughly oriented in the north-south direction, therefore the zonal wind speed is considered for U. The effect of saturation during the ascent on the stratification (N) is neglected. Note that ideally, F should be calculated away from the orography using the upstream undisturbed values of U and N. The blocking distance of the Western Ghats extends offshore by 150-300 km (Phadtare et al., 2022). Mangalore is well within the blocking region of the Western Ghats. Therefore, the flow at Mangalore is already decelerated due to the orographic blocking and the F calculated here will be an underestimation of the actual F values. On the other hand, in the precipitating environment, offshore stratification is weaker than coastal stratification due to the piling up of cold pools over the mountain slopes (Phadtare, 2018). This is evident in figures 10a,l during the onshore mode. Therefore, the F values calculated from the offshore sounding will be an overestimation of the actual F values. Amini Divi is an island station (Figure 1) located around 300 km offshore from the Western Ghats, i.e., away from its blocking distance. Figure 11d-f shows U, N, and F values, respectively, averaged over 50-1000 m altitude above the surface from the 0000 UTC Amini Divi radiosondes and the corresponding values of these parameters from the hourly output of the WRF simulation; the 1200 UTC radiosondes were not released from Amini Divi during this period.

Given these limitations in estimating the true F of the flow impinging on the Western Ghats, we avoid the terms ‘blocked’ or

'unblocked' in describing its regime. Instead, phrases like 'weakly blocked'/'strongly blocked' are used. The main aim of this exercise is to show the difference in the observed and simulated flow blocking. The model overestimates U and underestimates N most of the time at the coast, and hence, overestimates F of the flow implying weaker orographic blocking. According to the Mangalore (Amini Divi) radiosonde observations, the F values at 000 UTC hover around 0.5 (1) during the offshore mode. After 26 June, F values are higher and stay between 0.7-1 (2-5) at Mangalore (Amini Divi). The true F of the flow may lie between the F values calculated from the Mangalore and Amini Divi soundings. In D4 and D1 domains, F values are 2-3 times higher than the observed values at Mangalore. During the offshore mode, the simulated F values greater than 1 (2) are consistently seen at Mangalore (Amini Divi). This suggests that the onshore flow in the model is weakly blocked, instead of strongly blocked as suggested by the radiosondes.

In summary, stronger winds, weaker PBL stratification, and hence weakly blocked onshore flow lead to enhanced orographic lifting in the model. Stronger and warmer onshore flow also allows a greater supply of instability towards the orographic slopes. Therefore, the model tends to simulate stronger convection (Fig. 9) and higher rainfall (Fig. 3, 4) over the slopes of the Western Ghats, even during the offshore mode.

4 | SENSITIVITY EXPERIMENTS

This section investigates the sensitivity of the simulated west coast rainfall modes to the orographic influence and mesoscale convective processes in the model. Section 3.2.4 showed that the orographic blocking is weak in the model compared to the observations. Despite this, domains D4 and D1 simulated the offshore and onshore modes of rainfall somewhat satisfactorily. This hints that the west coast rainfall modes may not be as sensitive to the presence of the Western Ghats as previously assumed and are entirely driven by the large-scale variability, e.g., BSISO, as suggested by previous studies (Shige et al., 2017; Fletcher et al., 2020; Hunt et al., 2021). We explicitly show the influence of orography on the rainfall modes by performing a 'No orography' simulation (henceforth referred to as the *NoOrog* experiment) in which the Western Ghats are flattened entirely (Figure 1b). Note that the orography is flattened in all domains. Zhang and Smith (2018) performed a similar experiment in the WRF model and concluded that the offshore rainfall along the west coast was not caused by the orographic blocking from the Western Ghats. However, their focus was on the 'wet period' in which rainfall occurred onshore as well as offshore. Here, we focus on the offshore-onshore modes and the transition.

Zhang and Smith (2018) and Fletcher et al. (2020) emphasized the importance of offshore deep convection in suppressing rainfall over the west coast by cooling and drying the boundary layer. Domain D12 does not simulate the offshore heavy rainfall events probably due to the convective parameterization scheme. In the second experiment, we rerun the control simulation by turning off the convective parameterization scheme in D12 (henceforth referred to as the *NoCu* experiment). The aim of the second experiment is to check if explicit convection at 12-km horizontal grid spacing gives heavy rainfall and consequently, allows the west coast rainfall modes, and so whether the key difference between D12 and D4/D1 is the convective parameterization scheme rather than the resolution.

4.1 | Orography

Figures 12a-c show Hovmöller diagrams of 12-14°N averaged rainfall in the three domains for the *NoOrog* experiment. Note that the convective parameterization scheme in D12 is active in this experiment. Figures 12b,c show that the offshore rainfall mode is simulated in domains D4 and D1 even without the Western Ghats. The onshore rainfall is weak over the coast throughout the simulation. This is due to the absence of orographic uplifting. The offshore rainbands are practically unaffected by the removal of orography. Removal of the Western Ghats did not affect the diurnal cycle of rainfall either along the coast or in the offshore

region; we see early morning rainfall events in the *NoOrog* simulation quite similar to those when the orography was present (Fig. 2). This suggests that the land-sea contrast, more than the orography, affects the diurnal cycle of rainfall along the coast.

Figure 13 shows 850 hPa mean winds and geopotential field during the offshore and onshore modes for the *NoOrog* simulation. The evolution of large-scale fields is somewhat similar to the control run. During the offshore mode, a trough is present over the peninsula and the Arabian Sea, and during the onshore mode, an LPS has developed north of the Western Ghats. The winds are north-westerlies during the offshore mode, and during the onshore mode, they are stronger and westerly. Thus, the offshore and onshore modes of rainfall are linked to the evolution of the large-scale fields (as proposed by Shige et al. (2017); Fletcher et al. (2020); Hunt et al. (2021)). The Western Ghats merely modulate the intensity of rainfall over the coast through different orographic blocking regimes of the low-level flow which can be identified by classifying the onshore flow according to its Froude number as shown by Phadtare et al. (2022).

4.2 | Convective parameterization

In the *NoCu* experiment, the event was simulated employing only D12 but with explicit convection. Figure 12d shows a Hovmöller diagram of 12-14°N averaged rainfall for the *NoCu* experiment. It shows rainbands starting from the rain shadow region and propagating westwards over the Arabian Sea during 20-24 June. The intensity, as well as the organization of these rainfall episodes, seem abnormally high when compared with observations. This is an outcome of anomalously strong convection, possibly due to inadequate entrainment of dry air by the turbulent eddies into the convective core at 12 km horizontal grid spacing (Tang and Kirshbaum, 2020; Kirshbaum, 2020). The two modes seen in this experiment can be characterized as 'offshore propagation' and 'onshore propagation'. Offshore propagation of rainfall appears as one of the features of the offshore mode as it was seen in the other simulations (control and *NoOrog*) as well. Observations from IMERG suggest that a mixture of stationary and offshore-propagating rainfall episodes are present during the offshore mode. A trough present over the Indian peninsula and the Arabian Sea during the offshore mode might be promoting the westward propagation of rainfall. A similar phenomenon over the Indian region was noted by Phadtare and Bhat (2019) where deep clouds predominantly formed in the western flank of the trough and moved further westward.

In the *NoCu* experiment, the processes that suppress convection over the rain shadow region during the offshore mode are too weak or absent. Thus, convection gets triggered over the land during daytime due to the presence of the trough and moves westward with time. It arrives over the Arabian Sea during late-night to morning hours and further propagates offshore. On 25 June, there is a sudden change in the regime of rainfall formation and propagation. Hereafter, the storms form just off the coast and propagate onshore. The eastern limit of this propagation is set by the Western Ghats peak. Propagation of mesoscale systems depends on features such as downdrafts, cold pools, and gravity bores (Bukovsky et al., 2006), which are associated with heavily precipitating convective cores, or it can be a simple advection by the background flow. The former mechanism seems more likely during the offshore mode when the systems propagate upwind, while the latter is likely important during the onshore mode. It appears that as the explicit representation of convection simulates high-intensity rainfall, the aforementioned processes are stronger, which results in long-lasting (but constrained by the diurnal cycle) propagating mesoscale systems. With the convective scheme, rainfall intensities are weak and propagating systems are absent.

5 | CONCLUSIONS AND DISCUSSION

Simulations of the summer monsoon rainfall modes over the west coast of India were performed using the WRF model in order to understand the underlying mechanism driving these modes and the impacts of model resolution and the representation of convection on their simulation. It is concluded that the offshore and onshore rainfall modes are largely a consequence of

the large-scale atmospheric variability over this region. A schematic in Figure 14 summarizes the meteorological conditions controlling these rainfall modes. During the offshore mode, a trough extended over the Arabian Sea from the peninsula. It provided favourable conditions for offshore convection. As noted by Fletcher et al. (2020) in their observations, the low-level winds during this mode were weak. Shige et al. (2017) and Hunt et al. (2021) reported a positive vorticity anomaly over the offshore region during the offshore mode which is also a consequence of the trough. During the onshore mode, a ridge moved over the west coast and offshore region, which suppressed the large-scale convective activity over the offshore region. However, the low-level westerly winds were strong, resulting in the direct orographic uplift of winds and hence, heavy rainfall over the Western Ghats and west coast region. The following conclusions were drawn from the model simulations of this phenomenon performed in this study:

- **Orographic blocking**: The WRF model domains at 4- and 1.33-km grid spacing with explicit convection were able to simulate the broad features of the west coast rainfall modes. However, the coastal boundary layer in the model was too warm (by about 4-5 °C) and weakly stratified. This reduced the orographic blocking of the flow leading to an overestimation of the convective instability over the coast. As a result, there was anomalous deep convection and rainfall over the Western Ghats in the model simulations.
- **Diurnal cycle**: None of the domains simulated the observed diurnal cycle of rainfall over the west coast during the offshore mode correctly. All domains produced a daytime rainfall maximum over land which was not seen in the observations.
- **Convection scheme**: The model domain at 12-km horizontal resolution with a convection scheme could simulate the large-scale fields of the offshore and onshore modes but failed at simulating the rainfall modes associated with them. Convection, as well as rainfall intensity, in this domain, was very weak. On the other hand, turning off the convection scheme at this resolution resulted in an unrealistic overestimation of the rainfall intensity even over the rainshadow region.
- **Western Ghats**: The no-orography sensitivity experiment showed that the Western Ghats do not independently drive the offshore-onshore modes. However, they act as a barrier along the coast, keeping the rainfall predominantly offshore during the offshore mode. The coastal rainfall in the onshore mode is greatly enhanced due to the orographic uplifting.

Although the accuracy of IMERG rainfall can be questioned over the Western Ghats region, Flynn et al. (2017) reported that simulated rainfall over the west coast and Western Ghats was much greater in model simulations compared to their rain gauge observations. Given the uncertainties involved in model simulations, doubts can be raised regarding the pertinence of the conclusions of this study. Nevertheless, the rainfall accumulations in the offshore and onshore modes reported by Martin et al. (2020) (see figure 6 in that paper) in the MetUM are similar to those reported by the present study in Figure 4. Overestimation of orographic rainfall in the MetUM and other models based on the MetUM (e.g., NCUM) is also common (Martin et al., 2020). This suggests that the model biases reported here stem from the physics parameterization rather than the simulation uncertainties. Although this bias was blamed on the inadequate representation of convection in the models (Flynn et al., 2017), the simulated rainfall pattern in the present study is reminiscent of the idealized modelling experiments in which the Froude number of the flow was increased beyond 1 (Chu and Lin, 2000; Chen and Lin, 2005b,a; Jiang, 2003; Reeves and Lin, 2007; Miglietta and Rotunno, 2009). Our study points out that the underestimation of the orographic blocking by the model seems to be the primary cause behind it. The model does not adequately simulate the cold-air damming along the coast (Figs. 10 and 11), hence producing an anomalously warm and well-mixed PBL that weakens the orographic blocking by the Western Ghats. Although the model simulates the cold pools formed by the evaporation of rainfall (Fig. 7) and the temperature drop is also similar to that reported in observations by Fletcher et al. (2020) (figure 11b of that paper), the time scale for subsequent mixing and recovery of the PBL should be compared with the real world observations. In situ, high-resolution measurements on- and offshore are needed for this purpose.

Apart from the PBL scheme, the factors that can affect the structure of simulated PBL are the elevation of the lowest model

level and the number of levels within PBL. The lowest level in our simulations was at 20 m above the surface and there were 10 levels below 1500 m. Systematic model experiments can be performed to understand the sensitivity of these factors on the simulated PBL stratification. An underestimation low-level stratification can also result in reduced orographic drag in the upper atmosphere via weakened upward-propagating gravity waves (Wallace et al., 1983; Boer et al., 1984; Palmer et al., 1986; Bacmeister, 1993; Fritts and Alexander, 2003; Teixeira, 2014). This can have several consequences on the simulation of the Indian monsoon, including anomalously strong winds (Figure 6), stronger ventilation of the Indian peninsula by stronger winds, and hence, a weakened monsoon trough. Thus, in addition to the efforts of improving the representation of clouds and convection, land-atmosphere interaction, and aerosol effects, modelling of boundary layer processes and upscale propagation of orographic effects also needs attention in order to improve model simulations of the Indian monsoon.

REFERENCES

Bacmeister, J. T. (1993) Mountain-wave drag in the stratosphere and mesosphere inferred from observed winds and a simple mountain-wave parameterization scheme. *Journal of Atmospheric Sciences*, **50**, 377–399.

Birch, C., Webster, S., Peatman, S., Parker, D., Matthews, A., Li, Y. and Hassim, M. (2016) Scale interactions between the MJO and the western Maritime Continent. *Journal of Climate*, **29**, 2471–2492.

Birch, C. E., Roberts, M. J., Garcia-Carreras, L., Ackerley, D., Reeder, M. J., Lock, A. P. and Schiemann, R. (2015) Sea-breeze dynamics and convection initiation: The influence of convective parameterization in weather and climate model biases. *Journal of Climate*, **28**, 8093–8108.

Boer, G., McFarlane, N., Laprise, R., Henderson, J. and Blanchet, J.-P. (1984) The Canadian Climate Centre spectral atmospheric general circulation model. *Atmosphere-Ocean*, **22**, 397–429.

Bukovsky, M. S., Kain, J. S. and Baldwin, M. E. (2006) Bowing convective systems in a popular operational model: Are they for real? *Weather and forecasting*, **21**, 307–324.

Chen, F. and Dudhia, J. (2001) Coupling an advanced land surface–hydrology model with the Penn State–NCAR MM5 modeling system. Part I: Model implementation and sensitivity. *Monthly weather review*, **129**, 569–585.

Chen, S.-H. and Lin, Y.-L. (2005a) Effects of moist Froude number and CAPE on a conditionally unstable flow over a mesoscale mountain ridge. *Journal of the Atmospheric Sciences*, **62**, 331–350.

— (2005b) Orographic effects on a conditionally unstable flow over an idealized three-dimensional mesoscale mountain. *Meteorology and Atmospheric Physics*, **88**, 1–21.

Chen, Y., Chen, J., Chen, D., Xu, Z., Sheng, J. and Chen, F. (2021) A simulated radar reflectivity calculation method in numerical weather prediction models. *Weather and Forecasting*, **36**, 341–359.

Chu, C.-M. and Lin, Y.-L. (2000) Effects of orography on the generation and propagation of mesoscale convective systems in a two-dimensional conditionally unstable flow. *Journal of the Atmospheric Sciences*, **57**, 3817–3837.

Fletcher, J. K., Parker, D. J., Turner, A. G., Menon, A., Martin, G. M., Birch, C. E., Mitra, A. K., Mrudula, G., Hunt, K. M., Taylor, C. M. et al. (2020) The dynamic and thermodynamic structure of the monsoon over southern India: New observations from the INCOMPASS IOP. *Quarterly Journal of the Royal Meteorological Society*, **146**, 2867–2890.

Flynn, W. J., Nesbitt, S. W., Anders, A. M. and Garg, P. (2017) Mesoscale precipitation characteristics near the Western Ghats during the Indian Summer Monsoon as simulated by a high-resolution regional model. *Quarterly Journal of the Royal Meteorological Society*, **143**, 3070–3084.

Francis, P. and Gadgil, S. (2006) Intense rainfall events over the west coast of India. *Meteorology and Atmospheric Physics*, **94**, 27–42.

Fritts, D. C. and Alexander, M. J. (2003) Gravity wave dynamics and effects in the middle atmosphere. *Reviews of Geophysics*, **41**.

Gerard, L., Piriou, J.-M., Brožková, R., Geleyn, J.-F. and Banciu, D. (2009) Cloud and precipitation parameterization in a meso-gamma-scale operational weather prediction model. *Monthly Weather Review*, **137**, 3960–3977.

Grossman, R. L. and Durran, D. R. (1984) Interaction of low-level flow with the Western Ghat mountains and offshore convection in the summer monsoon. *Monthly Weather Review*, **112**, 652–672.

Hersbach, H., Bell, B., Berrisford, P., Biavati, G., Horányi, A., Muñoz Sabater, J., Nicolas, J., Peubey, C., Radu, R., Rozum, I. et al. (2018) ERA5 hourly data on pressure levels from 1979 to present. *Copernicus Climate Change Service (C3S) Climate Data Store (CDS)*. (Accessed on 12 NOV 2022), 10.24381/cds.bd0915c6.

Hong, S.-Y. and Lim, J.-O. J. (2006) The WRF single-moment 6-class microphysics scheme (WSM6). *Asia-Pacific Journal of Atmospheric Sciences*, **42**, 129–151.

Hong, S.-Y., Noh, Y. and Dudhia, J. (2006) A new vertical diffusion package with an explicit treatment of entrainment processes. *Monthly Weather Review*, **134**, 2318–2341.

Honnert, R. (2016) Representation of the grey zone of turbulence in the atmospheric boundary layer. *Advances in Science and Research*, **13**, 63–67.

Huffman, G. J., Bolvin, D. T., Nelkin, E. J. and Tan, J. (2015) Integrated Multi-satellitE Retrievals for GPM (IMERG) technical documentation. *NASA/GSFC Code*, **612**, 2019.

Hunt, K. M. and Menon, A. (2020) The 2018 Kerala floods: A climate change perspective. *Climate Dynamics*, **54**, 2433–2446.

Hunt, K. M., Turner, A. G., Stein, T. H., Fletcher, J. K. and Schiemann, R. K. (2021) Modes of coastal precipitation over southwest India and their relationship with intraseasonal variability. *Quarterly Journal of the Royal Meteorological Society*, **147**, 181–201.

Iacono, M. J., Delamere, J. S., Mlawer, E. J., Shephard, M. W., Clough, S. A. and Collins, W. D. (2008) Radiative forcing by long-lived greenhouse gases: Calculations with the AER radiative transfer models. *Journal of Geophysical Research: Atmospheres*, **113**.

Jiang, Q. (2003) Moist dynamics and orographic precipitation. *Tellus A: Dynamic Meteorology and Oceanography*, **55**, 301–316.

Kirshbaum, D. J. (2020) Numerical simulations of orographic convection across multiple gray zones. *Journal of the Atmospheric Sciences*, **77**, 3301–3320.

Kirshbaum, D. J., Adler, B., Kalthoff, N., Barthlott, C. and Serafin, S. (2018) Moist orographic convection: Physical mechanisms and links to surface-exchange processes. *Atmosphere*, **9**, 80.

Krishnan, R., Zhang, C. and Sugi, M. (2000) Dynamics of breaks in the Indian summer monsoon. *Journal of the atmospheric sciences*, **57**, 1354–1372.

Kumar, A., Dudhia, J., Rotunno, R., Niyogi, D. and Mohanty, U. (2008) Analysis of the 26 July 2005 heavy rain event over Mumbai, India using the Weather Research and Forecasting (WRF) model. *Quarterly Journal of the Royal Meteorological Society*, **134**, 1897–1910.

Kumar, S. and Bhat, G. (2017) Vertical structure of orographic precipitating clouds observed over south Asia during summer monsoon season. *Journal of Earth System Science*, **126**, 1–12.

Mahoney, K. M. (2016) The representation of cumulus convection in high-resolution simulations of the 2013 Colorado Front Range flood. *Monthly Weather Review*, **144**, 4265–4278.

Martin, G. M., Brooks, M. E., Johnson, B., Milton, S. F., Webster, S., Jayakumar, A., Mitra, A. K., Rajan, D. and Hunt, K. M. (2020) Forecasting the monsoon on daily to seasonal time-scales in support of a field campaign. *Quarterly Journal of the Royal Meteorological Society*, **146**, 2906–2927.

Miglietta, M. M. and Rotunno, R. (2009) Numerical simulations of conditionally unstable flows over a mountain ridge. *Journal of the Atmospheric Sciences*, **66**, 1865–1885.

Mohandas, S., Francis, T., Singh, V., Jayakumar, A., George, J. P., Sandeep, A., Xavier, P. and Rajagopal, E. (2020) NWP perspective of the extreme precipitation and flood event in Kerala (India) during August 2018. *Dynamics of Atmospheres and Oceans*, **91**, 101158.

Murali Krishna, U., Das, S. K., Deshpande, S. M., Doiphode, S. and Pandithurai, G. (2017) The assessment of Global Precipitation Measurement estimates over the Indian subcontinent. *Earth and Space Science*, **4**, 540–553.

Palmer, T., Shutts, G. and Swinbank, R. (1986) Alleviation of a systematic westerly bias in general circulation and numerical weather prediction models through an orographic gravity wave drag parametrization. *Quarterly Journal of the Royal Meteorological Society*, **112**, 1001–1039.

Peatman, S. C., Matthews, A. J. and Stevens, D. P. (2014) Propagation of the Madden–Julian Oscillation through the Maritime Continent and scale interaction with the diurnal cycle of precipitation. *Quarterly Journal of the Royal Meteorological Society*, **140**, 814–825.

Phadtare, J. (2018) Role of Eastern Ghats orography and cold pool in an extreme rainfall event over Chennai on 1 December 2015. *Monthly Weather Review*, **146**, 943–965.

Phadtare, J. and Bhat, G. (2019) Characteristics of deep cloud systems under weak and strong synoptic forcing during the Indian summer monsoon season. *Monthly Weather Review*, **147**, 3741–3758.

Phadtare, J. A., Fletcher, J. K., Ross, A. N., Turner, A. G. and Schiemann, R. K. (2022) Froude number-based Rainfall Regimes over the Western Ghats Mountains of India. *Quarterly Journal of the Royal Meteorological Society*.

Prakash, S. and Srinivasan, J. (2021) A comprehensive evaluation of near-real-time and research products of IMERG precipitation over India for the southwest monsoon period. *Remote Sensing*, **13**, 3676.

Rajendran, K., Kitoh, A., Srinivasan, J., Mizuta, R. and Krishnan, R. (2012) Monsoon circulation interaction with Western Ghats orography under changing climate. *Theoretical and Applied Climatology*, **110**, 555–571.

Reeves, H. D. and Lin, Y.-L. (2007) The effects of a mountain on the propagation of a preexisting convective system for blocked and unblocked flow regimes. *Journal of the Atmospheric Sciences*, **64**, 2401–2421.

Rojas, Y., Minder, J. R., Campbell, L. S., Massmann, A. and Garreaud, R. (2021) Assessment of GPM IMERG satellite precipitation estimation and its dependence on microphysical rain regimes over the mountains of south-central Chile. *Atmospheric Research*, **253**, 105454.

Saha, U., Gupta, M. D. and Mitra, A. K. (2021) Monitoring the Quality of AWS/ARG Rainfall Observations over India during Monsoon Season. Available at `https://www.ncmrwf.gov.in/Reports-eng/Report_AWS_ARG_Feb_2021_Final_Upal_Saha_NCMRWF.pdf`.

Sheppard, P. (1956) Airflow over mountains. *Quarterly Journal of the Royal Meteorological Society*, **82**, 528–529.

Shige, S., Nakano, Y. and Yamamoto, M. K. (2017) Role of orography, diurnal cycle, and intraseasonal oscillation in summer monsoon rainfall over the Western Ghats and Myanmar Coast. *Journal of Climate*, **30**, 9365–9381.

Shrestha, D., Deshar, R. and Nakamura, K. (2015) Characteristics of summer precipitation around the Western Ghats and the Myanmar West Coast. *International Journal of Atmospheric Sciences*, **2015**.

Skamarock, W. C., Klemp, J. B., Dudhia, J., Gill, D. O., Barker, D. M., Wang, W. and Powers, J. G. (2008) A description of the advanced research WRF version 3. *Tech. rep.*, University Corporation for Atmospheric Research.

Smith, R. B. (1979) The influence of mountains on the atmosphere. In *Advances in Geophysics*, vol. 21, 87–230. Elsevier.

Smith, S., Vosper, S. and Field, P. (2015) Sensitivity of orographic precipitation enhancement to horizontal resolution in the operational Met Office Weather forecasts. *Meteorological Applications*, **22**, 14–24.

Stensrud, D. J. (2009) *Parameterization schemes: keys to understanding numerical weather prediction models*. Cambridge University Press.

Tang, S. L. and Kirshbaum, D. (2020) On the sensitivity of deep-convection initiation to horizontal grid resolution. *Quarterly Journal of the Royal Meteorological Society*, **146**, 1085–1105.

Teixeira, M. A. (2014) The physics of orographic gravity wave drag. *Frontiers in Physics*, **2**, 43.

Tiedtke, M. (1989) A comprehensive mass flux scheme for cumulus parameterization in large-scale models. *Monthly Weather Review*, **117**, 1779–1800.

Turner, A. G., Bhat, G., Martin, G., Parker, D. J., Taylor, C., Mitra, A. K., Tripathi, S. N., Milton, S., Rajagopal, E., Evans, J. G. et al. (2020) Interaction of convective organization with monsoon precipitation, atmosphere, surface and sea: The 2016 INCOMPASS field campaign in India. *Quarterly Journal of the Royal Meteorological Society*, **146**, 2828–2852.

Wallace, J. M., Tibaldi, S. and Simmons, A. J. (1983) Reduction of systematic forecast errors in the ECMWF model through the introduction of an envelope orography. *Quarterly Journal of the Royal Meteorological Society*, **109**, 683–717.

Wyngaard, J. C. (2004) Toward numerical modeling in the "Terra Incognita". *Journal of the Atmospheric Sciences*, **61**, 1816–1826.

Xu, W. and Rutledge, S. A. (2015) Morphology, intensity, and rainfall production of MJO convection: Observations from DYNAMO shipborne radar and TRMM. *Journal of the Atmospheric Sciences*, **72**, 623–640.

Zhang, C., Wang, Y. and Hamilton, K. (2011) Improved representation of boundary layer clouds over the southeast Pacific in ARW-WRF using a modified Tiedtke cumulus parameterization scheme. *Monthly Weather Review*, **139**, 3489–3513.

Zhang, D. and Anthes, R. A. (1982) A high-resolution model of the planetary boundary layer—Sensitivity tests and comparisons with SESAME-79 data. *Journal of Applied Meteorology (1962-1982)*, 1594–1609.

Zhang, G. and Smith, R. B. (2018) Numerical study of physical processes controlling summer precipitation over the Western Ghats region. *Journal of Climate*, **31**, 3099–3115.

Zheng, Y., Alapaty, K., Herwehe, J. A., Del Genio, A. D. and Niyogi, D. (2016) Improving high-resolution weather forecasts using the Weather Research and Forecasting (WRF) Model with an updated Kain–Fritsch scheme. *Monthly Weather Review*, **144**, 833–860.

6 | ACKNOWLEDGEMENTS

This work and its contributors (JAP, JKF, ANR, AGT, RKHS, HLB) were funded through the Weather and Climate Science for Service Partnership (WCSSP) India, a collaborative initiative between the Met Office, supported by the UK Government's Newton Fund, and the Indian Ministry of Earth Sciences (MoES). This work was undertaken on ARC4, part of the High Performance Computing facilities at the University of Leeds, UK. The ERA5 data was obtained via the Climate Data Store (CDS). JAP thanks Thorwald H.M. Stein and Kieran M.R. Hunt at the University of Reading and A. Jayakumar at the National Centre for Medium Range Weather Forecasting (NCMRWF) for their constructive comments on this study.

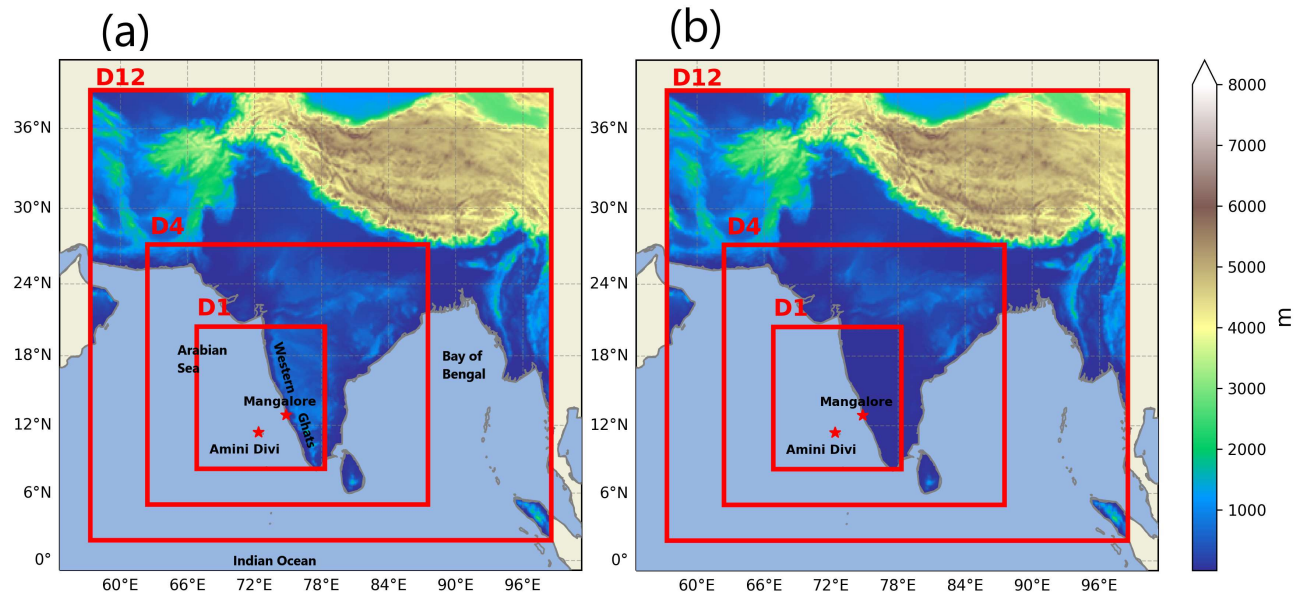

FIGURE 1 Model domains and orography for (a) Control run, and (b) *NoOrog* run described in section 4.1. Grid spacings: D12 - 12 km, D4 - 4 km, and D1 - 1.33 km.

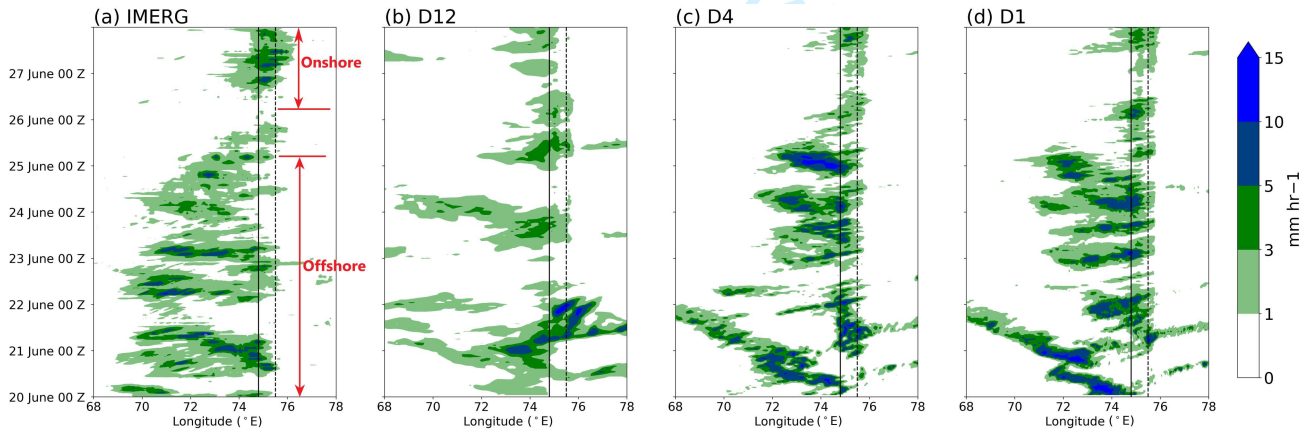

FIGURE 2 Hovmöller plot of 12-14°N averaged rainfall in (a) IMERG, (b) D12, (c) D4, and (d) D1 during 20-27 June 2016. The solid black line shows the mean longitude of the coast and the dotted line shows the mean longitude of the Western Ghats peak between 12-14°N.

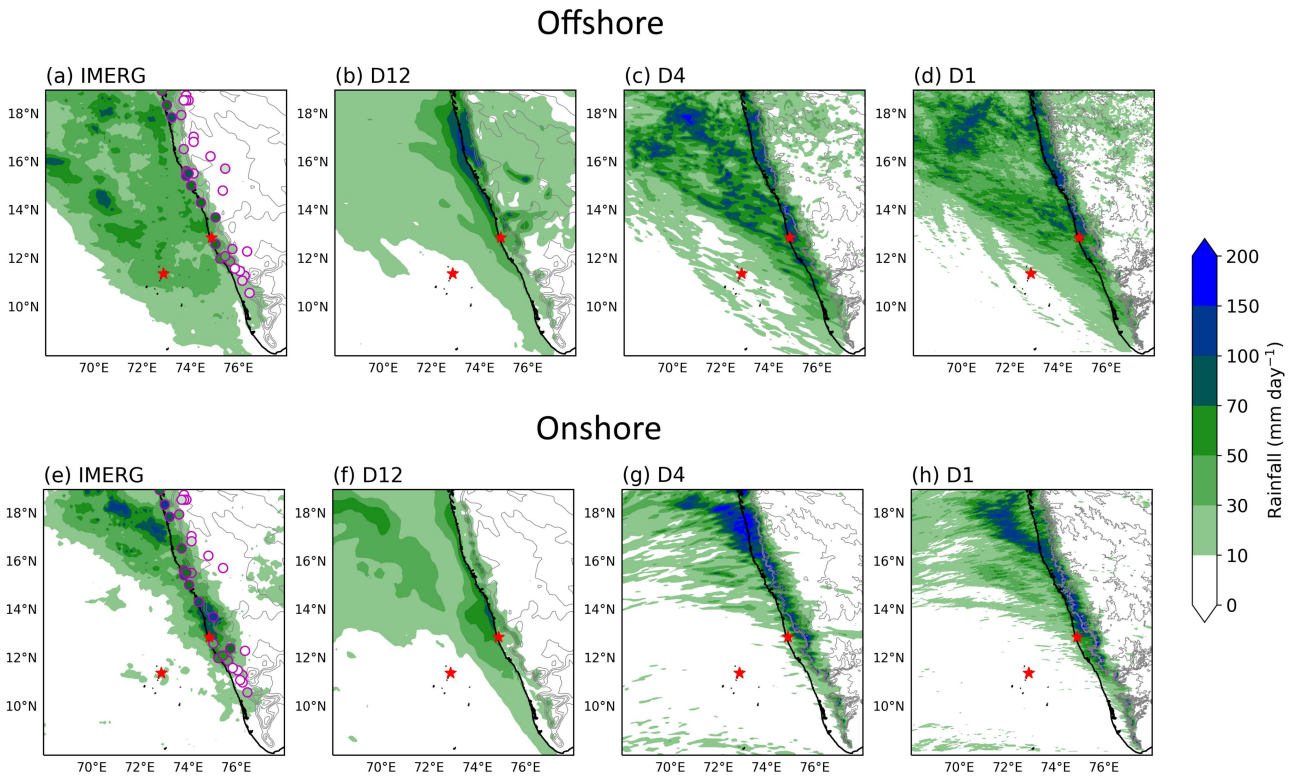

FIGURE 3 Mean rainfall during the offshore mode (20-24 June) in (a) IMERG, (b) D12, (c) D4, and (d) D1. (e)-(g) are the same as (a)-(d), respectively, but for the onshore mode (26-27 June). The stars show the locations of Mangalore (coast) and Amini Divi (island) stations. The circles along the west coast in (a) and (e) show the locations of rain gauges from which data is used and their face colours show the mean rainfall recorded by them during respective modes.

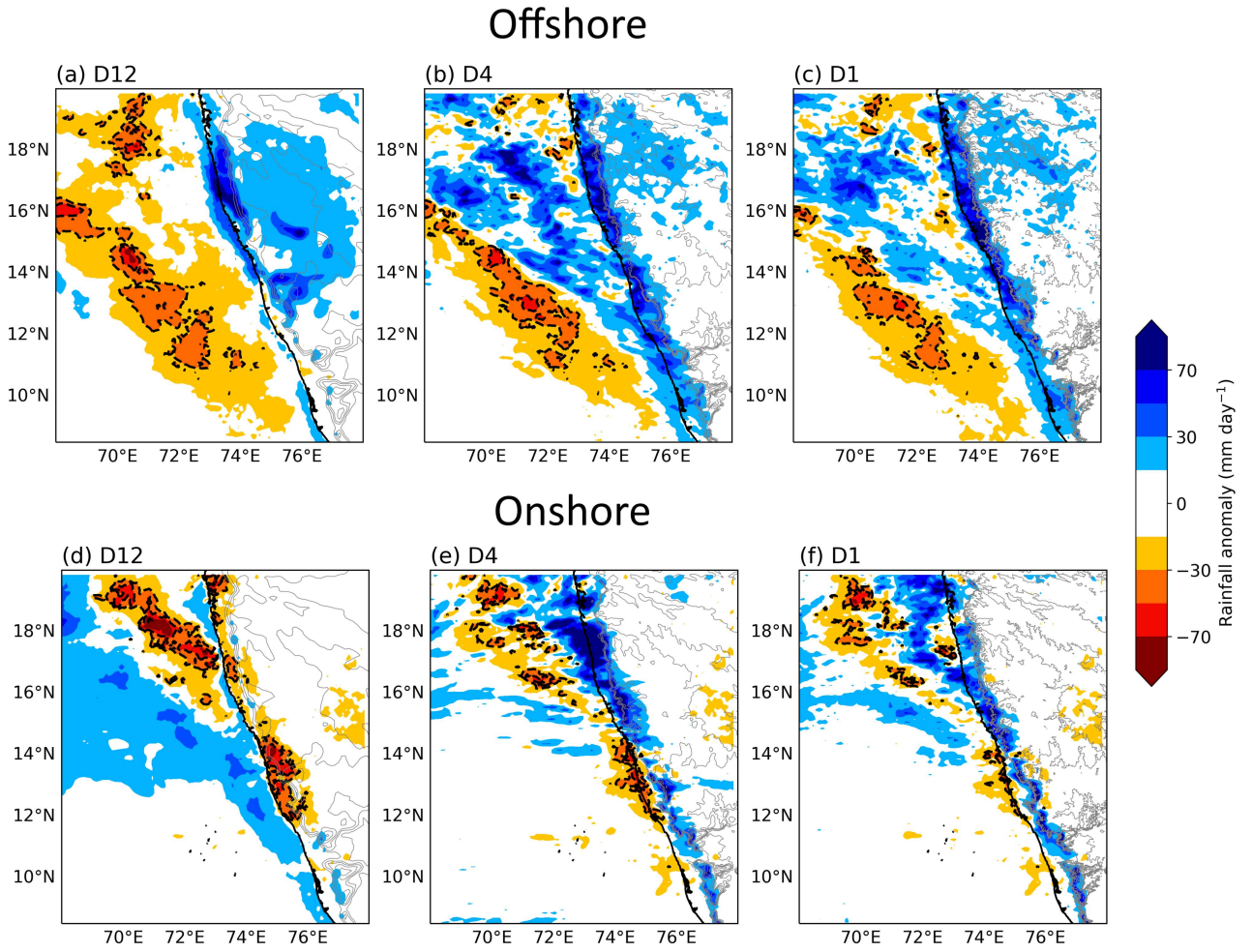

FIGURE 4 Rainfall anomaly in (a) D12, (b) D4, and (c) D1 with respect to the IMERG rainfall during the offshore mode. (d)-(f) Same as (a)-(c), respectively, but during the onshore mode.

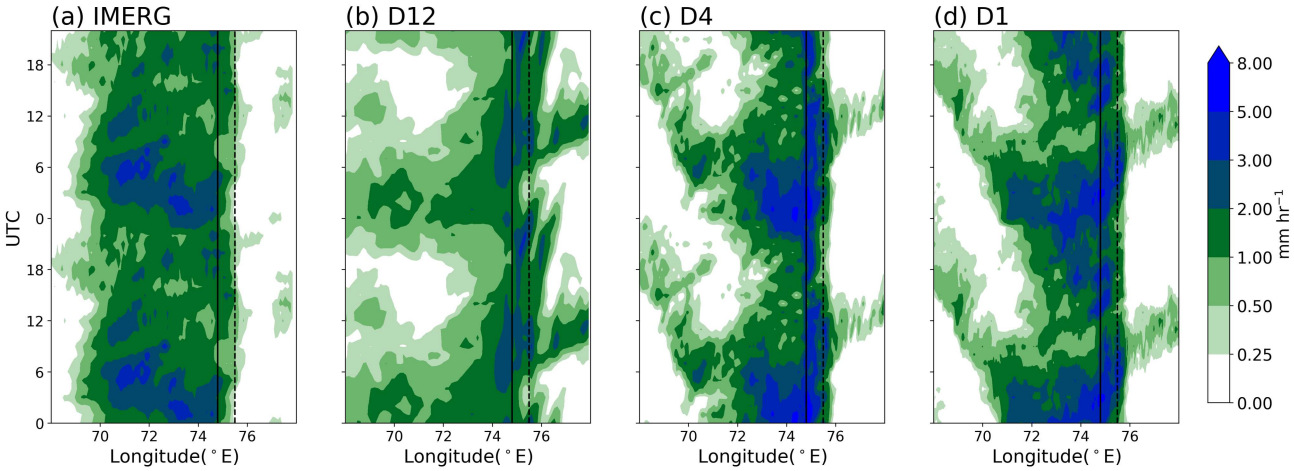

FIGURE 5 Diurnal variation of mean rainfall over 12-14°N band in (a) IMERG, (b) D12, (c) D4, and (d) D1 during the offshore mode.

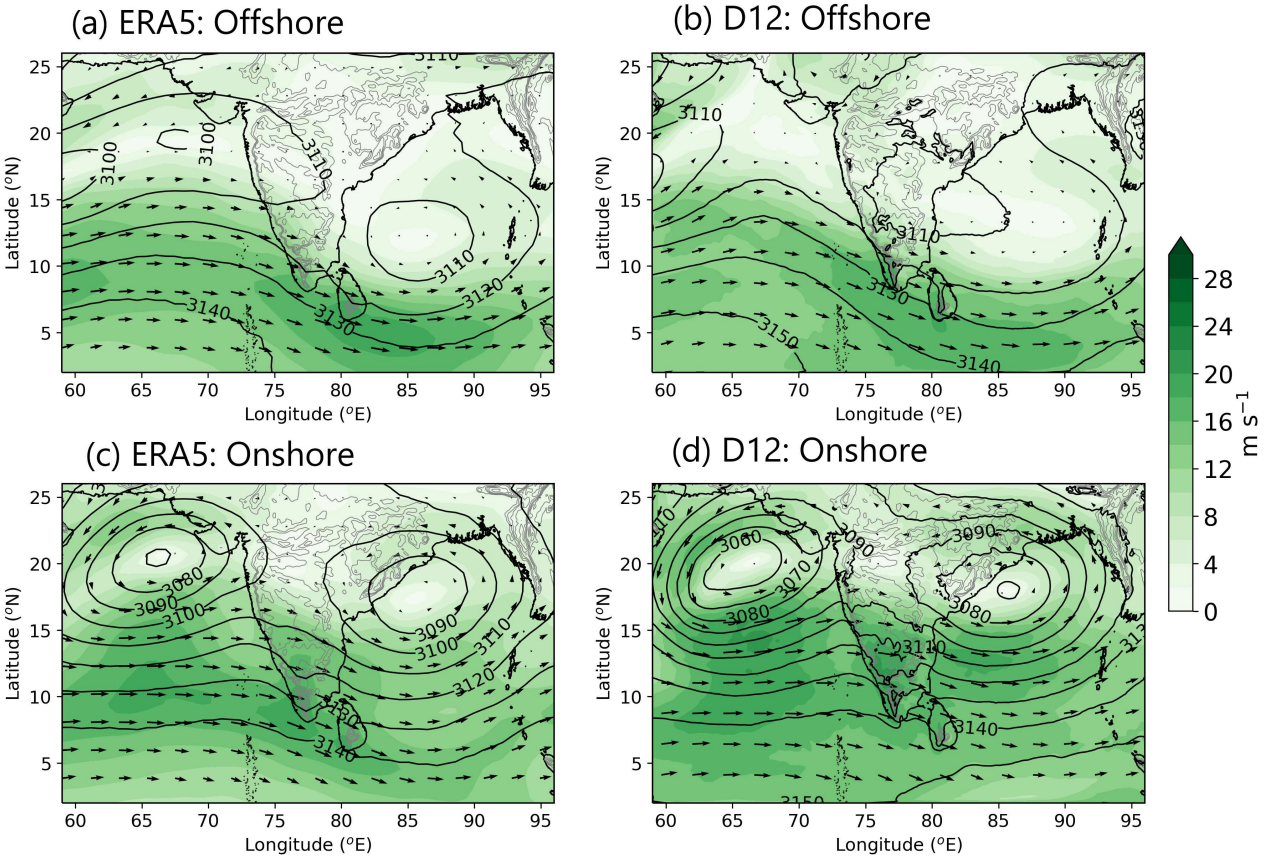

FIGURE 6 Mean 700 hPa geopotential height (m) contours and wind speed (shading) from (a) ERA5 and (b) D12 during the offshore mode. (c),(d) same as (a),(b) but for the onshore mode.

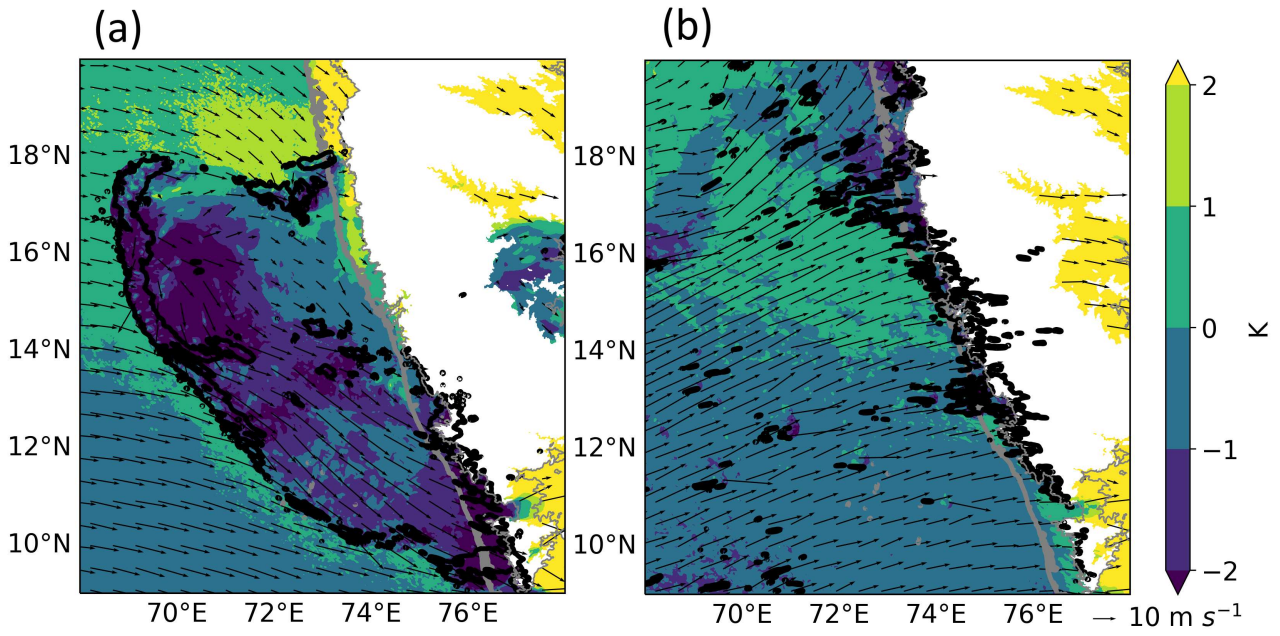

FIGURE 7 Virtual potential temperature perturbation (shading) and winds at 950 hPa in D1 at (a) 0500 UTC 20 June (offshore mode) and (b) 0500 UTC 27 June (onshore mode); The black contours delineate regions where rainfall ≥ 5 mm hr^{-1}.

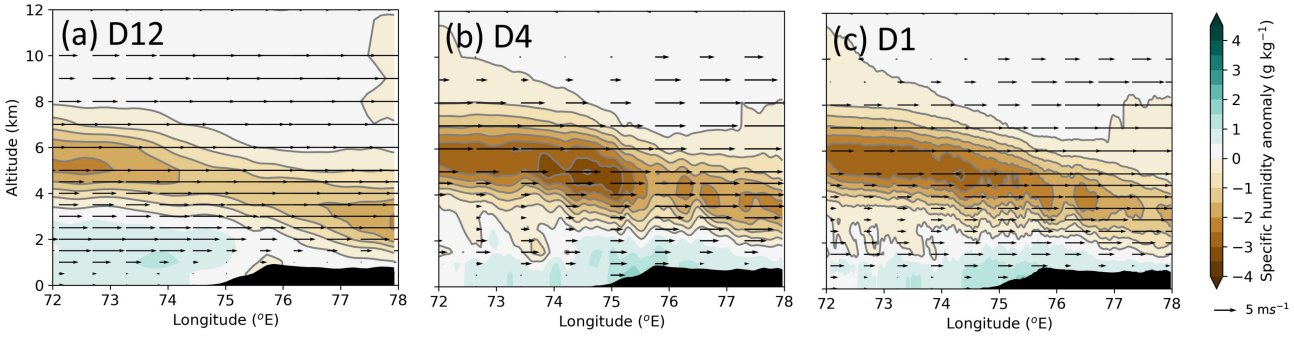

FIGURE 8 Difference between the mean zonal winds (vectors) and specific humidity (shading) over the 12-14°N band during the onshore and offshore modes (onshore-offshore) simulated by (a) D12, (b) D4 and (c) D1. The grey contours delineate negative anomalies of the specific humidity.

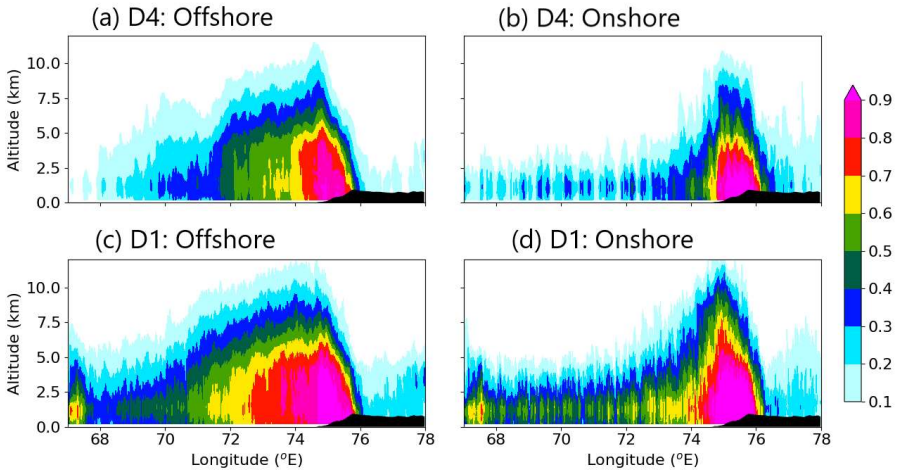

FIGURE 9 Temporal fraction for which the simulated radar reflectivity was ≥ 20 dBZ in at least one grid box in the 12-14°N band in D4 during the (a) offshore and (b) onshore modes. (c)-(d) are same as (a)-(b), respectively, but for the D1 domain.

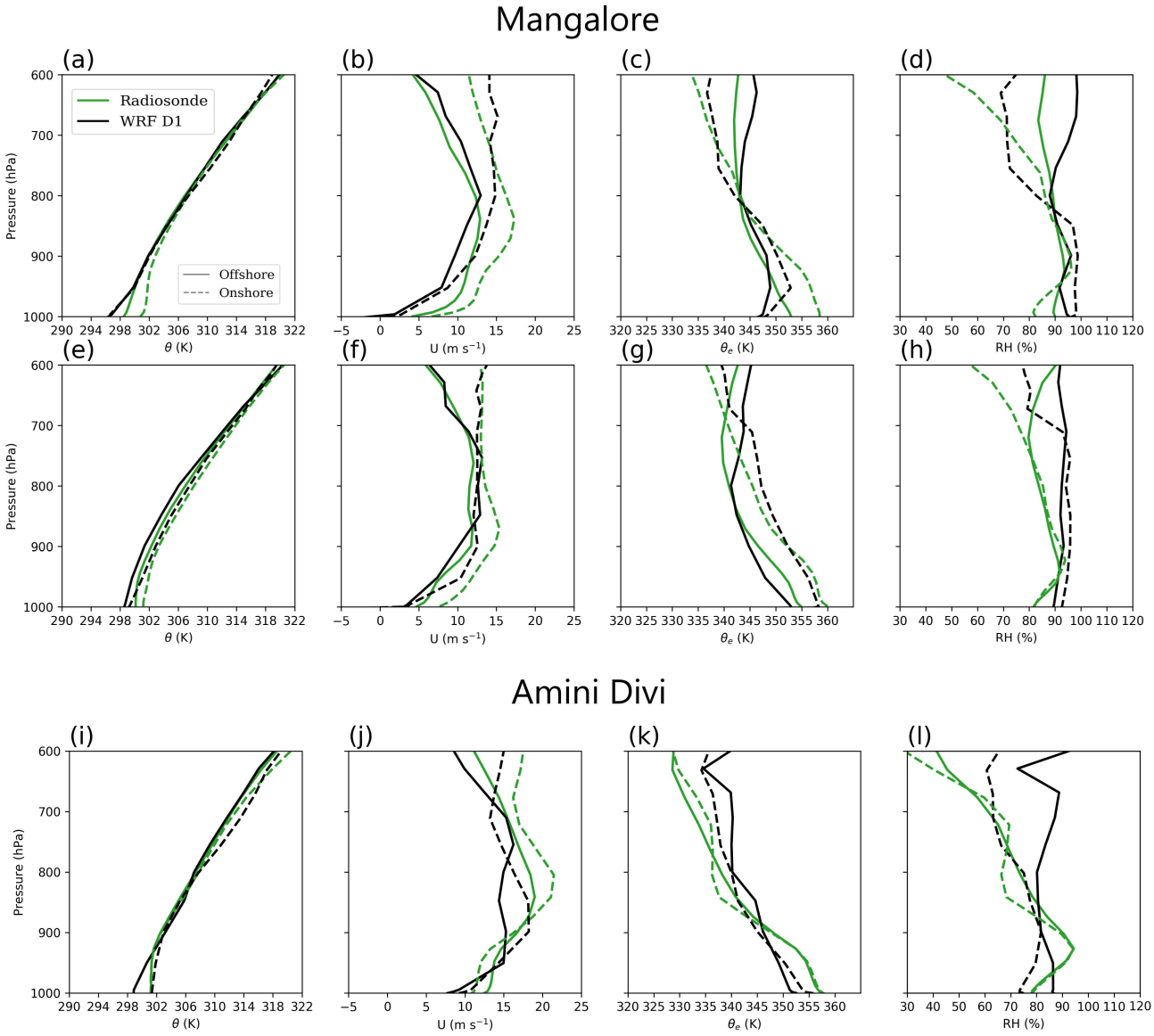

FIGURE 10 Mean vertical profiles of (a) Potential temperature (θ), (b) zonal winds (U), (c) equivalent potential temperature (θ_e), and (d) relative humidity during the offshore and onshore modes from the 0000 UTC Mangalore (a coastal station) radiosondes and the corresponding simulated soundings in D1. (e)-(h) are the same as (a)-(d) but for the 1200 UTC radiosondes. (i)-(l) are the same as (a)-(d) but for the 0000 UTC Amini Divi (an island station) radiosondes. The simulated profiles are averaged over a 12 km box centred over the sounding location.

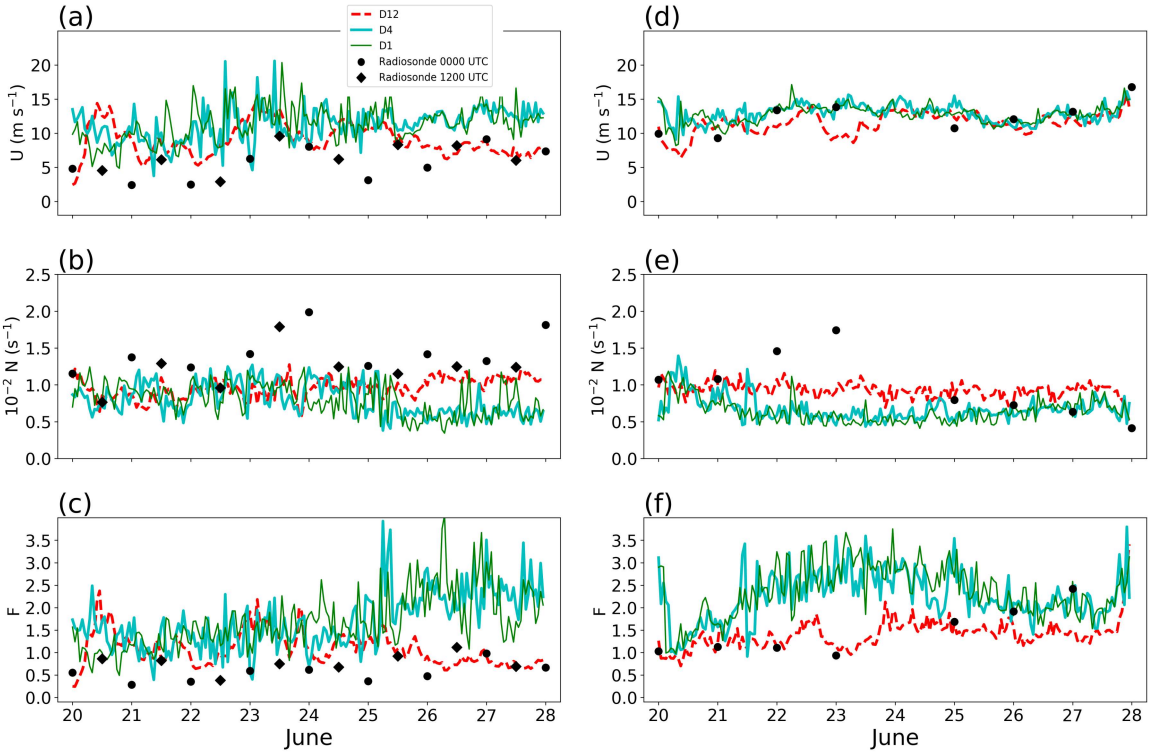

FIGURE 11 Mean values of (a) Zonal winds (U), (b) Brunt-Väisälä frequency (N), and (c) Froude number (F) over the 50-1000 m layer calculated from the 0000 and 1200 UTC Mangalore (a coastal station) radiosonde soundings and the hourly simulated soundings in the three WRF grids (D12, D4, and D1) over the same location as Mangalore. (d)-(f) are same as (a)-(c) but for the Amini Divi (an island station) radiosonde soundings.

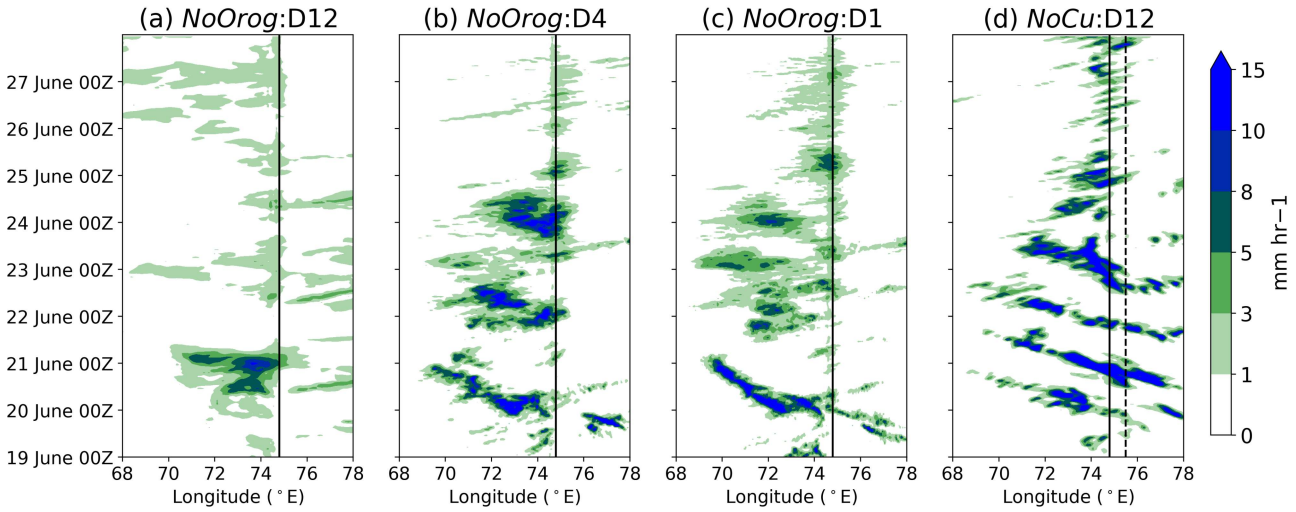

FIGURE 12 Hovmöller plot of 12-14°N averaged rainfall in (a) D12, (b) D4, and (c) D1 from the *NoOrog* simulation. (d) Same as (a) but for the *NoCu* simulation. The solid black line shows the mean longitude of the coast and the dotted line shows the mean longitude of the Western Ghats peak between 12-14°N.

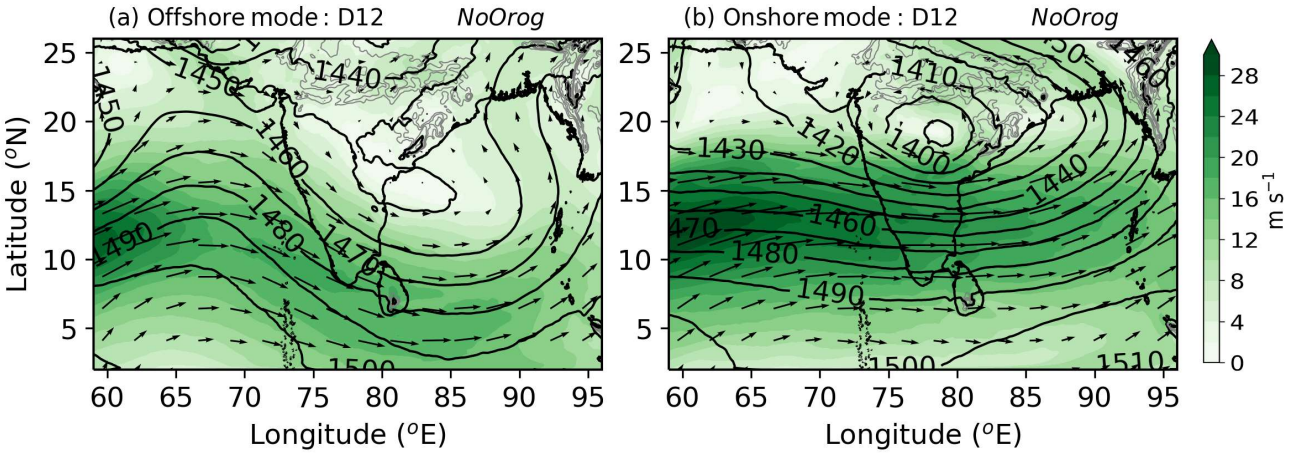

FIGURE 13 Mean 850 hPa geopotential height (m) contours and wind speed (shading) during the (a) offshore and (b) onshore modes in the D12 domain from the *NoOrog* simulation.

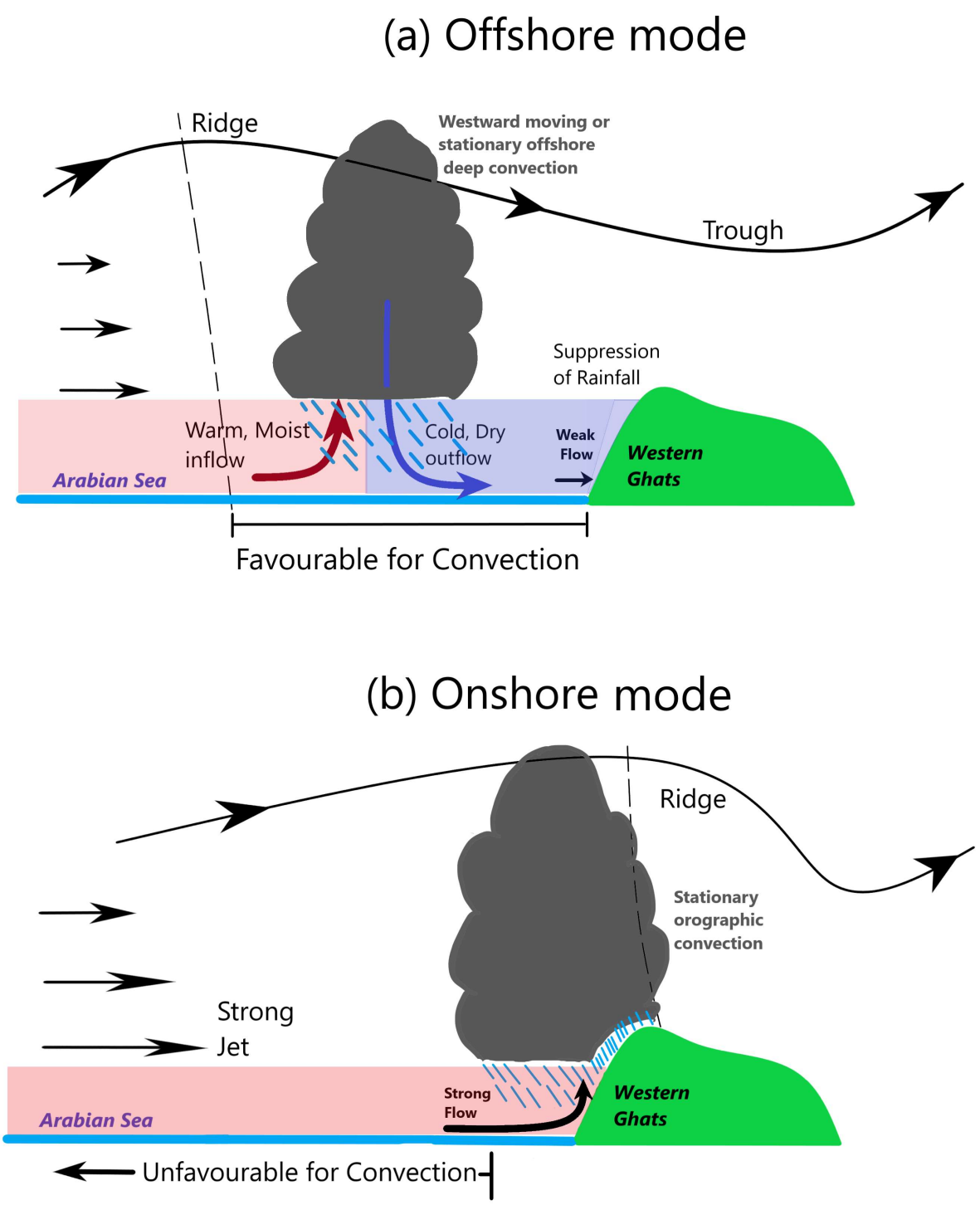

FIGURE 14 Schematics of the (a) offshore and (b) onshore rainfall modes over the west coast of India. An offshore trough facilities offshore convection and rainfall over the Arabian Sea. The cold and dry outflows from the offshore rainfall suppress rainfall over the Western Ghats. During onshore mode, a ridge over the coast suppresses offshore rainfall. Westerlies are stronger during this phase and enhanced rainfall over the coast and Western Ghats results from the orographic uplifting.

ORIGINAL ARTICLE

Unravelling the Mechanism of Summer Monsoon Rainfall Modes over the West Coast of India using Model Simulations

Jayesh A. Phadtare[1,2*] | Jennifer K. Fletcher[1,2] | Andrew N. Ross[1] | Andrew G. Turner[3,4] | Reinhard K. H. Schiemann[4] | Helen L. Burns[5]

[1]School of Earth and Environment, University of Leeds, UK

[2]National Centre for Atmospheric Science, University of Leeds, UK

[3]Department of Meteorology, University of Reading, UK

[4]National Centre for Atmospheric Science, University of Reading, UK

[5]Centre for Environmental Modelling And Computation, University of Leeds, UK

Correspondence
Jayesh Phadtare, Department of Civil and Environmental Engineering and Earth Sciences, University of Notre Dame, Notre Dame, IN 46556
Email: jayesh.phadtare@gmail.com

Present address
*Department of Civil and Environmental Engineering and Earth Sciences, University of Notre Dame, Notre Dame, IN 46556

Funding information
Weather and Climate Science for Service Partnership (WCSSP) India, a collaborative initiative between the Met Office, supported by the UK Government's Newton Fund, and the Indian Ministry of Earth Sciences (MoES).

A transition from a predominantly offshore to an onshore rainfall phase over the west coast of India was simulated using three one-way nested domains with 12-, 4-, and 1.33-km horizontal grid spacing in the Weather Research and Forecasting model. The mechanism of offshore-onshore rainfall oscillation and the orographic effects of the Western Ghats are studied. A convective parameterization scheme was employed only in the 12-km domain. A trough extending offshore from the west coast facilitates offshore rainfall. This trough is absent during the onshore phase, and rainfall occurs over the coast mainly via orographic uplift by the Western Ghats. The model overestimates rainfall over the Western Ghats at all resolutions as it consistently underestimates the boundary layer stratification along the coast. Weaker stratification weakens the blocking effect of the Western Ghats, resulting in anomalous deep convection and rainfall over its windward slopes. The 4- and 1.33-km domains simulate the offshore-to-onshore transition of rainfall but fail to capture a sufficient contrast in rainfall between land and sea compared to observations. The 12-km domain produces light rainfall, anchored along the coast, throughout the simulation period, and hence gravely underestimates the offshore rainfall. The offshore rainfall persisted in the 4- and 1.33-

km domains in a sensitivity experiment in which the Western Ghats were flattened. This suggests that orographic effects do not significantly influence offshore rainfall. In another experiment, the convective parameterization scheme in the 12-km domain was turned off. This experiment simulated the offshore and onshore rainfall phases correctly to some extent but the rainfall intensity was unrealistically high. Thus, a model with a horizontal grid spacing of O(∼ 1 km), in which convection evolves explicitly, is desired for simulating the west coast rainfall variations. However, improvements in the representation of boundary layer processes are needed to capture the land-sea contrast.

KEYWORDS

Orographic effects, Indian Summer monsoon, Coastal rainfall

1 | INTRODUCTION

The west coast of the Indian peninsula is one of the rainiest places on our planet and a host to rainforests with a high level of biodiversity, thanks to the Western Ghats mountain range. This region is prone to flash floods and landslides during the summer monsoon season (Francis and Gadgil, 2006; Kumar et al., 2008; Hunt and Menon, 2020; Mohandas et al., 2020). In June 2016, the Interaction of Convective Organization and Monsoon Precipitation, Atmosphere, Surface and Sea (INCOMPASS) field campaign took place over the Indian region in order to understand the interaction between the convective and large-scale weather systems in the summer monsoon (Turner et al., 2020). One of its southern legs involved aircraft and ground-based observations over the west coast of India and the adjacent Arabian Sea during 21-26 June (henceforth referred to as the 'INCOMPASS IOP'). Heavy rainfall shifted from the offshore region (henceforth referred to as the 'offshore mode') to the onshore region (henceforth referred to as the 'onshore mode') during this period. It was speculated that the interactions between the monsoonal westerly jet, a mid-tropospheric dry air intrusion, and convection lead to the offshore and onshore rainfall modes (Fletcher et al., 2020). A climatological study by Hunt et al. (2021) supports this hypothesis. Grossman and Durran (1984), with the help of field observations and a simple 2D model of flow over an orographic barrier, suggest that the offshore rainfall over the Arabian Sea may result from upstream blocking and uplift of the monsoonal jet by the Western Ghats. On the other hand, a study involving WRF model simulations by Zhang and Smith (2018) suggests that the offshore rainfall results from large-scale instabilities, and that the Western Ghats merely serve as the eastern boundary for it. Shige et al. (2017) and Hunt et al. (2021) showed that the offshore-onshore oscillation of rainfall over the Indian west coast is associated with large-scale forcing from the Boreal Summer Intraseasonal Oscillation (BSISO) phases.

Current operational numerical weather models still have issues in realistically simulating rainfall over this coastal hilly region. A 10-day weather forecasting exercise in support of the INCOMPASS field campaign showed that the operational Met Office Unified Model (MetUM) at a horizontal resolution of N768 (17 km) with a convection scheme, as well as its limited-area model (LAM) version at 4.4 km using explicit convection, overestimate the onshore rainfall and underestimate the offshore rainfall over the west coast (figure 10 in Martin et al. (2020)); this could be a direct consequence of poor representation of the offshore-onshore rainfall modes. Mohandas et al. (2020) reported that medium-range forecasts from the global National Centre for Medium-Range Weather Forecasting (NCMRWF) Unified Model (NCUM), a version of MetUM, simulate the observed

circulation patterns over the west coast but do not get the rainfall distribution right. Rajendran et al. (2012) argues that capturing the convective-regional-global scale interaction is necessary in order to simulate the observed long-term rainfall trends over this region in the models. Thus, a realistic simulation of offshore-onshore rainfall modes over the west coast and their relationship with large-scale weather systems is imperative for regional and global models in order to produce useful short-term and long-term forecasts of rainfall.

Smith et al. (2015) show that the MetUM simulates the observed rainfall intensity over the hills on the west coast of the UK at 1.5 km resolution; rainfall intensity reduces when the resolution is decreased. They suggest that the sensitivity of the orographic rainfall to the horizontal grid spacing is different for different mountain ranges and it is mainly governed by the geometry of the orographic features. In general, the horizontal grid spacing that is adequate to faithfully represent the effects of orography on simulated rainfall appears to be a few to 10 km (see Smith et al. (2015) and references therein). Some of the latest operational numerical weather prediction (NWP) models employ grid spacing of O($\sim$ 1 km). The fundamental assumption in the convective parameterization is that the convective cells are much smaller than the model grid box and remain unresolved. At O($\sim$ 1 km) resolution, convective cells are partially resolved. Thus, the usage of a convective parameterization scheme at this resolution is questionable as individual convective cells can occupy more than one grid box. This scale is generally referred to as the 'grey zone' of convective parameterization (Gerard et al., 2009; Kirshbaum, 2020). Peatman et al. (2014) showed that the models which rely on convective parameterization fail to simulate the observed interaction between convection and sea breeze over the islands of the Maritime Continent. High-resolution convection-permitting simulations produced a much improved diurnal cycle of circulation and rainfall (Birch et al., 2015, 2016). Nevertheless, there are many studies where the usage of a convective parameterization scheme within and near the grey zone of convection has improved the overall model simulation of a meteorological event (e.g., Zheng et al. (2016); Mahoney (2016); Phadtare (2018)). This can be due to the prescribed CAPE consumption and entrainment-detrainment rates for shallow and deep convection in the scheme. Recently, convective schemes are being improved by including a scale-dependency in these factors (e.g. Zheng et al. (2016)).

The grid spacing of a few km, however, is inadequate to resolve the eddies within the planetary boundary layer (PBL). Thus, a PBL scheme is needed to represent the boundary layer processes (Wyngaard, 2004; Honnert, 2016; Kirshbaum, 2020). The boundary layer processes determine the orographic influence by controlling the near-surface stratification of the atmosphere. One of the key parameters controlling the orographic effects is the Froude Number (F) of the impinging flow:

$$F = \frac{U}{N H} \tag{1}$$

where U is the mean wind speed upstream of the orographic barrier, N is the mean Brunt-Väisälä frequency of the atmosphere, and H is the height of the orography (Sheppard, 1956; Smith, 1979; Kirshbaum et al., 2018). When F < 1, flow is blocked by the orographic barrier, whereas when F > 1, the flow has sufficient kinetic energy to overcome the orographic barrier and move to the lee side. Several idealized simulation experiments (Chu and Lin, 2000; Chen and Lin, 2005b,a; Jiang, 2003; Reeves and Lin, 2007; Miglietta and Rotunno, 2009) have shown that in the blocked case, precipitating systems remain upstream of the orography, and in the unblocked case, precipitation occurs over the orographic slopes (heavy) and the lee region (light to moderate). A recent study by Phadtare et al. (2022) showed that when the incident low-level flow over the west coast of India is classified according to F, the classification leads to the offshore-onshore rainfall pattern – the low F values are associated with the offshore mode, and high F values with the onshore mode. Further, they show that the offshore mode is characterised by strong land-sea breeze variations and greater control of the local diurnal cycle over the west coast rainfall. Conversely, the onshore mode has suppressed land-sea breeze and the rainfall has a weak diurnal cycle. Thus, the mechanisms by which the release of convective instability takes place in the two modes are different. Mechanical uplifting is dominant during the onshore mode, whereas during the offshore mode, it is mainly facilitated by daytime heating. Therefore, even though the majority of the literature suggests that

the offshore-onshore modes are caused by the large-scale variability of the atmosphere, the blocking/uplifting from the Western Ghats, as well as its thermal forcing, seem to play an important role. Thus, a pertinent question that needs to be answered is: are the representation of orographic effects and the diurnal cycle of rainfall in the present-day models adequate for simulating the offshore-onshore rainfall modes?

The purpose of this study is to understand the impacts of horizontal grid resolution and the presence of a convective parameterization scheme on the model simulation of the offshore-onshore rainfall modes over the west coast of India and understand the role of the Western Ghats in these modes. The INCOMPASS IOP is chosen as a case study. Section 2 of this article describes the datasets used and model setup, section 3 shows how model domains at different horizontal resolutions perform at simulating the observed offshore-onshore rainfall transition and the evolution of dynamics, section 4 presents the results of model sensitivity experiments relating to the convective parameterization and the presence of the Western Ghats. Section 5 presents the main conclusions and discussion on the future avenues for research.

2 | DATA AND MODEL SETUP

2.1 | IMERG rainfall

The Integrated Multi-satellitE Retrievals for GPM (IMERG) product, version 06B (Huffman et al., 2015), is used for describing the patterns of rainfall over the Indian west coast during the offshore-onshore modes. IMERG provides global surface rainfall on a 0.1° spatial grid at 30-minute intervals. The dataset is provided by the National Aeronautics and Space Administration (NASA). IMERG is produced by merging passive microwave and infrared rainfall estimates which are further calibrated with the rain gauges on a monthly basis. Satellite-based rainfall estimates over the west coast of India are known to have biases. The Tropical Rainfall Measuring Mission (TRMM) 3B42 product gives the maximum rainfall off the coast instead of the Western Ghats slopes. This is because the coastal clouds are deeper than those over the Western Ghats (Shrestha et al., 2015; Kumar and Bhat, 2017), and hence the infrared rainfall estimates undervalue the orographic rainfall. The latest IMERG product places the maximum rainfall correctly over the Western Ghats slopes (e.g., Prakash and Srinivasan (2021); Phadtare et al. (2022)), but still underestimates the intensity of heavy rainfall episodes (> 25 mm h^{-1}) compared to the rain gauges (Murali Krishna et al., 2017). Rojas et al. (2021) concluded that IMERG underestimated the overall rainfall over the mountainous region of Chile by 16% and warm rain events by 50%. Thus, it is possible that the IMERG underestimates the actual rainfall over the orography of the Western Ghats by about 16-50%.

2.2 | Rain gauges

To validate the IMERG rainfall, we have used rainfall data from the rain gauge network of the India Meteorological Department (IMD). The network comprises automatic weather stations (AWS) and automatic rain gauges (ARG) (Saha et al., 2021). These automatic stations use tipping-bucket rain gauges. The dataset was obtained from IMD in support of the Indo-UK joint INCOMPASS project. A total of 44 rain gauges were selected along the west coast. Rain gauges with more than 10% missing data were excluded from the analysis.

2.3 | Radiosondes

We use the upper-air radiosonde observations from Mangalore (74.83°E, 12.95°N and 31 m elevation) and Amini Divi (72.73°E, 11.12°N and 4 m elevation) stations in order to evaluate the model simulation for the near-surface stratification and winds. This data was obtained from the Atmospheric Soundings web portal of the University of Wyoming (`weather.uwyo.edu/upperair/`

sounding.html). Mangalore is located over the west coast, whereas Amini Divi is an island in the Arabian Sea. Radiosonde observations are ideal for determining the near-surface stratification as they provide high-resolution in situ observations. The near-surface atmospheric stratification directly influences the orographic blocking as well as the sub-grid orographic drag parameterization (Stensrud, 2009).

2.4 | Reanalysis

The fifth-generation European Centre for Medium-Range Weather Forecasts Reanalysis (ERA5) dataset is used for evaluating the model simulated large-scale fields. ERA5 is available at hourly intervals on a 0.25° horizontal grid and 137 vertical levels starting from the surface and up to a height of 80 km (Hersbach et al., 2018).

2.5 | WRF model

The Advanced Research version of the Weather Research and Forecasting (WRF 4.1.3) model (Skamarock et al., 2008) is used to simulate the INCOMPASS IOP. Three one-way nested grids, all centred over the Indian west coast, were employed for the simulations (Fig. 1). The outermost grid will be referred to as D12, the intermediate as D4, and the innermost as D1 as the grid spacings of these domains are 12, 4, and 1.33 km, respectively. D12 is large enough to include the entire Arabian Sea to the west, the Bay of Bengal to the east and the Himalayas to the north. D1 is large enough to include the entire Western Ghats over the Indian peninsula and the mesoscale systems over the offshore region of the Arabian Sea. The physics schemes recommended in the tropical suite of the WRF model are used. The modified Tiedtke convective parameterization scheme (Tiedtke, 1989; Zhang et al., 2011) is used only in D12. This scheme accounts for deep, middle, and shallow convection. The domains D4 and D1 allow convection to develop explicitly. More details on the grids used and other physics schemes are given in Table 1. 35 vertical eta levels are used with a lid at 50 hPa; the lowest level is at 20 m elevation above the surface and there are 10 levels below 1500 m. Note that one-way nesting was used here in order to understand the differences in the simulation of each domain. In two-way nesting, the inner/finer domain gets the boundary conditions from the outer/coarser domain, and the output of the inner domain is fed back to the outer grid to improve the overall simulation; in one-way nesting, only the former part is true. The initial and lateral boundary conditions to D12 are taken from ERA5.

Each mode of the offshore-onshore rainfall oscillation can last for about 4-7 days (Fletcher et al., 2020; Hunt et al., 2021). Thus, in order to allow sufficient time for such variability to develop in the model simulation, we start the simulation at 0000 UTC 13 June 2016 and end it on 0000 UTC 28 June 2016; only the simulation between 0000 UTC 20 June - 0000 UTC 28 June, a period which coincides with the INCOMPASS IOP, is analyzed.

3 | CONTROL SIMULATION

The purpose of the control simulation is to simulate the event as realistically as possible using actual topographical and meteorological conditions as input. Model biases in the simulated rainfall and other meteorological parameters are identified for all domains in this run. The sensitivity simulations described in section 4 will be compared with the control run in order to understand the effect of the modified topography and convection representation in the model.

Domains	D12	D4	D1
Grid cells	356×348	649×601	889×985
Grid spacing	12 km	4 km	1.33 km
Boundary conditions	ERA5	D12	D4
Convection	New Tiedke (Tiedtke, 1989; Zhang et al., 2011)	-	-
Microphysics	WRF Single-moment 6-class (Hong and Lim, 2006)		
Planetary boundary layer	Yonsei University (Hong et al., 2006)		
Surface layer	MM5 (Zhang and Anthes, 1982)		
Land surface	Noah (Chen and Dudhia, 2001)		
Radiation	RRTMG (Iacono et al., 2008)		

TABLE 1 Details of the WRF domains shown in Figure 1 and the physics schemes used.

3.1 | Rainfall

First, we identify the offshore and onshore modes of rainfall, if they exist, in different domains of the model. The model evaluation can then be done on the basis of the time periods of these modes, and the overall distribution and the diurnal cycle of rainfall in each mode.

3.1.1 | Offshore and onshore modes

Figure 2 shows Hovmöller diagrams of 12-14°N mean rainfall during 20-27 June from the IMERG rainfall product and the three WRF domains. The latitudinal band of 12-14°N is chosen as this was the region where the INCOMPASS IOP was conducted and the transition of rainfall from offshore-to-onshore region was seen (Fletcher et al., 2020). Rainfall occurs over the offshore region during 20-24 June ('Offshore' mode), and over the onshore region ('Onshore' mode) during 26-27 June; the offshore region gets little rainfall during the onshore mode (Fig. 2a). Domains D4 and D1 simulate the offshore and onshore modes of rainfall somewhat similar to the observed modes (Fig. 2c,d). Distinct offshore and onshore modes are not seen in domain D12, which employs a convection scheme (Fig. 2b). According to the IMERG observations, the offshore mode is characterized by rainfall episodes occurring in the early morning hours over the sea, and the onshore mode by a stationary system over the coast and the Western Ghats. Domains D4 and D1 qualitatively simulate these characteristics of offshore and onshore modes. However, note that during the offshore mode, the intensity of rainfall over the coast in these domains is much greater than observed.

3.1.2 | Mean rainfall

In IMERG, two prominent offshore rainfall zones are seen during the offshore mode, a northwest-southeast oriented rain band over the Arabian Sea and an off-the-coast rain band (Figure 3). Heavy rainfall (> 30 mm/day) is widespread over the sea while rainfall is mostly light over the coast. During the onshore mode, rainfall around Mangalore increases (>50 mm/day), with the slopes of the Western Ghats at 14°N receiving the heaviest rainfall (> 80 mm/day). Note that the onshore mode is seen only to the south of 15°N in this case. An Offshore rainband is seen north of 15°N. A clear land-sea contrast in rainfall is quite evident during both modes in the 12-14°N belt. In domain D12, rainfall is located along the coast during both modes. Domains D4 and D1 do get the offshore and onshore modes right to some extent. Although there is heavy rainfall over the sea during the

offshore mode in these domains, it is not located as far offshore as in the IMERG field. In addition, there is heavy rainfall (> 80 mm/day) over the coast during the offshore mode and the observed land-sea contrast in rainfall is missing in D4 and D1. During the onshore mode, heavy rainfall in domains D4 and D1 is mainly over the Western Ghats slopes. In these domains, the coastal region receives only light rainfall during this mode. In reality, a broad patch of heavy rainfall accumulation, extending from the Western Ghats slopes to the coastal zone, is seen in the IMERG field during the onshore mode. Thus, although the convection-permitting domains simulate the offshore and onshore rainfall during the respective modes, it is erroneously shifted eastwards, i.e., towards the orography. This discrepancy is further emphasized in the next figure.

Figure 4 shows rainfall anomalies in the WRF domains with respect to the IMERG rainfall. The rainfall fields in these domains are regridded to the IMERG resolution for ease of comparison. The anomalous rainfall intensity over the west coast during the offshore mode is between 50-100 mm day^{-1} which is far higher than the reported underestimation of orographic rainfall by the IMERG product (16-50%). During the onshore mode, D12 gravely underestimates the west coast rainfall. The D4 and D1 overestimate rainfall over the Western Ghats slopes by 50-100 mm day^{-1} at most places and slightly underestimate rainfall along the coast south of 15°N where the onshore mode is seen.

3.1.3 | Diurnal cycle

Phadtare et al. (2022) showed that the rainfall during the offshore regime is controlled by a strong diurnal cycle, whereas that during the onshore regime has a weak diurnal cycle. Therefore, here we analyze if the model can simulate the observed diurnal cycle of rainfall during the offshore mode. Figure 5 shows the diurnal variation of mean rainfall over a latitudinal band of 12-14°N during the offshore mode of this case study from IMERG and model simulations. Just off the coast, the IMERG rainfall increases in the early morning period of 0000-0300 UTC (0530-0830 IST), and during 0300-0600 UTC rainfall increases further offshore. The D4 and D1 domains simulate the near-coast heavy rainfall mode during 0000-0300 UTC correctly but miss the enhancement further offshore during 0300-0600 UTC. Notice that the early morning rainfall in IMERG stays strictly off the coast (Fig. 5a), whereas the simulated offshore rainfall in D4 and D1 intrudes over the land. These domains also simulate onshore rainfall maxima during 0600-1200 UTC. Onshore daytime rainfall is not seen at all in the IMERG dataset. Thus, anomalous morning, as well as daytime rainfall over land in D4 and D1, lead to anomalous rainfall over the coast during the offshore mode. In domain D12, offshore rainfall increases during 0000-0600 UTC but the intensity remains less than half of the observed intensity. Rainfall over the coast increases around 0400 UTC and remains high throughout the day.

To summarize, the west coast rainfall modes are entirely absent in D12; the rainfall is anchored along the coast almost all the time and offshore rainfall is very weak in this domain. The D4 and D1 domains do simulate the offshore-onshore modes, but they fail to capture the land-sea contrast and the diurnal cycle of rainfall along the coast during the offshore phase. Both domains produce daytime maximum rainfall over land which is not seen in the observations.

3.2 | Dynamics and thermodynamics

This section evaluates the model simulation for its dynamic (synoptic, mesoscale) and thermodynamic (humidity, convection) fields. In the process, explanations for the discrepancies in the simulated rainfall fields reported in section 3.1 are given.

3.2.1 | Large-scale dynamics

During the offshore mode, there was a northwest-southeast oriented trough over the region extending from the northern Arabian Sea to the southern Bay of Bengal. Note that the rainfall over the Arabian Sea occurs over the trough region with its limits being a ridge to the west and the Western Ghats to the east (Figures 2a, 3a). During the onshore mode, the trough over the Bay of

Bengal moved northeastwards and transformed into a well-developed cyclonic circulation. The western end over the northern Arabian Sea also intensified and developed into a closed cyclonic circulation. A ridge sits over the west coast during this mode which provides an unfavourable environment for the organised large-scale rainfall. However, the westerly jet is stronger during this mode and rainfall over the west coast mainly results from the orographic lifting (Phadtare et al., 2022). Note that the offshore mode is not the same as the break phase (Krishnan et al., 2000) of the summer monsoon. Organized rainbands are absent over the Indian region during the break phase, but they do appear over the eastern Arabian Sea during the offshore phase. However, the offshore-onshore mode oscillation is likely to happen during the break-to-active transition as organized rainbands propagate northward (Shige et al., 2017; Hunt et al., 2021). The model simulates the main features of the offshore and onshore modes correctly (Figure 6b,d), but overestimates the wind speed, especially downstream of the Western Ghats, i.e. over the Indian peninsula and the Bay of Bengal, during the onshore mode. This wind bias is also seen in the D4 and D1 domains (not shown).

The offshore rainfall not only cools the boundary layer over the sea, but the cold pools also present a substantial barrier to the low-level monsoonal flow. Figure 7 shows 950 hPa virtual potential temperature perturbation and winds during the simulated rainfall events in the offshore and onshore modes from domain D1. During the offshore event (Fig. 7a) the rainfall has a squall-line-like north-south organization. This system was propagating westward (Fig. 2d) and it leaves a trail of cold air behind it. The low-level monsoonal flow is obstructed by this cold pool, and the outflow itself is directed southward. As a consequence, the flow along the coast is cooler and has a northwesterly direction leading to suppression of rainfall over the coast. On the other hand, during the onshore mode (Fig. 7b), the flow is westerly and almost perpendicular to the Western Ghats. The air parcels reaching the coast during the onshore event are warmer than those during the offshore events by about 2-3 K. As a result, rainfall is enhanced over the Western Ghats. These simulated features of offshore and onshore rainfall events are in accordance with the observations of Fletcher et al. (2020). The onshore mode is also characterized by a drier mid-troposphere and moister lower-troposphere over the Arabian Sea (Fletcher et al., 2020; Hunt et al., 2021). The simulated humidity fields in the three domains are analyzed next.

3.2.2 | Mid-tropospheric humidity

Figure 8 shows the difference in the vertical cross-section of specific humidity averaged over the 12-14°N band during the onshore and offshore modes in the three model domains. All domains simulate a drier mid-troposphere and moister lower-troposphere during the onshore mode. The westerlies are also stronger during the onshore mode. However, note that in domain D12, the onshore winds do not strengthen and the Western Ghats slopes are drier during the onshore mode compared to the offshore mode. This is contrary to the observations of the case study (Fletcher et al., 2020) and this is the reason that the Western Ghats receive less rainfall during the onshore mode than the offshore mode in D12 (Figure 4). In domains D4 and D1, the low-level wind and moisture anomalies during the onshore mode are strongest over the west coast. This leads to rainfall enhancement over the Western Ghats slopes during the onshore mode.

3.2.3 | Convection

Figure 9 shows the vertical cross-sections of the temporal fraction for which the simulated radar reflectivity was at least 20 dBZ in any grid-box in the 12-14°N latitudinal band in the D4 and D1 model domains. The 20 dBZ threshold is typically used to identify precipitation features in a radar dataset, e.g., Xu and Rutledge (2015). In D12 domain, the convective rain is a subgrid entity produced by the convective parameterization scheme, and it is not reflected in the grid-resolved hydrometeor fields (Chen et al., 2021). Therefore, simulated radar reflectivity from domain D12 is not shown. In domains D4 and D1, there is a frequent widespread deep convection over the Arabian Sea and the west coast during the offshore mode. During the onshore mode, convection is less frequent and remains below 2.5 km altitude over the Arabian Sea. During this mode, deep convection is

confined to the coast. The simulated transformation in the deep convective activity in D4 and D1 is similar to that reported by Fletcher et al. (2020) and Hunt et al. (2021). The only difference is that the model domains simulate deep convection over the coast and orography even during the offshore mode, whereas in the observations it occurred only over the sea. This suggests that there is an anomalous supply of conditional instability to the coast during the offshore mode in D4 and D1. Notice that the dry air intrusion spans the entire region during the onshore mode and not just the offshore part (Fig. 8). Nevertheless, deep convection develops over the coast. This suggests that if the low-level supply of conditional instability and an uplifting mechanism (orography in this case) are present, deep convection can develop despite a dry mid-troposphere.

3.2.4 | Orographic blocking

The model simulates warmer and weakly stratified PBL over the coast during both modes compared to the radiosonde observations (Figure 10a,e). The nighttime temperature anomaly at the surface is around 4 K during the onshore mode. The anomaly reduces in the daytime to around 2 K. Thus, the model severely underestimates the nocturnal cooling of the surface and PBL. The zonal wind speed profiles from the radiosondes (Figure 10b,f) show a stronger monsoonal jet during the onshore mode than the offshore mode. The model captures this variation, however, it overestimates wind speed below 800 hPa at both times. The 0000 UTC equivalent potential temperatures (θ_e) are also higher (by 7-10 K) in the PBL, suggesting that the model transports more instability towards the Western Ghats during nighttime (Figure 10c). During the daytime, the PBL warms up; the simulated θ_e values are closer to the observations at 1200 UTC (Figure 10g). Due to the warmer temperatures, the relative humidity in the PBL is also lower in the simulation compared to the observations (Figures 10d,h). Profiles from the D12 and D4 domains also exhibit similar PBL biases over but they are not shown for the sake of brevity.

The radiosonde profile during the onshore mode shows a well-mixed PBL over the Arabian Sea, whereas the offshore mode has a stratified PBL (Figure 10i). The PBL stratification may be due to the evaporative cold pools produced by the rainfall. Since rainfall is absent over the offshore region during the onshore mode, the offshore PBL is well mixed. The model consistently produces a well-mixed PBL irrespective of the rainfall mode. It simulates the wind speed within the PBL correctly but overestimates the jet speed at 800 hPa by about 4-5 m s^{-1}.

As a result of the bias towards stronger wind and weaker PBL stratification, the orographic blocking is weak in the model. Figure 11a-c shows U, N, and F values, respectively, averaged over 50-1000 m altitude above the surface (refer to equation 1) from the 0000 and 1200 UTC Mangalore radiosondes and the corresponding values of these parameters from the hourly output of the WRF simulation. The simulated soundings are averaged over a 12 km horizontal box centred over the radiosonde location. The mean height of the Western Ghats within the 12-14°N band is considered for H, which is about 1000 m. The Western Ghats range is roughly oriented in the north-south direction, therefore the zonal wind speed is considered for U. The effect of saturation during the ascent on the stratification (N) is neglected. Note that ideally, F should be calculated away from the orography using the upstream undisturbed values of U and N. The blocking distance of the Western Ghats extends offshore by 150-300 km (Phadtare et al., 2022). Mangalore is well within the blocking region of the Western Ghats. Therefore, the flow at Mangalore is already decelerated due to the orographic blocking and the F calculated here will be an underestimation of the actual F values. On the other hand, in the precipitating environment, offshore stratification is weaker than coastal stratification due to the piling up of cold pools over the mountain slopes (Phadtare, 2018). This is evident in figures 10a,l during the onshore mode. Therefore, the F values calculated from the offshore sounding will be an overestimation of the actual F values. Amini Divi is an island station (Figure 1) located around 300 km offshore from the Western Ghats, i.e., away from its blocking distance. Figure 11d-f shows U, N, and F values, respectively, averaged over 50-1000 m altitude above the surface from the 0000 UTC Amini Divi radiosondes and the corresponding values of these parameters from the hourly output of the WRF simulation; the 1200 UTC radiosondes were not released from Amini Divi during this period.

Given these limitations in estimating the true F of the flow impinging on the Western Ghats, we avoid the terms 'blocked' or

'unblocked' in describing its regime. Instead, phrases like 'weakly blocked'/'strongly blocked' are used. The main aim of this exercise is to show the difference in the observed and simulated flow blocking. The model overestimates U and underestimates N most of the time at the coast, and hence, overestimates F of the flow implying weaker orographic blocking. According to the Mangalore (Amini Divi) radiosonde observations, the F values at 000 UTC hover around 0.5 (1) during the offshore mode. After 26 June, F values are higher and stay between 0.7-1 (2-5) at Mangalore (Amini Divi). The true F of the flow may lie between the F values calculated from the Mangalore and Amini Divi soundings. In D4 and D1 domains, F values are 2-3 times higher than the observed values at Mangalore. During the offshore mode, the simulated F values greater than 1 (2) are consistently seen at Mangalore (Amini Divi). This suggests that the onshore flow in the model is weakly blocked, instead of strongly blocked as suggested by the radiosondes.

In summary, stronger winds, weaker PBL stratification, and hence weakly blocked onshore flow lead to enhanced orographic lifting in the model. Stronger and warmer onshore flow also allows a greater supply of instability towards the orographic slopes. Therefore, the model tends to simulate stronger convection (Fig. 9) and higher rainfall (Fig. 3, 4) over the slopes of the Western Ghats, even during the offshore mode.

4 | SENSITIVITY EXPERIMENTS

This section investigates the sensitivity of the simulated west coast rainfall modes to the orographic influence and mesoscale convective processes in the model. Section 3.2.4 showed that the orographic blocking is weak in the model compared to the observations. Despite this, domains D4 and D1 simulated the offshore and onshore modes of rainfall somewhat satisfactorily. This hints that the west coast rainfall modes may not be as sensitive to the presence of the Western Ghats as previously assumed and are entirely driven by the large-scale variability, e.g., BSISO, as suggested by previous studies (Shige et al., 2017; Fletcher et al., 2020; Hunt et al., 2021). We explicitly show the influence of orography on the rainfall modes by performing a 'No orography' simulation (henceforth referred to as the *NoOrog* experiment) in which the Western Ghats are flattened entirely (Figure 1b). Note that the orography is flattened in all domains. Zhang and Smith (2018) performed a similar experiment in the WRF model and concluded that the offshore rainfall along the west coast was not caused by the orographic blocking from the Western Ghats. However, their focus was on the 'wet period' in which rainfall occurred onshore as well as offshore. Here, we focus on the offshore-onshore modes and the transition.

Zhang and Smith (2018) and Fletcher et al. (2020) emphasized the importance of offshore deep convection in suppressing rainfall over the west coast by cooling and drying the boundary layer. Domain D12 does not simulate the offshore heavy rainfall events probably due to the convective parameterization scheme. In the second experiment, we rerun the control simulation by turning off the convective parameterization scheme in D12 (henceforth referred to as the *NoCu* experiment). The aim of the second experiment is to check if explicit convection at 12-km horizontal grid spacing gives heavy rainfall and consequently, allows the west coast rainfall modes, and so whether the key difference between D12 and D4/D1 is the convective parameterization scheme rather than the resolution.

4.1 | Orography

Figures 12a-c show Hovmöller diagrams of 12-14°N averaged rainfall in the three domains for the *NoOrog* experiment. Note that the convective parameterization scheme in D12 is active in this experiment. Figures 12b,c show that the offshore rainfall mode is simulated in domains D4 and D1 even without the Western Ghats. The onshore rainfall is weak over the coast throughout the simulation. This is due to the absence of orographic uplifting. The offshore rainbands are practically unaffected by the removal of orography. Removal of the Western Ghats did not affect the diurnal cycle of rainfall either along the coast or in the offshore

region; we see early morning rainfall events in the *NoOrog* simulation quite similar to those when the orography was present (Fig. 2). This suggests that the land-sea contrast, more than the orography, affects the diurnal cycle of rainfall along the coast.

Figure 13 shows 850 hPa mean winds and geopotential field during the offshore and onshore modes for the *NoOrog* simulation. The evolution of large-scale fields is somewhat similar to the control run. During the offshore mode, a trough is present over the peninsula and the Arabian Sea, and during the onshore mode, an LPS has developed north of the Western Ghats. The winds are north-westerlies during the offshore mode, and during the onshore mode, they are stronger and westerly. Thus, the offshore and onshore modes of rainfall are linked to the evolution of the large-scale fields (as proposed by Shige et al. (2017); Fletcher et al. (2020); Hunt et al. (2021)). The Western Ghats merely modulate the intensity of rainfall over the coast through different orographic blocking regimes of the low-level flow which can be identified by classifying the onshore flow according to its Froude number as shown by Phadtare et al. (2022).

4.2 | Convective parameterization

In the *NoCu* experiment, the event was simulated employing only D12 but with explicit convection. Figure 12d shows a Hovmöller diagram of 12-14°N averaged rainfall for the *NoCu* experiment. It shows rainbands starting from the rain shadow region and propagating westwards over the Arabian Sea during 20-24 June. The intensity, as well as the organization of these rainfall episodes, seem abnormally high when compared with observations. This is an outcome of anomalously strong convection, possibly due to inadequate entrainment of dry air by the turbulent eddies into the convective core at 12 km horizontal grid spacing (Tang and Kirshbaum, 2020; Kirshbaum, 2020). The two modes seen in this experiment can be characterized as 'offshore propagation' and 'onshore propagation'. Offshore propagation of rainfall appears as one of the features of the offshore mode as it was seen in the other simulations (control and *NoOrog*) as well. Observations from IMERG suggest that a mixture of stationary and offshore-propagating rainfall episodes are present during the offshore mode. A trough present over the Indian peninsula and the Arabian Sea during the offshore mode might be promoting the westward propagation of rainfall. A similar phenomenon over the Indian region was noted by Phadtare and Bhat (2019) where deep clouds predominantly formed in the western flank of the trough and moved further westward.

In the *NoCu* experiment, the processes that suppress convection over the rain shadow region during the offshore mode are too weak or absent. Thus, convection gets triggered over the land during daytime due to the presence of the trough and moves westward with time. It arrives over the Arabian Sea during late-night to morning hours and further propagates offshore. On 25 June, there is a sudden change in the regime of rainfall formation and propagation. Hereafter, the storms form just off the coast and propagate onshore. The eastern limit of this propagation is set by the Western Ghats peak. Propagation of mesoscale systems depends on features such as downdrafts, cold pools, and gravity bores (Bukovsky et al., 2006), which are associated with heavily precipitating convective cores, or it can be a simple advection by the background flow. The former mechanism seems more likely during the offshore mode when the systems propagate upwind, while the latter is likely important during the onshore mode. It appears that as the explicit representation of convection simulates high-intensity rainfall, the aforementioned processes are stronger, which results in long-lasting (but constrained by the diurnal cycle) propagating mesoscale systems. With the convective scheme, rainfall intensities are weak and propagating systems are absent.

5 | CONCLUSIONS AND DISCUSSION

Simulations of the summer monsoon rainfall modes over the west coast of India were performed using the WRF model in order to understand the underlying mechanism driving these modes and the impacts of model resolution and the representation of convection on their simulation. It is concluded that the offshore and onshore rainfall modes are largely a consequence of

the large-scale atmospheric variability over this region. A schematic in Figure 14 summarizes the meteorological conditions controlling these rainfall modes. During the offshore mode, a trough extended over the Arabian Sea from the peninsula. It provided favourable conditions for offshore convection. As noted by Fletcher et al. (2020) in their observations, the low-level winds during this mode were weak. Shige et al. (2017) and Hunt et al. (2021) reported a positive vorticity anomaly over the offshore region during the offshore mode which is also a consequence of the trough. During the onshore mode, a ridge moved over the west coast and offshore region, which suppressed the large-scale convective activity over the offshore region. However, the low-level westerly winds were strong, resulting in the direct orographic uplift of winds and hence, heavy rainfall over the Western Ghats and west coast region. The following conclusions were drawn from the model simulations of this phenomenon performed in this study:

- **Orographic blocking**: The WRF model domains at 4- and 1.33-km grid spacing with explicit convection were able to simulate the broad features of the west coast rainfall modes. However, the coastal boundary layer in the model was too warm (by about 4-5 °C) and weakly stratified. This reduced the orographic blocking of the flow leading to an overestimation of the convective instability over the coast. As a result, there was anomalous deep convection and rainfall over the Western Ghats in the model simulations.
- **Diurnal cycle**: None of the domains simulated the observed diurnal cycle of rainfall over the west coast during the offshore mode correctly. All domains produced a daytime rainfall maximum over land which was not seen in the observations.
- **Convection scheme**: The model domain at 12-km horizontal resolution with a convection scheme could simulate the large-scale fields of the offshore and onshore modes but failed at simulating the rainfall modes associated with them. Convection, as well as rainfall intensity, in this domain, was very weak. On the other hand, turning off the convection scheme at this resolution resulted in an unrealistic overestimation of the rainfall intensity even over the rainshadow region.
- **Western Ghats**: The no-orography sensitivity experiment showed that the Western Ghats do not independently drive the offshore-onshore modes. However, they act as a barrier along the coast, keeping the rainfall predominantly offshore during the offshore mode. The coastal rainfall in the onshore mode is greatly enhanced due to the orographic uplifting.

Although the accuracy of IMERG rainfall can be questioned over the Western Ghats region, Flynn et al. (2017) reported that simulated rainfall over the west coast and Western Ghats was much greater in model simulations compared to their rain gauge observations. Given the uncertainties involved in model simulations, doubts can be raised regarding the pertinence of the conclusions of this study. Nevertheless, the rainfall accumulations in the offshore and onshore modes reported by Martin et al. (2020) (see figure 6 in that paper) in the MetUM are similar to those reported by the present study in Figure 4. Overestimation of orographic rainfall in the MetUM and other models based on the MetUM (e.g., NCUM) is also common (Martin et al., 2020). This suggests that the model biases reported here stem from the physics parameterization rather than the simulation uncertainties. Although this bias was blamed on the inadequate representation of convection in the models (Flynn et al., 2017), the simulated rainfall pattern in the present study is reminiscent of the idealized modelling experiments in which the Froude number of the flow was increased beyond 1 (Chu and Lin, 2000; Chen and Lin, 2005b,a; Jiang, 2003; Reeves and Lin, 2007; Miglietta and Rotunno, 2009). Our study points out that the underestimation of the orographic blocking by the model seems to be the primary cause behind it. The model does not adequately simulate the cold-air damming along the coast (Figs. 10 and 11), hence producing an anomalously warm and well-mixed PBL that weakens the orographic blocking by the Western Ghats. Although the model simulates the cold pools formed by the evaporation of rainfall (Fig. 7) and the temperature drop is also similar to that reported in observations by Fletcher et al. (2020) (figure 11b of that paper), the time scale for subsequent mixing and recovery of the PBL should be compared with the real world observations. In situ, high-resolution measurements on- and offshore are needed for this purpose.

Apart from the PBL scheme, the factors that can affect the structure of simulated PBL are the elevation of the lowest model

level and the number of levels within PBL. The lowest level in our simulations was at 20 m above the surface and there were 10 levels below 1500 m. Systematic model experiments can be performed to understand the sensitivity of these factors on the simulated PBL stratification. An underestimation low-level stratification can also result in reduced orographic drag in the upper atmosphere via weakened upward-propagating gravity waves (Wallace et al., 1983; Boer et al., 1984; Palmer et al., 1986; Bacmeister, 1993; Fritts and Alexander, 2003; Teixeira, 2014). This can have several consequences on the simulation of the Indian monsoon, including anomalously strong winds (Figure 6), stronger ventilation of the Indian peninsula by stronger winds, and hence, a weakened monsoon trough. Thus, in addition to the efforts of improving the representation of clouds and convection, land-atmosphere interaction, and aerosol effects, modelling of boundary layer processes and upscale propagation of orographic effects also needs attention in order to improve model simulations of the Indian monsoon.

REFERENCES

Bacmeister, J. T. (1993) Mountain-wave drag in the stratosphere and mesosphere inferred from observed winds and a simple mountain-wave parameterization scheme. *Journal of Atmospheric Sciences*, **50**, 377–399.

Birch, C., Webster, S., Peatman, S., Parker, D., Matthews, A., Li, Y. and Hassim, M. (2016) Scale interactions between the MJO and the western Maritime Continent. *Journal of Climate*, **29**, 2471–2492.

Birch, C. E., Roberts, M. J., Garcia-Carreras, L., Ackerley, D., Reeder, M. J., Lock, A. P. and Schiemann, R. (2015) Sea-breeze dynamics and convection initiation: The influence of convective parameterization in weather and climate model biases. *Journal of Climate*, **28**, 8093–8108.

Boer, G., McFarlane, N., Laprise, R., Henderson, J. and Blanchet, J.-P. (1984) The Canadian Climate Centre spectral atmospheric general circulation model. *Atmosphere-Ocean*, **22**, 397–429.

Bukovsky, M. S., Kain, J. S. and Baldwin, M. E. (2006) Bowing convective systems in a popular operational model: Are they for real? *Weather and forecasting*, **21**, 307–324.

Chen, F. and Dudhia, J. (2001) Coupling an advanced land surface–hydrology model with the Penn State–NCAR MM5 modeling system. Part I: Model implementation and sensitivity. *Monthly weather review*, **129**, 569–585.

Chen, S.-H. and Lin, Y.-L. (2005a) Effects of moist Froude number and CAPE on a conditionally unstable flow over a mesoscale mountain ridge. *Journal of the Atmospheric Sciences*, **62**, 331–350.

— (2005b) Orographic effects on a conditionally unstable flow over an idealized three-dimensional mesoscale mountain. *Meteorology and Atmospheric Physics*, **88**, 1–21.

Chen, Y., Chen, J., Chen, D., Xu, Z., Sheng, J. and Chen, F. (2021) A simulated radar reflectivity calculation method in numerical weather prediction models. *Weather and Forecasting*, **36**, 341–359.

Chu, C.-M. and Lin, Y.-L. (2000) Effects of orography on the generation and propagation of mesoscale convective systems in a two-dimensional conditionally unstable flow. *Journal of the Atmospheric Sciences*, **57**, 3817–3837.

Fletcher, J. K., Parker, D. J., Turner, A. G., Menon, A., Martin, G. M., Birch, C. E., Mitra, A. K., Mrudula, G., Hunt, K. M., Taylor, C. M. et al. (2020) The dynamic and thermodynamic structure of the monsoon over southern India: New observations from the INCOMPASS IOP. *Quarterly Journal of the Royal Meteorological Society*, **146**, 2867–2890.

Flynn, W. J., Nesbitt, S. W., Anders, A. M. and Garg, P. (2017) Mesoscale precipitation characteristics near the Western Ghats during the Indian Summer Monsoon as simulated by a high-resolution regional model. *Quarterly Journal of the Royal Meteorological Society*, **143**, 3070–3084.

Francis, P. and Gadgil, S. (2006) Intense rainfall events over the west coast of India. *Meteorology and Atmospheric Physics*, **94**, 27–42.

Fritts, D. C. and Alexander, M. J. (2003) Gravity wave dynamics and effects in the middle atmosphere. *Reviews of Geophysics*, **41**.

Gerard, L., Piriou, J.-M., Brožková, R., Geleyn, J.-F. and Banciu, D. (2009) Cloud and precipitation parameterization in a meso-gamma-scale operational weather prediction model. *Monthly Weather Review*, **137**, 3960–3977.

Grossman, R. L. and Durran, D. R. (1984) Interaction of low-level flow with the Western Ghat mountains and offshore convection in the summer monsoon. *Monthly Weather Review*, **112**, 652–672.

Hersbach, H., Bell, B., Berrisford, P., Biavati, G., Horányi, A., Muñoz Sabater, J., Nicolas, J., Peubey, C., Radu, R., Rozum, I. et al. (2018) ERA5 hourly data on pressure levels from 1979 to present. *Copernicus Climate Change Service (C3S) Climate Data Store (CDS)*. (Accessed on 12 NOV 2022), 10.24381/cds.bd0915c6.

Hong, S.-Y. and Lim, J.-O. J. (2006) The WRF single-moment 6-class microphysics scheme (WSM6). *Asia-Pacific Journal of Atmospheric Sciences*, **42**, 129–151.

Hong, S.-Y., Noh, Y. and Dudhia, J. (2006) A new vertical diffusion package with an explicit treatment of entrainment processes. *Monthly Weather Review*, **134**, 2318–2341.

Honnert, R. (2016) Representation of the grey zone of turbulence in the atmospheric boundary layer. *Advances in Science and Research*, **13**, 63–67.

Huffman, G. J., Bolvin, D. T., Nelkin, E. J. and Tan, J. (2015) Integrated Multi-satellitE Retrievals for GPM (IMERG) technical documentation. *NASA/GSFC Code*, **612**, 2019.

Hunt, K. M. and Menon, A. (2020) The 2018 Kerala floods: A climate change perspective. *Climate Dynamics*, **54**, 2433–2446.

Hunt, K. M., Turner, A. G., Stein, T. H., Fletcher, J. K. and Schiemann, R. K. (2021) Modes of coastal precipitation over southwest India and their relationship with intraseasonal variability. *Quarterly Journal of the Royal Meteorological Society*, **147**, 181–201.

Iacono, M. J., Delamere, J. S., Mlawer, E. J., Shephard, M. W., Clough, S. A. and Collins, W. D. (2008) Radiative forcing by long-lived greenhouse gases: Calculations with the AER radiative transfer models. *Journal of Geophysical Research: Atmospheres*, **113**.

Jiang, Q. (2003) Moist dynamics and orographic precipitation. *Tellus A: Dynamic Meteorology and Oceanography*, **55**, 301–316.

Kirshbaum, D. J. (2020) Numerical simulations of orographic convection across multiple gray zones. *Journal of the Atmospheric Sciences*, **77**, 3301–3320.

Kirshbaum, D. J., Adler, B., Kalthoff, N., Barthlott, C. and Serafin, S. (2018) Moist orographic convection: Physical mechanisms and links to surface-exchange processes. *Atmosphere*, **9**, 80.

Krishnan, R., Zhang, C. and Sugi, M. (2000) Dynamics of breaks in the Indian summer monsoon. *Journal of the atmospheric sciences*, **57**, 1354–1372.

Kumar, A., Dudhia, J., Rotunno, R., Niyogi, D. and Mohanty, U. (2008) Analysis of the 26 July 2005 heavy rain event over Mumbai, India using the Weather Research and Forecasting (WRF) model. *Quarterly Journal of the Royal Meteorological Society*, **134**, 1897–1910.

Kumar, S. and Bhat, G. (2017) Vertical structure of orographic precipitating clouds observed over south Asia during summer monsoon season. *Journal of Earth System Science*, **126**, 1–12.

Mahoney, K. M. (2016) The representation of cumulus convection in high-resolution simulations of the 2013 Colorado Front Range flood. *Monthly Weather Review*, **144**, 4265–4278.

Martin, G. M., Brooks, M. E., Johnson, B., Milton, S. F., Webster, S., Jayakumar, A., Mitra, A. K., Rajan, D. and Hunt, K. M. (2020) Forecasting the monsoon on daily to seasonal time-scales in support of a field campaign. *Quarterly Journal of the Royal Meteorological Society*, **146**, 2906–2927.

Miglietta, M. M. and Rotunno, R. (2009) Numerical simulations of conditionally unstable flows over a mountain ridge. *Journal of the Atmospheric Sciences*, **66**, 1865–1885.

Mohandas, S., Francis, T., Singh, V., Jayakumar, A., George, J. P., Sandeep, A., Xavier, P. and Rajagopal, E. (2020) NWP perspective of the extreme precipitation and flood event in Kerala (India) during August 2018. *Dynamics of Atmospheres and Oceans*, **91**, 101158.

Murali Krishna, U., Das, S. K., Deshpande, S. M., Doiphode, S. and Pandithurai, G. (2017) The assessment of Global Precipitation Measurement estimates over the Indian subcontinent. *Earth and Space Science*, **4**, 540–553.

Palmer, T., Shutts, G. and Swinbank, R. (1986) Alleviation of a systematic westerly bias in general circulation and numerical weather prediction models through an orographic gravity wave drag parametrization. *Quarterly Journal of the Royal Meteorological Society*, **112**, 1001–1039.

Peatman, S. C., Matthews, A. J. and Stevens, D. P. (2014) Propagation of the Madden–Julian Oscillation through the Maritime Continent and scale interaction with the diurnal cycle of precipitation. *Quarterly Journal of the Royal Meteorological Society*, **140**, 814–825.

Phadtare, J. (2018) Role of Eastern Ghats orography and cold pool in an extreme rainfall event over Chennai on 1 December 2015. *Monthly Weather Review*, **146**, 943–965.

Phadtare, J. and Bhat, G. (2019) Characteristics of deep cloud systems under weak and strong synoptic forcing during the Indian summer monsoon season. *Monthly Weather Review*, **147**, 3741–3758.

Phadtare, J. A., Fletcher, J. K., Ross, A. N., Turner, A. G. and Schiemann, R. K. (2022) Froude number-based Rainfall Regimes over the Western Ghats Mountains of India. *Quarterly Journal of the Royal Meteorological Society*.

Prakash, S. and Srinivasan, J. (2021) A comprehensive evaluation of near-real-time and research products of IMERG precipitation over India for the southwest monsoon period. *Remote Sensing*, **13**, 3676.

Rajendran, K., Kitoh, A., Srinivasan, J., Mizuta, R. and Krishnan, R. (2012) Monsoon circulation interaction with Western Ghats orography under changing climate. *Theoretical and Applied Climatology*, **110**, 555–571.

Reeves, H. D. and Lin, Y.-L. (2007) The effects of a mountain on the propagation of a preexisting convective system for blocked and unblocked flow regimes. *Journal of the Atmospheric Sciences*, **64**, 2401–2421.

Rojas, Y., Minder, J. R., Campbell, L. S., Massmann, A. and Garreaud, R. (2021) Assessment of GPM IMERG satellite precipitation estimation and its dependence on microphysical rain regimes over the mountains of south-central Chile. *Atmospheric Research*, **253**, 105454.

Saha, U., Gupta, M. D. and Mitra, A. K. (2021) Monitoring the Quality of AWS/ARG Rainfall Observations over India during Monsoon Season. Available at `https://www.ncmrwf.gov.in/Reports-eng/Report_AWS_ARG_Feb_2021_Final_Upal_Saha_NCMRWF.pdf`.

Sheppard, P. (1956) Airflow over mountains. *Quarterly Journal of the Royal Meteorological Society*, **82**, 528–529.

Shige, S., Nakano, Y. and Yamamoto, M. K. (2017) Role of orography, diurnal cycle, and intraseasonal oscillation in summer monsoon rainfall over the Western Ghats and Myanmar Coast. *Journal of Climate*, **30**, 9365–9381.

Shrestha, D., Deshar, R. and Nakamura, K. (2015) Characteristics of summer precipitation around the Western Ghats and the Myanmar West Coast. *International Journal of Atmospheric Sciences*, **2015**.

Skamarock, W. C., Klemp, J. B., Dudhia, J., Gill, D. O., Barker, D. M., Wang, W. and Powers, J. G. (2008) A description of the advanced research WRF version 3. *Tech. rep.*, University Corporation for Atmospheric Research.

Smith, R. B. (1979) The influence of mountains on the atmosphere. In *Advances in Geophysics*, vol. 21, 87–230. Elsevier.

Smith, S., Vosper, S. and Field, P. (2015) Sensitivity of orographic precipitation enhancement to horizontal resolution in the operational Met Office Weather forecasts. *Meteorological Applications*, **22**, 14–24.

Stensrud, D. J. (2009) *Parameterization schemes: keys to understanding numerical weather prediction models*. Cambridge University Press.

Tang, S. L. and Kirshbaum, D. (2020) On the sensitivity of deep-convection initiation to horizontal grid resolution. *Quarterly Journal of the Royal Meteorological Society*, **146**, 1085–1105.

Teixeira, M. A. (2014) The physics of orographic gravity wave drag. *Frontiers in Physics*, **2**, 43.

Tiedtke, M. (1989) A comprehensive mass flux scheme for cumulus parameterization in large-scale models. *Monthly Weather Review*, **117**, 1779–1800.

Turner, A. G., Bhat, G., Martin, G., Parker, D. J., Taylor, C., Mitra, A. K., Tripathi, S. N., Milton, S., Rajagopal, E., Evans, J. G. et al. (2020) Interaction of convective organization with monsoon precipitation, atmosphere, surface and sea: The 2016 INCOMPASS field campaign in India. *Quarterly Journal of the Royal Meteorological Society*, **146**, 2828–2852.

Wallace, J. M., Tibaldi, S. and Simmons, A. J. (1983) Reduction of systematic forecast errors in the ECMWF model through the introduction of an envelope orography. *Quarterly Journal of the Royal Meteorological Society*, **109**, 683–717.

Wyngaard, J. C. (2004) Toward numerical modeling in the "Terra Incognita". *Journal of the Atmospheric Sciences*, **61**, 1816–1826.

Xu, W. and Rutledge, S. A. (2015) Morphology, intensity, and rainfall production of MJO convection: Observations from DYNAMO shipborne radar and TRMM. *Journal of the Atmospheric Sciences*, **72**, 623–640.

Zhang, C., Wang, Y. and Hamilton, K. (2011) Improved representation of boundary layer clouds over the southeast Pacific in ARW-WRF using a modified Tiedtke cumulus parameterization scheme. *Monthly Weather Review*, **139**, 3489–3513.

Zhang, D. and Anthes, R. A. (1982) A high-resolution model of the planetary boundary layer—Sensitivity tests and comparisons with SESAME-79 data. *Journal of Applied Meteorology (1962-1982)*, 1594–1609.

Zhang, G. and Smith, R. B. (2018) Numerical study of physical processes controlling summer precipitation over the Western Ghats region. *Journal of Climate*, **31**, 3099–3115.

Zheng, Y., Alapaty, K., Herwehe, J. A., Del Genio, A. D. and Niyogi, D. (2016) Improving high-resolution weather forecasts using the Weather Research and Forecasting (WRF) Model with an updated Kain–Fritsch scheme. *Monthly Weather Review*, **144**, 833–860.

6 | ACKNOWLEDGEMENTS

This work and its contributors (JAP, JKF, ANR, AGT, RKHS, HLB) were funded through the Weather and Climate Science for Service Partnership (WCSSP) India, a collaborative initiative between the Met Office, supported by the UK Government's Newton Fund, and the Indian Ministry of Earth Sciences (MoES). This work was undertaken on ARC4, part of the High Performance Computing facilities at the University of Leeds, UK. The ERA5 data was obtained via the Climate Data Store (CDS). JAP thanks Thorwald H.M. Stein and Kieran M.R. Hunt at the University of Reading and A. Jayakumar at the National Centre for Medium Range Weather Forecasting (NCMRWF) for their constructive comments on this study.

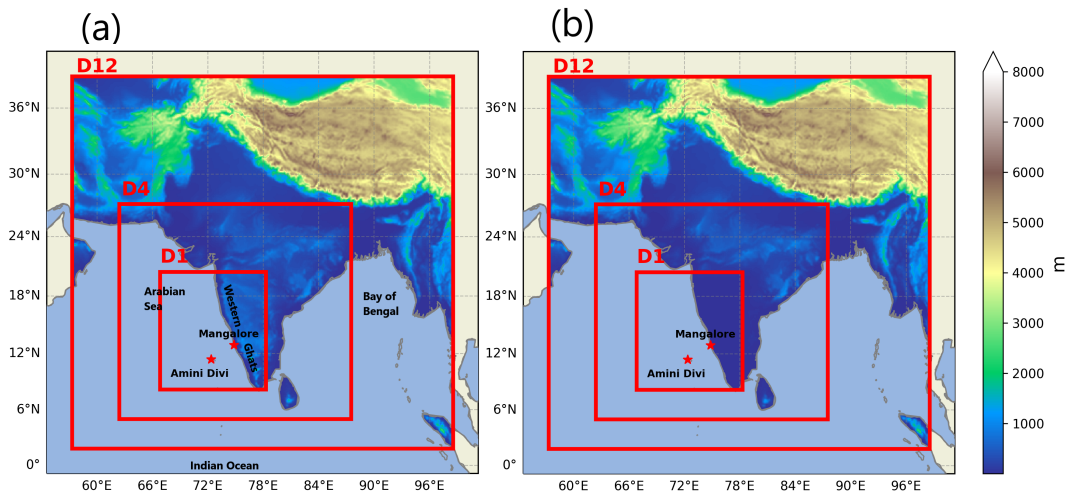

FIGURE 1 Model domains and orography for (a) Control run, and (b) *NoOrog* run described in section 4.1. Grid spacings: D12 - 12 km, D4 - 4 km, and D1 - 1.33 km.

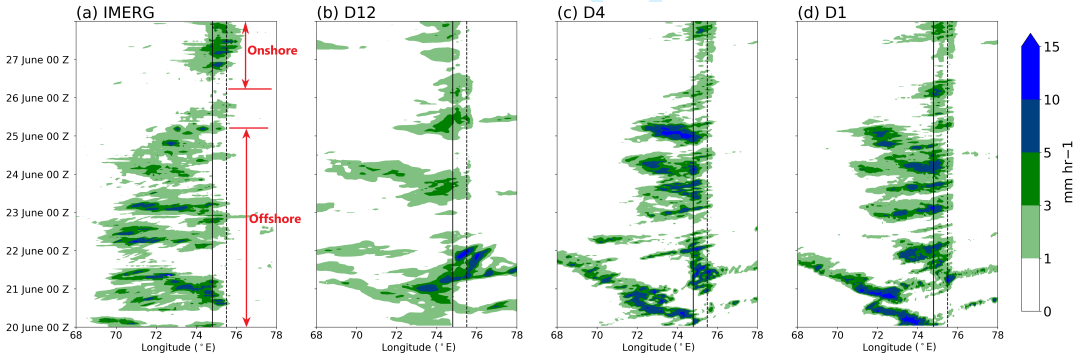

FIGURE 2 Hovmöller plot of 12-14°N averaged rainfall in (a) IMERG, (b) D12, (c) D4, and (d) D1 during 20-27 June 2016. The solid black line shows the mean longitude of the coast and the dotted line shows the mean longitude of the Western Ghats peak between 12-14°N.

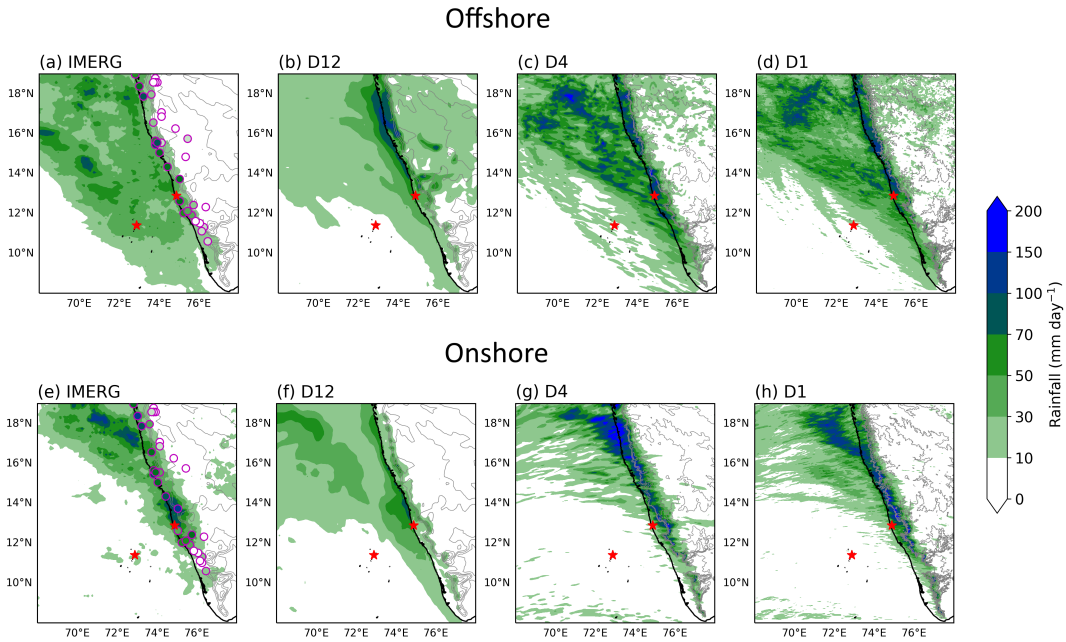

FIGURE 3 Mean rainfall during the offshore mode (20-24 June) in (a) IMERG, (b) D12, (c) D4, and (d) D1. (e)-(g) are the same as (a)-(d), respectively, but for the onshore mode (26-27 June). The stars show the locations of Mangalore (coast) and Amini Divi (island) stations. The circles along the west coast in (a) and (e) show the locations of rain gauges from which data is used and their face colours show the mean rainfall recorded by them during respective modes.

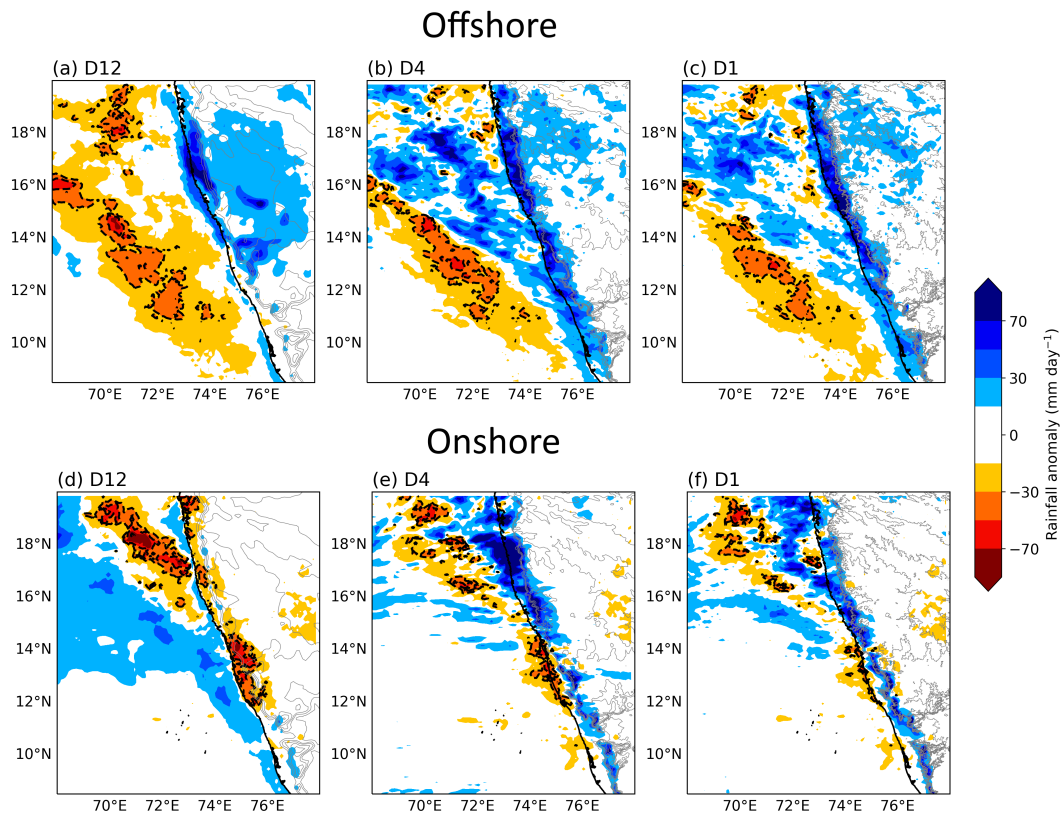

FIGURE 4 Rainfall anomaly in (a) D12, (b) D4, and (c) D1 with respect to the IMERG rainfall during the offshore mode. (d)-(f) Same as (a)-(c), respectively, but during the onshore mode.

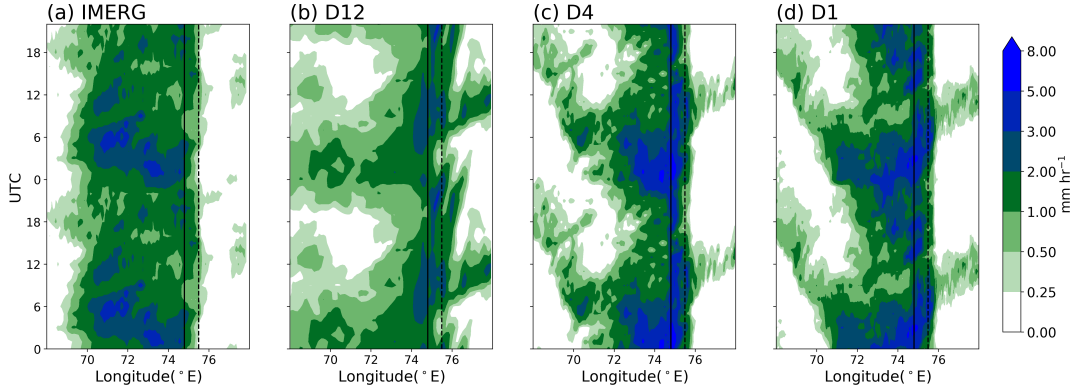

FIGURE 5 Diurnal variation of mean rainfall over 12-14°N band in (a) IMERG, (b) D12, (c) D4, and (d) D1 during the offshore mode.

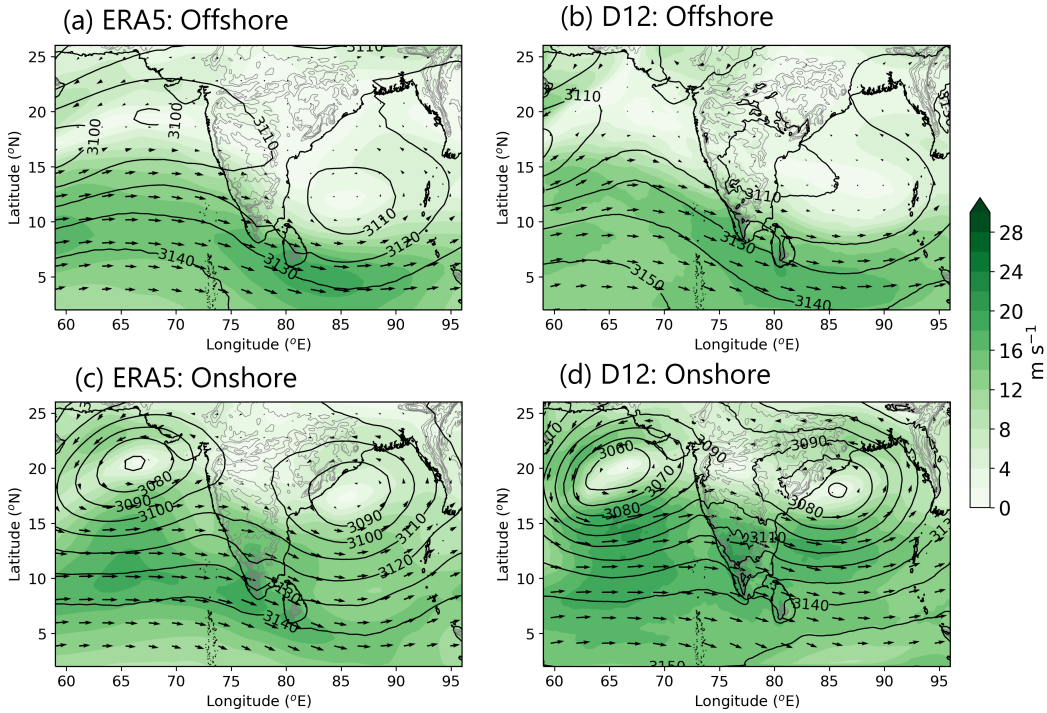

FIGURE 6 Mean 700 hPa geopotential height (m) contours and wind speed (shading) from (a) ERA5 and (b) D12 during the offshore mode. (c),(d) same as (a),(b) but for the onshore mode.

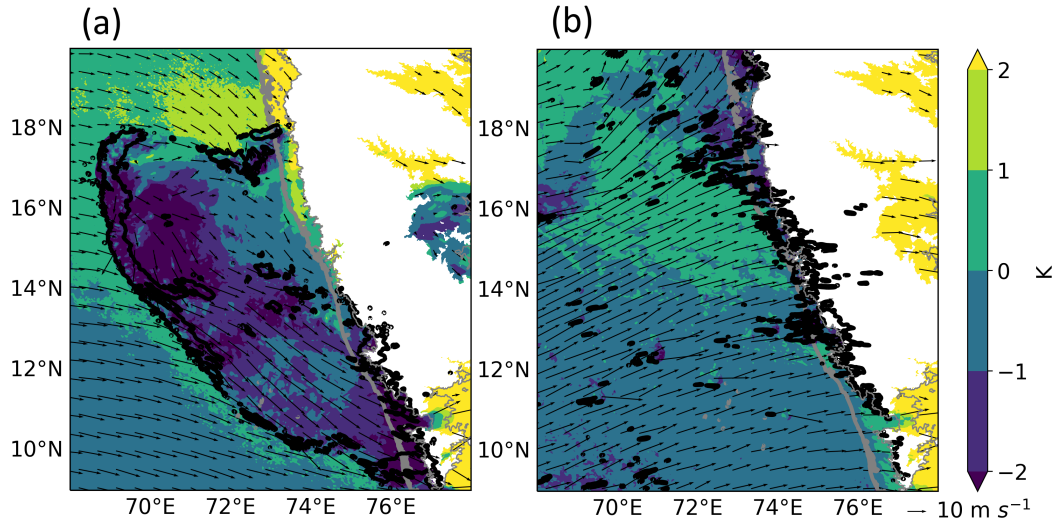

FIGURE 7 Virtual potential temperature perturbation (shading) and winds at 950 hPa in D1 at (a) 0500 UTC 20 June (offshore mode) and (b) 0500 UTC 27 June (onshore mode); The black contours delineate regions where rainfall ≥ 5 mm hr^{-1}.

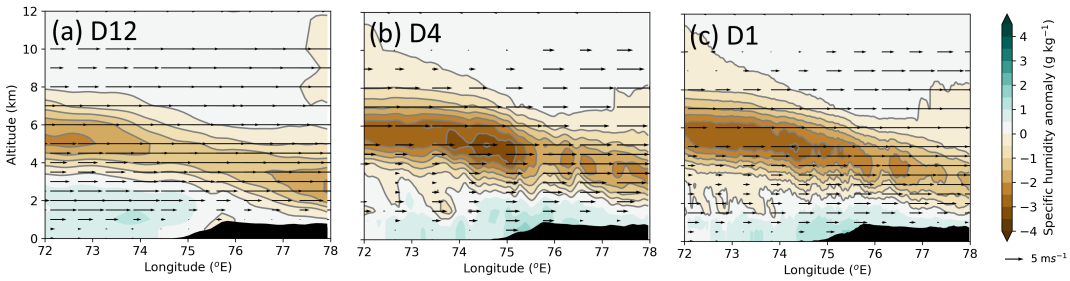

FIGURE 8 Difference between the mean zonal winds (vectors) and specific humidity (shading) over the 12-14°N band during the onshore and offshore modes (onshore-offshore) simulated by (a) D12, (b) D4 and (c) D1. The grey contours delineate negative anomalies of the specific humidity.

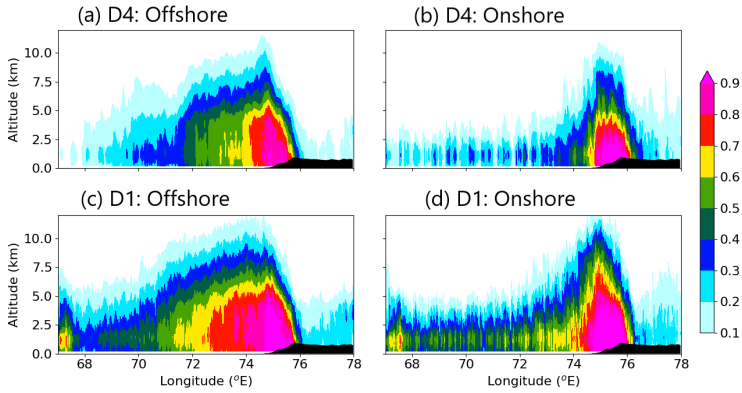

FIGURE 9 Temporal fraction for which the simulated radar reflectivity was ≥ 20 dBZ in at least one grid box in the 12-14°N band in D4 during the (a) offshore and (b) onshore modes. (c)-(d) are same as (a)-(b), respectively, but for the D1 domain.

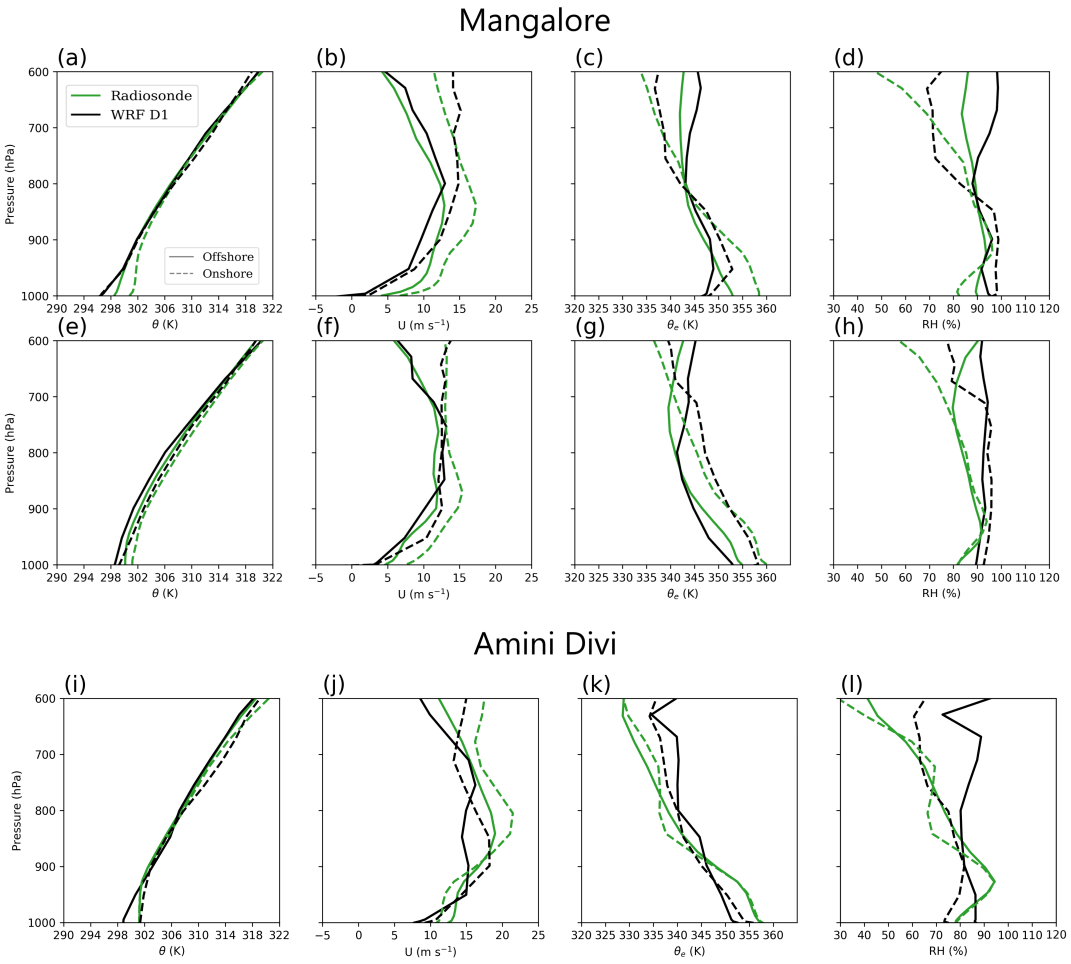

FIGURE 10 Mean vertical profiles of (a) Potential temperature (θ), (b) zonal winds (U), (c) equivalent potential temperature (θ_e), and (d) relative humidity during the offshore and onshore modes from the 0000 UTC Mangalore (a coastal station) radiosondes and the corresponding simulated soundings in D1. (e)-(h) are the same as (a)-(d) but for the 1200 UTC radiosondes. (i)-(l) are the same as (a)-(d) but for the 0000 UTC Amini Divi (an island station) radiosondes. The simulated profiles are averaged over a 12 km box centred over the sounding location.

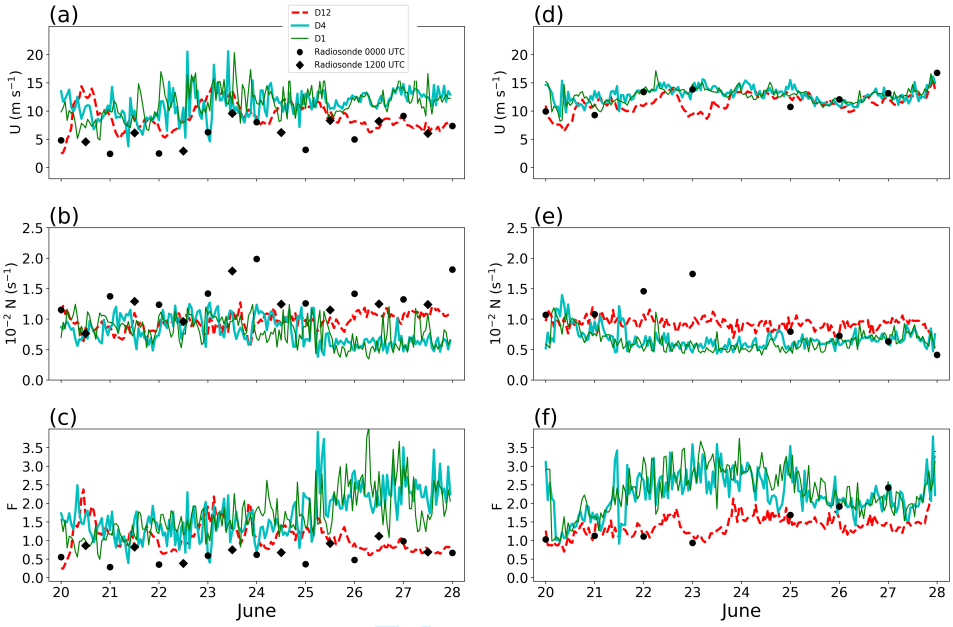

FIGURE 11 Mean values of (a) Zonal winds (*U*), (b) Brunt-Väisälä frequency (N), and (c) Froude number (F) over the 50-1000 m layer calculated from the 0000 and 1200 UTC Mangalore (a coastal station) radiosonde soundings and the hourly simulated soundings in the three WRF grids (D12, D4, and D1) over the same location as Mangalore. (d)-(f) are same as (a)-(c) but for the Amini Divi (an island station) radiosonde soundings.

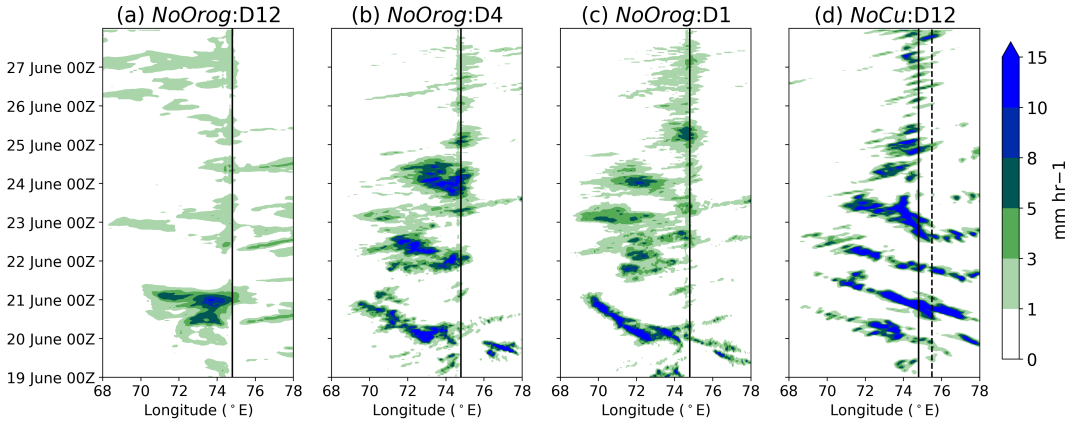

FIGURE 12 Hovmöller plot of 12-14°N averaged rainfall in (a) D12, (b) D4, and (c) D1 from the *NoOrog* simulation. (d) Same as (a) but for the *NoCu* simulation. The solid black line shows the mean longitude of the coast and the dotted line shows the mean longitude of the Western Ghats peak between 12-14°N.

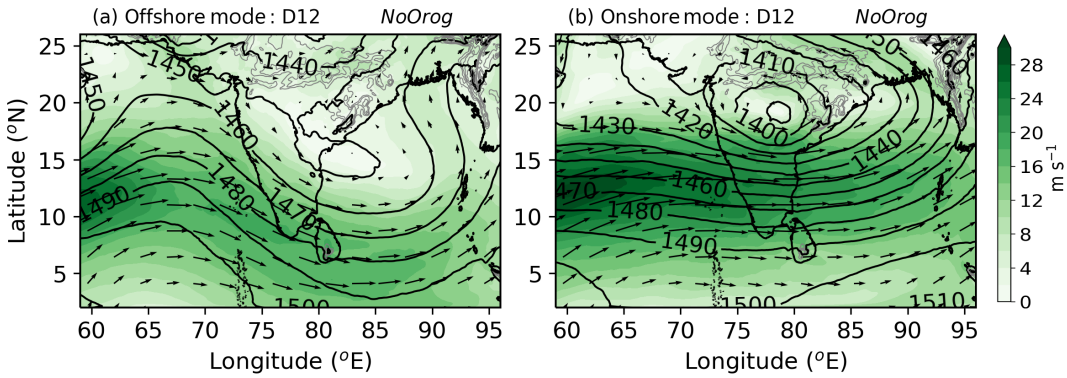

FIGURE 13 Mean 850 hPa geopotential height (m) contours and wind speed (shading) during the (a) offshore and (b) onshore modes in the D12 domain from the *NoOrog* simulation.

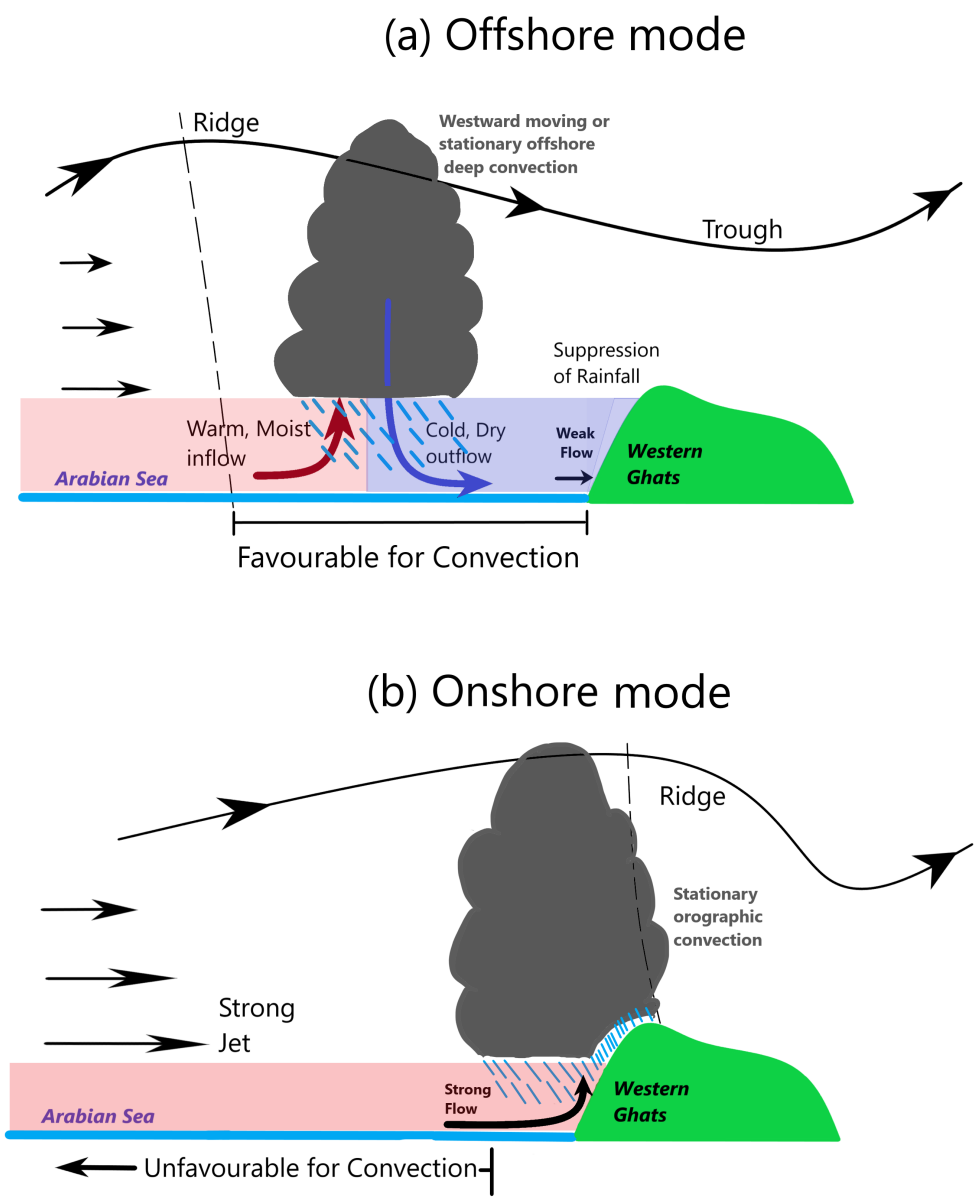

FIGURE 14 Schematics of the (a) offshore and (b) onshore rainfall modes over the west coast of India. An offshore trough facilities offshore convection and rainfall over the Arabian Sea. The cold and dry outflows from the offshore rainfall suppress rainfall over the Western Ghats. During onshore mode, a ridge over the coast suppresses offshore rainfall. Westerlies are stronger during this phase and enhanced rainfall over the coast and Western Ghats results from the orographic uplifting.

We sincerely thank all the reviewers for their critical review of this manuscript. We have tried to answer all the queries raised. The reviewer comments are in blue colour font and the reply in black. The revised text in the manuscript appears in red. The revised line numbers are mentioned in the reply.

Reviewer: 1

Overall this is an interesting piece of research in a region which is problematic for climate models. My main comments are (i) the lack of information on the IMERG product and possible errors over the mountains, along with the lack of any other observations (e.g. rain gauges), and (ii) how and where the Froude number is calculated. I give more detail in the comments below.

1. P4, L6-8: The Smith et al study concentrated on frontal rain over the UK. (i) The required resolution depends on the scale of the mountains in the simulation. (ii) Simulations of convection may need resolutions of a few hundred metres to properly represent convective circulations and rainfall. You could run a higher resolution simulation to see how similar it is to the 1.33km simulation.

This text in the Introduction section has been revised [Line no 65-69].

The 4- and 1.33-km simulations are quite similar. Thus, horizontal grid spacing of O(1km) is desired for realistically simulating the west coast rainfall regimes. However, both domains overestimate the orographic rainfall due to the stronger onshore winds and weaker stratification. The aim of choosing these resolutions was to see how the regional models perform at simulating the offshore-onshore modes. The results from the 1.33-km domain were not better than the 4-km domain. This suggests that the problem is with something else, e.g. PBL physics, rather than the horizontal resolution.

2. P4, L16-17: When used in this grey zone, convection schemes are often modified to do less.

The improvement in the simulation in some cases can be due to the prescribed rate of CAPE consumption as it prevents the build-up of unrealistic CAPE, or the prescribed entrainment-detrainment rates for shallow and deep convection. In 'scale-aware' schemes, these factors are made scale-dependent. This sentence is revised to include these points [Line no. 79-81].

3. P5, Section 2.1: More information should be given about the IMERG product. In particular, is this the version which is calibrated using rain gauges? As IMERG is used to verify the simulations, it is important to discuss its accuracy. Satellite precipitation observations, especially over mountains, are often inaccurate. For example, Rojas et al (2021) found that IMERG

underestimates orographic precipitation over orography, including the Andes and the smaller coastal mountains. These errors were as high as 50% (higher for warm rain events). It is important to mention this fact and to discuss the implications for verification of the simulations. Could this mean that the high-resolution simulations don't actually overdo orographic precipitation, at least as much as it first appears? Maybe produce another plot with IMERG orographic precipitation increased by 50% to get some idea of the difference this error would make? Rain gauge observations could be used over land, to get a better feeling for the satellite and simulation errors in this region. But again, you need to carefully consider possible observational errors and biases, such as due to their location with respect to maximum rainfall. Were there any INCOMPASS observations that could be useful, either here or elsewhere in the paper?

The IMERG V06B product is used. It is produced by merging passive microwave and infrared rainfall estimates and is further calibrated with the rain gauge data on a monthly basis.

A discussion on the accuracy of the IMERG is added in Section 2.1 [Line no. 115-124]. Murali Krishna et al., 2017 report that the IMERG underestimates heavy rainfall episodes (> 25 mm/h). Rojas et al. (2021) present observations from two field experiments: The Chilean Coastal Orographic Precipitation Experiment (CCOPE) and The Chilean Orographic and Mesoscale Precipitation Study (ChOMPS). During CCOPE, IMERG underestimated the total amount of rainfall by 50%, while during ChOMPS the underestimation was by 16%. ChOMPS was conducted over a much wider area compared to CCOPE and had far more observing stations (CCOPE had just 6!). Flynn et al. 2017 compared the WRF (at 5-km resolution) simulated rainfall with their rain-gauge network. They also concluded that the WRF overestimates rainfall over the west coast (see Figure R1).

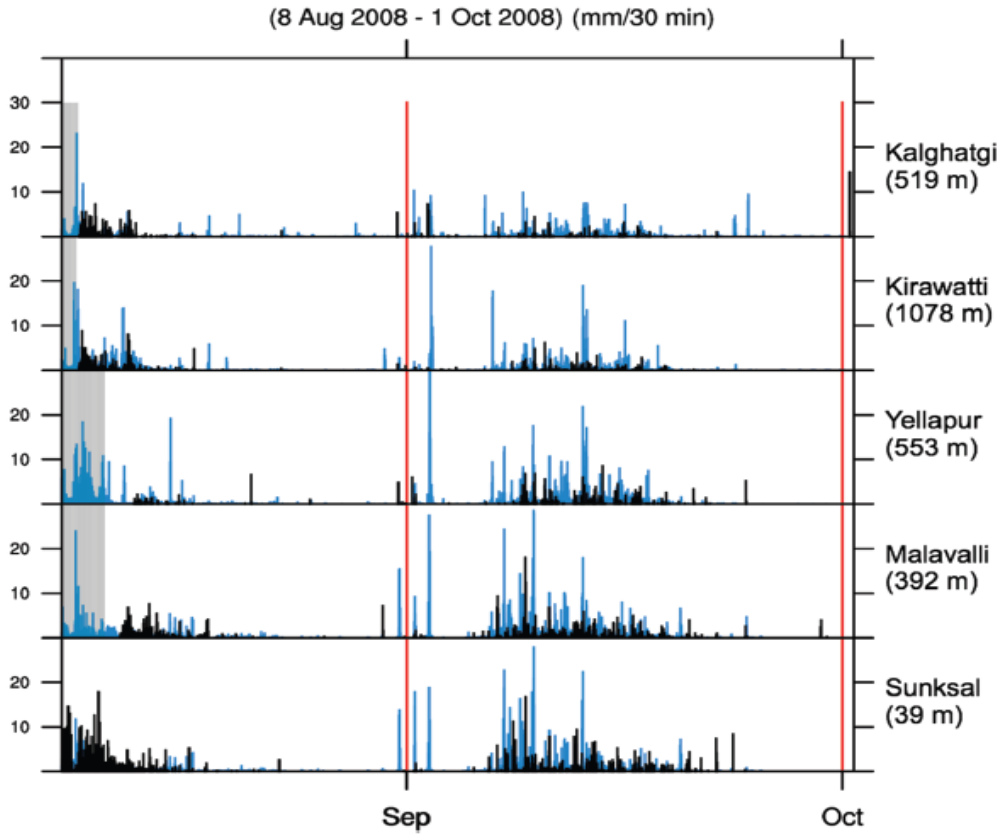

Figure R1. *Taken from Flynn et al. (2017) – 30-min rainfall rates at five gauge sites (black bars) and 30-min precipitation rates as simulated by WRF (blue bars), over the nearest and four adjoining model grid points.*

We have overlaid rainfall accumulations in the India Meteorological Department (IMD) station gauges over the IMERG plot in the revised Figure 3 of our manuscript. IMERG values of rainfall accumulation are comparable to the station rain gauges during the offshore and onshore phases. In the figure below, we have included a comparison between IMD's 0.25-degree gridded rainfall product and IMERG. The former is produced by averaging rain gauge values only. The values from rain gauges are also overlaid on IMERG. It shows that the IMERG somewhat underestimates the orographic rainfall where it rains very heavily. However, the rain gauge values are not as high as in the WRF simulation. Figure 4 in the revised manuscript gives the anomalous rainfall in the simulations compared to IMERG. The anomalous rainfall over the west coast in the model ranges between 50-100 mm/day. It is much higher than the underestimation of the actual rainfall by IMERG.

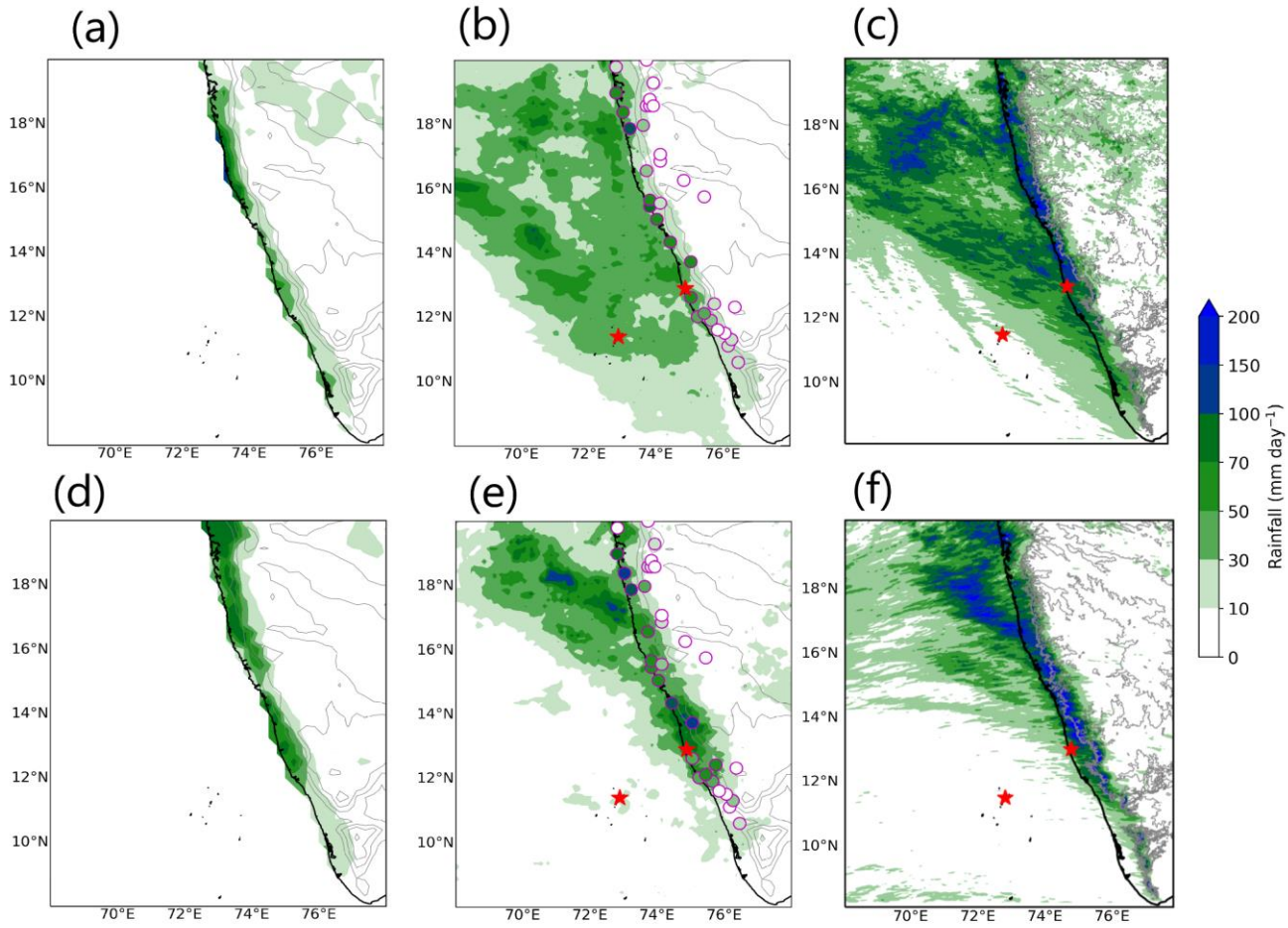

Figure R2. *Rainfall accumulation in (a) IMD 0.25-degree gridded rainfall product, (b) IMERG, and (c) WRF D1 during the offshore mode. (d)-(f) are the same as (a)-(c), respectively, but for the onshore phase. The rainfall accumulations in IMD's station rain gauges are shown in circles overlaid over (b) and (e).*

Note that the WRF also simulates higher instability and Froude number of the onshore flow along the coast compared to the radiosonde observations (Fig. 10 and 11 in the revised manuscript). This also suggests that the WRF might be overestimating the orographic rainfall.

4. P6, L41/42: the word "region" is missing.

Thank you. The word "region" has been added.

5. P6, L44/45 - I'm not sure that I agree that the off/onshore modes are completely missing from D12. It does look like D12 has more offshore rain before 24 June than after. Also, could the lack of onshore rain in D12 be at least partially due to insufficient resolution of the orography?

Yes, that's true. But this is light rain. Therefore, looking at Fig. 3, the accumulated rainfall patterns during offshore and onshore modes in D12 do not show clear offshore-onshore modes.

The convective parameterization was turned off in the *'NoCu'* experiment 12 km resolution. The D12 domain simulates coastal/onshore rainfall intensity in this simulation (Fig. R3). Therefore, the lack of rainfall in D12 when the convection is parameterized is mainly due to the convection scheme rather than the coarse resolution.

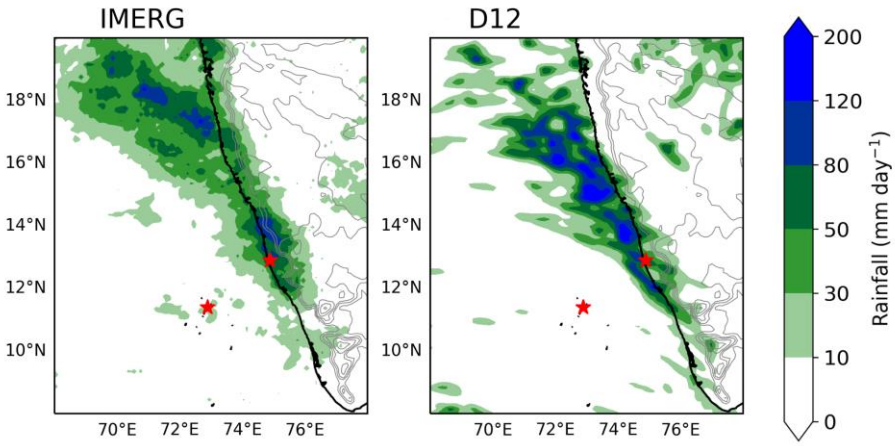

Figure R3. *Accumulation of rainfall in IMERG and D12 in the NoCu simulation during the onshore phase.*

6. P6, L46/47 - It looks like the precipitation over the sea during the offshore mode during the early morning is propagating westward.

Yes, the offshore mode is characterized by westward propagating as well as offshore stationary rainfall episodes. A discussion on this topic is included in Section 4.2. [Line no 368-378].

7. P6 L57/48 - P7 L1/2: the statement that the rain over the coast in D1/D4 simulations is much greater than observed needs rethinking in terms of IMERG accuracy problems over mountains (see previous comment).

It is true that IMERG underestimates relative to the IMD gauges, but the WRF model, as well as MetUM, overestimate rainfall over the west coast compared to the gauge measurements. This was addressed previously. Please refer to point 3. MetUM plots are shown in the reply to Reviewer 2, please refer to Point 1 and Figure R6.

8. P7, L25: drop the word "offshore" from "rainfall is suppressed over the offshore sea".

Thank you for pointing that out. The 'offshore' word has been removed.

9. P7, L45-46: Not sure that I agree that D4 and D1 rainfall remains strictly onshore during 0600-1200 UTC. I can see rain over the sea!

This line is modified to “These domains also simulate onshore rainfall maxima during 0600-1200 UTC.” [Line no 211-212].

P8, L21-22: I wouldn't say that the trough has vanished! It has advected eastwards.

The large-scale trough over the peninsula and the Bay of Bengal moved northeastwards. The low-level trough in the lee of Western Ghats exists in both modes due to the blocking of the mountains. Figure 6 is revised, and now 700 hPa fields are plotted instead of 850 hPa. The movement of the large-scale trough is more clear at 700 hPa as the orographic effects are reduced. The discussion in Section 3.2.1 is revised accordingly [Line no 224-229].

P8, L43-45: "...the onshore winds are weaker in domain D12 during the onshore mode". Do you mean weaker than in D4 and D1? And similarly for the following sentence.

The comparison is done between the two modes. These sentences are revised as follows: “However, note that in domain D12, the onshore winds do not strengthen, and the Western Ghats slopes are drier during the onshore mode compared to the offshore mode.” [Line no 252-253].

P9, Section 3.2.3 and Fig 9: how is the simulated radar reflectivity calculated? Does it include clouds and precipitation generated within the convection scheme?

Thank you for this query. The simulated radar reflectivity is obtained from the grid-resolved hydrometeor species. The wrf-python package is used for the post-processing of WRF output. The function call for the simulated radar reflectivity is of the following form: *wrf.dbz(pres, tkel, qv, qr, qs, qg).* Where ‘pres’ is pressure, ‘tkel’ temperature, ‘qv’ water vapor mixing ratio, ‘qr’ Rain mixing ratio, ‘qs’ Snow mixing ratio, and ‘qg’ Graupel mixing ratio.

According to the WRF manual, these variables do not include the hydrometeors from the convective rain produced by the convection scheme (Figure R4 below). This is the reason that the simulated radar reflectivity in the D12 domain is very weak. Therefore, Figure 9 is revised and radar reflectivity only from D4 and D1 domains is shown. The omission of radar reflectivity from the D12 domain is explained in Section 3.2.3. [Line no 261-263].

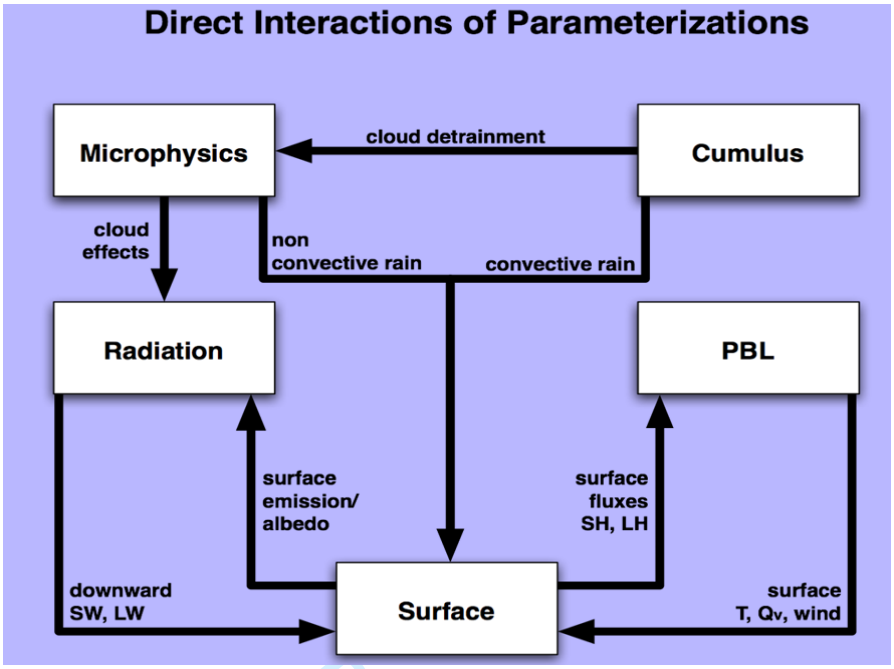

Figure R4. *Taken from 'Overview of WRF Physics'. Available at* https://homepages.see.leeds.ac.uk/~lecag/wiser/sample_wiser_files.dir/Physics_Dudhia.ppt.pdf

P9 L42 onwards (and Fig 11): how were U, N, and H calculated? For example, how is the mountain height defined (is it the max height or some average)? Is U the windspeed or the easterly flow component? Does N account for saturation during ascent, which will reduce the effective stability? The Froude number should be calculated using undisturbed values of U and N upstream of the mountain, but this is done at Mangalore on the coast, well within any blocked region. It would be better to use the upstream soundings for this purpose. Faster winds at Mangalore might be a result of reduced blocking, however.

'H' is the average height of the mountain between 12-14N. Since the Western Ghats range practically runs north-south, the zonal wind speed is assumed as 'U'. 'N' does not account for saturation during ascent.

It is true that the Froude number should be calculated using the undisturbed flow parameters. Ideally, away from orography at least by a distance given by the orographic radius of deformation, $R_d = NH/f$, where 'f' is the Coriolis parameter (Pierrehumbert and Wyman, 1985). For the Western Ghats, $R_d \sim 150–300$ km. However, in the precipitating atmosphere cold pool piles up against the mountain over a length scale R_d in the upwind direction (Phadtare 2018). Thus, the stratification of the flow within R_d is higher than that in the upstream undisturbed location and the Froude

number calculated at the undisturbed location will be an overestimation of the true Froude number.

Given all the limitations in calculating the true Froude number of the flow impinging on the Western Ghats, we do not comment on the nature of 'flow regime', i.e., blocked or unblocked. Instead phrases like 'weakly blocked'/'strongly blocked' are used. The main aim of this exercise was to show the difference in the observed and simulated flow blocking. A good measure of this is the Froude number of the flow arriving at the coast. Figure 11 is revised by adding plots for the Froude number from the Amini Divi station (an island in the Arabian Sea). Discussion related to this figure is revised. See Section 3.2.4 [Line no 292-315].

P11, L17/18: "12 12km" - remove one of the 12's.
Thank you, the extra '12' has been removed.

P12, L34-36: reduced orographic blocking should increase orographic wave drag aloft, not reduce it, as this would result in faster-moving air over the mountains and stronger wave forcing. However, the magnitude of the wave drag would be reduced by the reduced low-level stability in the model.
Thank you for pointing out this. The phrase 'orographic blocking' has been replaced with low-level stratification'. [Line no 426].

Reviewer: 2

 # General Comments

- Because the simulation duration is rather short and only a small number of single rainfall events are part of this investigation I think ensemble simulations should have been conducted. Such ensemble simulations are important to give an estimate of the model uncertainties. So far we only know the differences between one specific model simulation and the observations. But we do not know if those differences are significant or lie within a potential uncertainty range of the model simulations. Addressing the uncertainty is something important since it can indeed influence the conclusions drawn from this study. If the authors argue that it would not be feasible to conduct more simulations - which I think they should - then they should at least give an appropriate estimate of the model uncertainties. Following on from this, I doubt whether the considered time period is indeed long enough to give robust results.

Simulation of the INCOMPASS IOP was also performed in the UK Met Office Unified Model (MetUM). Model domains at similar horizontal resolutions were used (17 km, 4.4 km, and 1.5 km). The results from the MetUM simulations are shown below in figures R5-R7. The conclusions drawn with the WRF model simulation are also applicable to MetUM simulations:

1. Rainfall in the domain with convective parameterization (17 km) is anchored along the coast and the offshore rainfall is very weak (Figures R5 and R6).
2. The domains with explicit convection (4.4- and 1.5 km) simulate the offshore-onshore phases correctly but do not capture the observed land-sea contrast in the rainfall (Figure R6).
3. These high-resolution domains overestimate the orographic rainfall over the Western Ghat (Figures R6 and R2 a,e).
4. The boundary layer is anomalously warm, its stratification is weak, and the low-level winds are stronger in these domains. Hence, they have weaker orographic blocking (Figure R7).

Therefore, we believe that these model biases stem from the physics parameterization rather than the simulation uncertainties and the results from our WRF simulations are robust. A note on this has been added in the Discussion section [Line no 408-412].

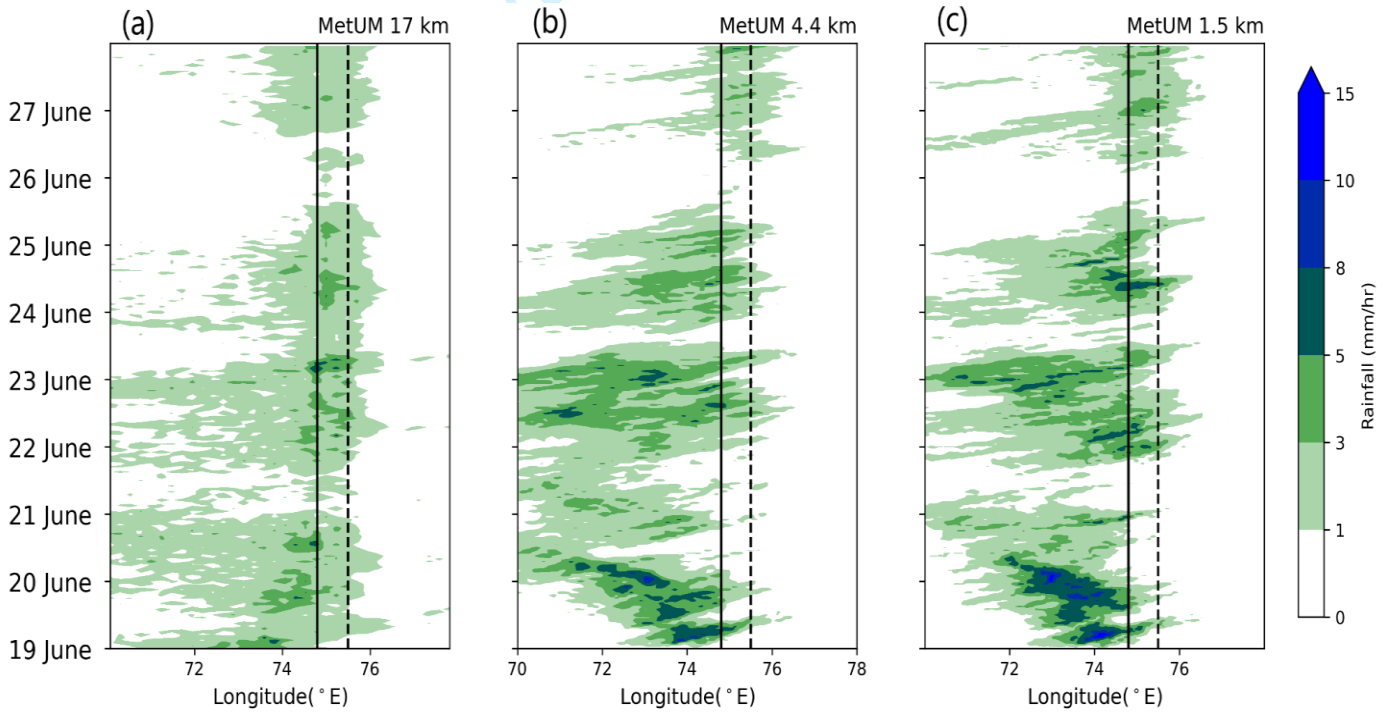

Figure R5. *Hovmoller plot of 12-14°N averaged rainfall in MetUM simulations at (a) 17 km, (b) 4.4 km, and (c) 1.5 km during 20-27 June 2016. The solid black line shows the mean longitude of the coast and the dotted line shows the mean longitude of the Western Ghats peak between 12-14°N.*

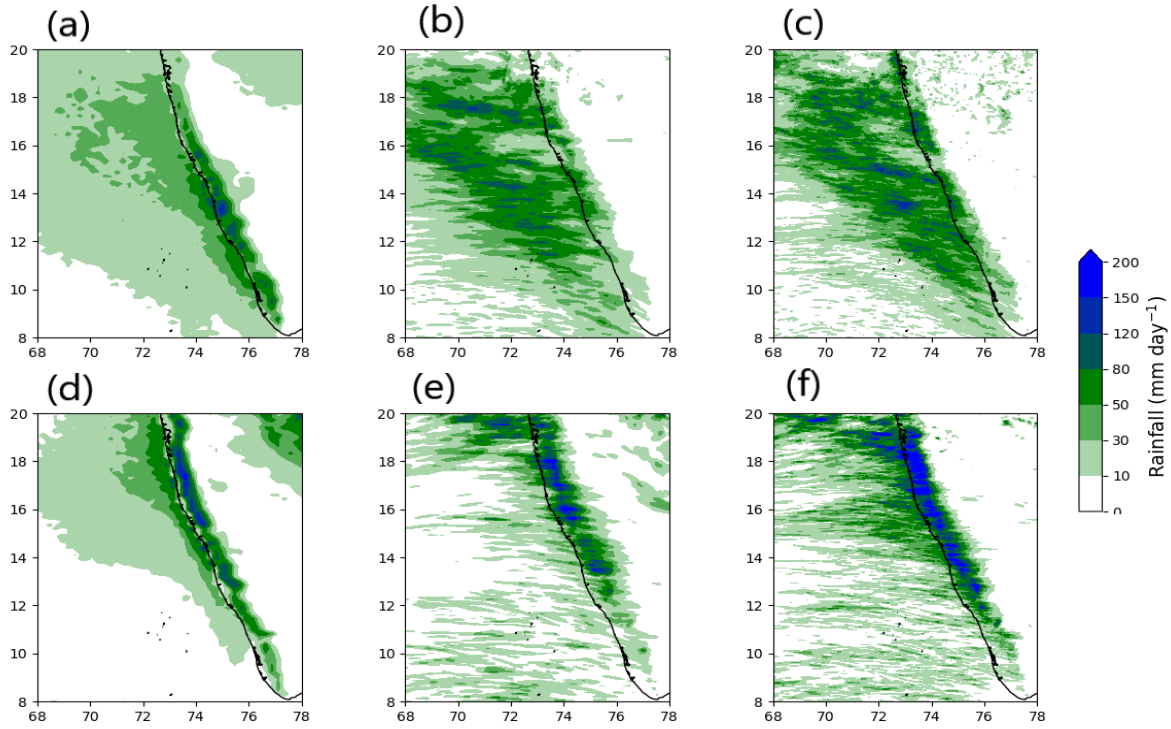

Figure R6. *Rainfall accumulation during the offshore phase in MetUM simulations at (a) 17 km, (b) 4.4 km, and (c) 1.5 km. (d)-(f) same as (a)-(c) but for the onshore phase.*

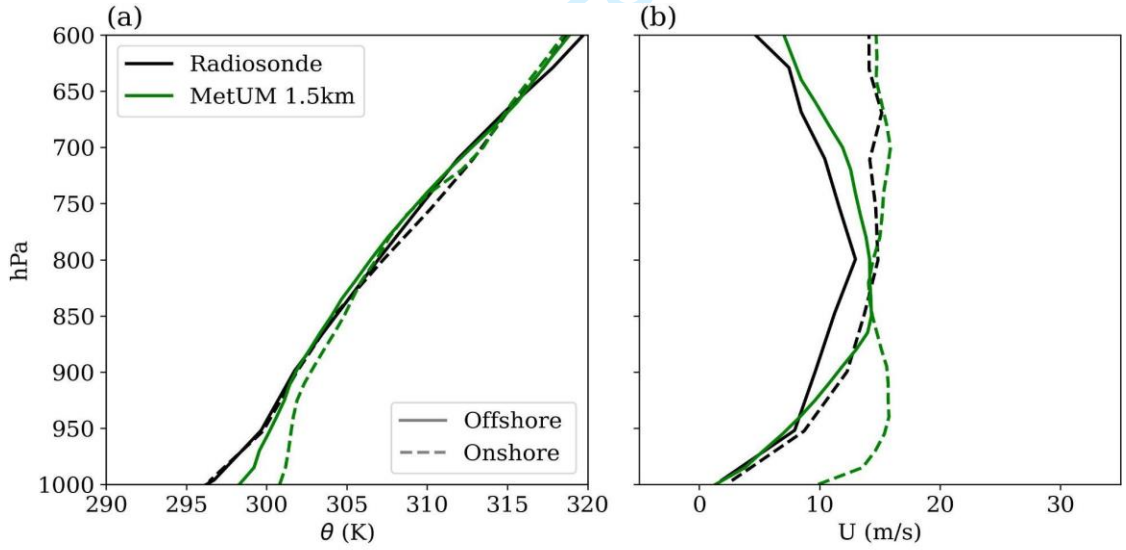

Figure R7. *(a) Mean potential temperature profiles from Mangalore radiosondes and the simulated soundings from the corresponding location from MetUM simulations during the offshore phase. (b) Same as (a) but shows zonal winds profiles.*

Since the diurnal cycle is an integral part of this study it would be beneficial if the authors could add a more comprehensive analysis to the diurnal cycle section. I'd suggest adding a more

quantitative analysis. The authors could add calculate and display the magnitudes of the diurnal cycle. For example by comparing maps the rainfall peaks as a fraction of the total daily rainfall. Or by comparing nighttime and daytime rainfall (like in Mori et al. 2004). A simple time plot displaying the average diurnal cycle would also be nice.

Figure 10 is revised and soundings from 0000 UTC and 1200 UTC are shown to understand the daytime and nighttime differences. The diurnal cycle is an important part of the offshore-onshore phases. An observational study involving multi-year data was done by Phadtare et al. (2022) in which the characteristics of the diurnal cycle of offshore and onshore modes were shown. In the present study, the purpose of mentioning the diurnal cycle was to show that the model simulates daytime maximum rainfall over the coast which does not exist in the observations. The underestimation of orographic blocking by the model is the reason behind this (Section 3.2.4).

Mori et al. 2004 studied the diurnal cycle with 3-years data. The duration of the offshore phase for which the diurnal cycle is shown in Figure 5, is just 5 days. This simulation period is not ideal for commenting on the characteristics of the complete diurnal cycle. Some of the authors of the present study are currently involved in a study exclusively focusing on the diurnal cycle of offshore-onshore phases with longer simulations.

Could you also please add tables showing the overall magnitudes of the differences between model simulations and observations? Or add least add numbers to the text?

Figure R8 below shows anomalous rainfall in WRF model domains with respect to the IMERG product. The WRF output was regridded to the IMERG resolution for obtaining this figure. The WRF overestimates rainfall over the Western Ghats and west coast by about 50-100 mm/day. Figure 4 in the manuscript is replaced by this figure. Please refer to Section 3.1.2 for the discussion on this figure [line no 197-202].

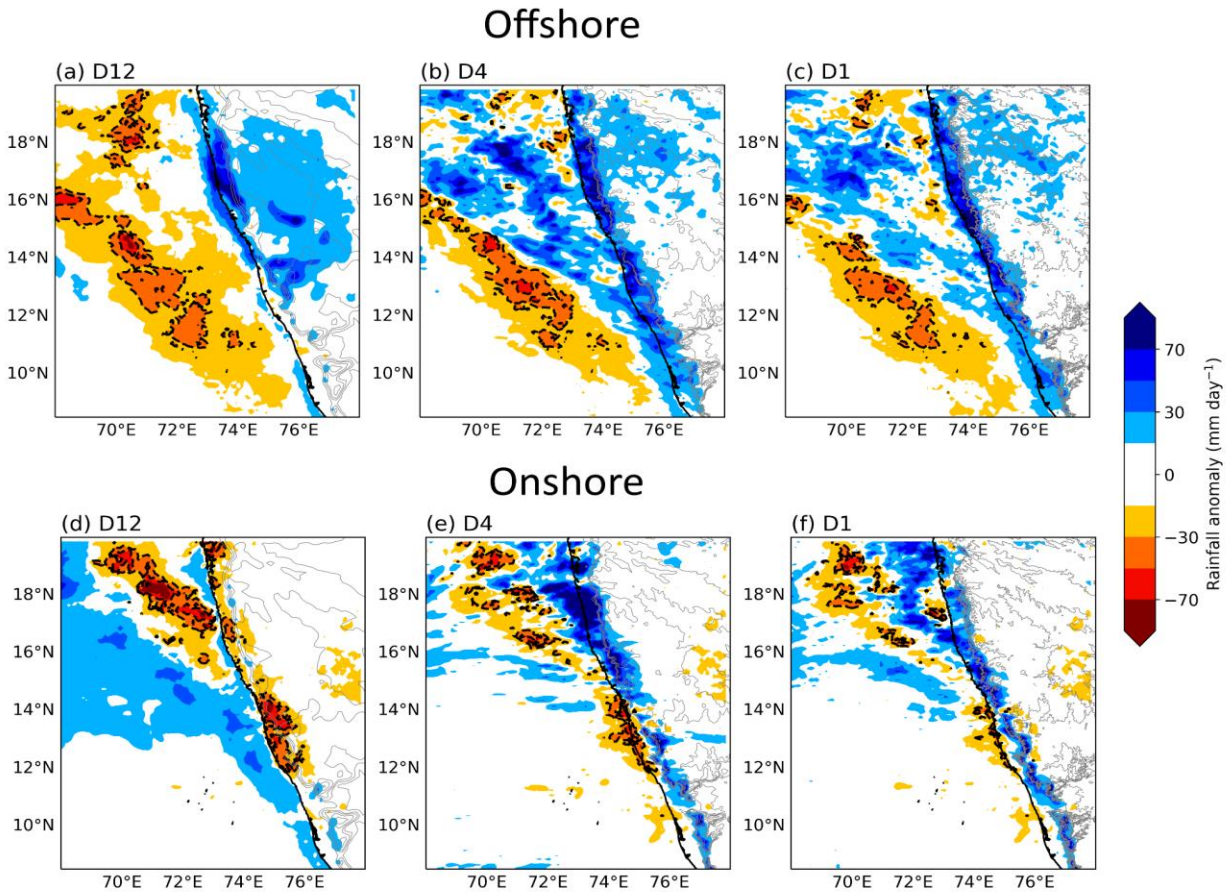

Figure R8. *Anomalous rainfall in (a) D12, (b) D4, and (c) D1 compared to IMERG during the offshore phase. (d)-(f) Same as (a)-(c) but for the onshore phase.*

Specific Comments:

P 4. Line 9 - 10: "The convective parameterization ideology". Ideology is a rather odd word in this context. I guess you meant something like a priori assumption or fundamental assumption.

This text is revised: *"The fundamental assumption in the convective parameterization is that the convective cells are much smaller than the model grid box. At O(∼ 1 km) resolution, convective cells are partially resolved. Thus, using a convective parameterization scheme at this resolution is questionable as individual convective cells can occupy more than one grid box ."[Line no 70-73].*

P 8. Line 26: The authors speculate that cold pools might suppress the occurrence of rainfall over the cost. Here it would be more clear if the authors would analyse the density potential temperature perturbation field rather than simply the potential temperature field.

Figure 7 is revised; virtual potential temperature perturbation is plotted instead of potential temperature. It shows the cold pool more clearly than the previous plot.

P 11. Line 18 P. 11: Remove the first "12" in 12 12 km.

Thank you for pointing that out. The extra “12” has been removed.

Reviewer: 3

Manuscript I read with a lot of interest. I have the following impression after reading the manuscript. There needs to be a look at how onshore and offshore convection is identified and how they are classified based on the existing literature on the ISMR active / break periods. The characteristics of the onshore/offshore large-scale conditions are similar to the active/break conditions. I think attention should be paid to the diurnal cycle of convection. It is unclear whether the latitudinal averaging is bringing the westward propagation of the precipitating zones over AS (in the case of offshore convection, as presented in the study). Adding more cases of onshore/offshore convection may be worthwhile to prove the hypothesis set. Please see specific comments below. I recommend major revision with the following note.

Abstract: The WRF can be expanded or avoided in the abstract. It is also not necessary to mention model configuration in the abstract. The onshore-offshore mode is not yet defined and appears without an introduction.

WRF has been expanded in the abstract. The abstract has been revised and the mention of ‘onshore-offshore modes’ is avoided. The modes are explicitly defined in the Introduction section [Line no. 43-44 and Line no. 92-98].

Regarding model configuration: What will happen with the two-way nested domain at a 1.33 km resolution is used?

The two-way nested domain at 1.33 km will override the output of the 4 km domain where the two domains overlap. Thus, when two-way nesting is used, we will lose the output of the 4 km domain over the coast.

It is suggested to replace with more apt words or phrases, e.g. ‘generally does a good job, becomes problematic etc.

These sentences have been revised. [Line no. 59-60 and 72-73]

Introduction:

The introduction of the grey zone needs a better description. Please bring in the idea in ln #40 in the abstract, indicating the objective and describing the onshore/offshore convection.

The discussion on the grey zone has been revised. [Line 70-73]. The offshore/onshore rainfall and the objectives are now described in the first two sentences of the abstract.

Looking at Figure 2a, the convection starts at the coastal areas and shifts westwards with time almost in the diurnal cycle. At Least 3 such events are noted.

Yes, the offshore/westward propagation of rainfall is one of the characteristics of the offshore rainfall mode. A discussion on this has been included in Section 4.2 [Line no. 372-378].

The onshore classification does not have long periods of observations or cases. Thus the emphasis on the onshore/offshore is not appealing. My suggestion is to investigate the patterns seen consistently over the period mentioned offshore.

Although the onshore mode persists for a couple more days after 27 June 2016, the rainfall simply remains anchored over the coast. A detailed investigation of offshore and onshore rainfall events on a mesoscale level is certainly desirable. However, the focus of this study was on simulating the overall rainfall fields of both modes and their transition. It is important to highlight some fundamental issues with the model simulations first, such as the lack of intense rainfall with a convective parameterization scheme, no land-sea contrast in any of the domains, and an imperfect diurnal cycle of coastal rainfall.

In the onshore case, this is the period of onset and LLJ was probably weak compared to the subsequent period when it got established. The major issue is that LLJ is not captured with accuracy (with its depth and strength) in the model. The vertical resolution of the model also matters in this case. The boundary layer over the Arabian Sea during these periods will be below 500m. The intermittent intrusion of dry air would weaken convection and the distribution of winds (especially the LLJ characteristics) in combination with convection features to be examined.

Thank you for this important suggestion. A discussion on this point is included in Section 5 [Line no 423-426]. We have also analyzed the simulation of this case study from the Met Office Unified Model (MetUM). It has 80 vertical levels; we have 35 in the WRF simulations. The simulated sounding from the MetUM is shown in Figure R6 above. It does show some improvement from the WRF simulation; however, the boundary layer is anomalously warm, its stratification is weak, and the low-level winds are stronger during the onshore mode. Thus, even with higher vertical resolution some issues mentioned in the present study persist. However, more systematic experiments are needed to determine the sensitivity of orographic precipitation to the lowest model level and vertical resolution in the PBL. The present study was focused on the effect of horizontal grid resolution and convective parameterization on the offshore-onshore oscillation

of rainfall. In our simulations, the lowest level was at 20 m and there were 10 levels below 1500 m. Experiments can be performed for understanding the sensitivity of these two factors on the orographic blocking. A note on this is added in the Discussion section [Line no 423-426].

The argument of enhanced instability in the model making enhanced convection than the observation is based on the comparison with radiosonde measurements. However, other additional measurements available from INCOMPASS need to be used to check spatial distribution.

Figure R9 shows radiosonde soundings from Mumbai and the corresponding simulated soundings from the WRF D1 domain. This figure also shows higher θe values compared to the radiosondes at 0000 UTC.

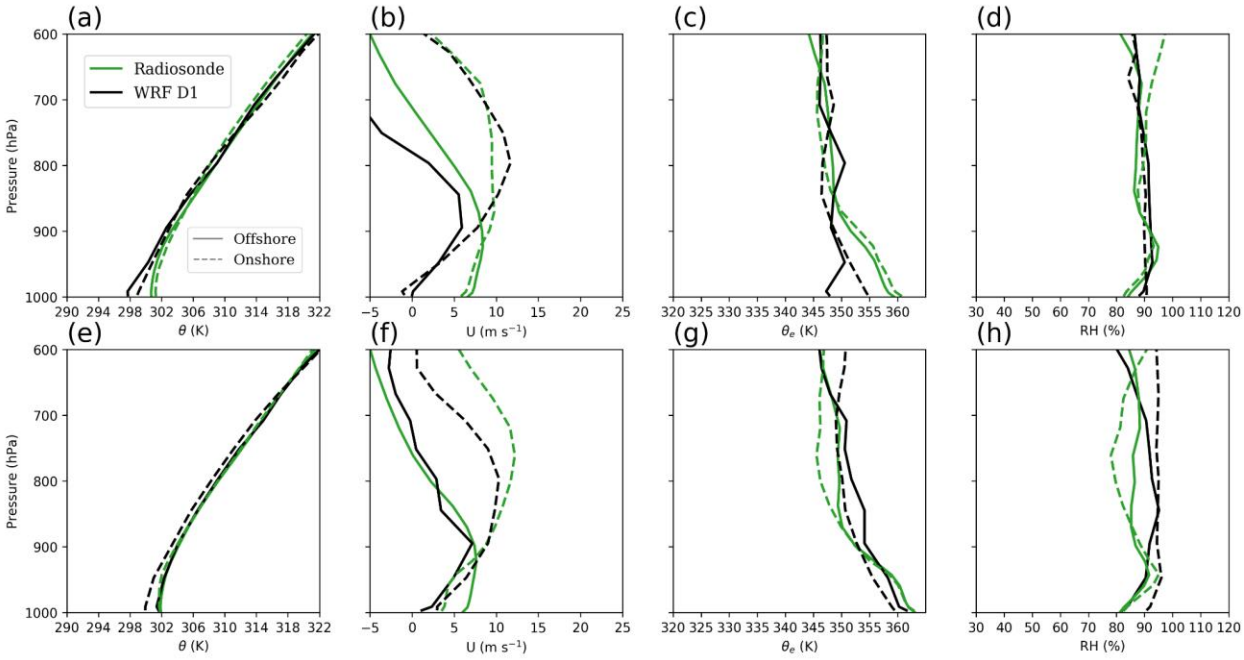

Figure R9. *Profiles of (a) Potential temperature (θ), (b) Zonal winds (U), (c) Equivalent potential temperature (θe), and (d) RH from the 0000 UTC Mumbai radiosonde soundings and the hourly simulated soundings in the WRF D1 over the same location as Mumbai. (e)-(h) are the same as (a)-(d) but for the 1200 UTC radiosondes. The simulated profiles are averaged over a 12km box centred over the radiosonde location.*

Regarding the results presented:

Figure 8: it is desirable to have two different sets of images for the onshore and offshore, and also plot the wind as resultant u and w; note that Wave effects are also propagating westward as well as eastward. Huge differences in winds are in the mid-troposphere with stronger westerlies, do you know why?

Figure 8 is produced by subtracting the simulated offshore phase from the onshore phase. This plot does not show model biases with respect to observations. It shows differences between the large-scale dynamic and thermodynamic environments during onshore and offshore phases.

Figure 10 for what timing on which day? Winds are very much off in the model throughout the lower-mid troposphere, with more differences in the onshore case, why is so? How was the initial condition compared with observations? Please add RH comparison as well.

Figure 10 in the manuscript has been revised. The simulated soundings are averaged over a 12-km box centred over the radiosonde location as you have suggested in the next point. These simulated profiles are close to the radiosonde profiles.

The initial sounding on 0000 UTC 13 June from ERA5 is shown in Figure R10. Initial conditions are quite close to the radiosonde soundings, except along the coast. The winds near the surface are stronger in ERA5 at the coast.

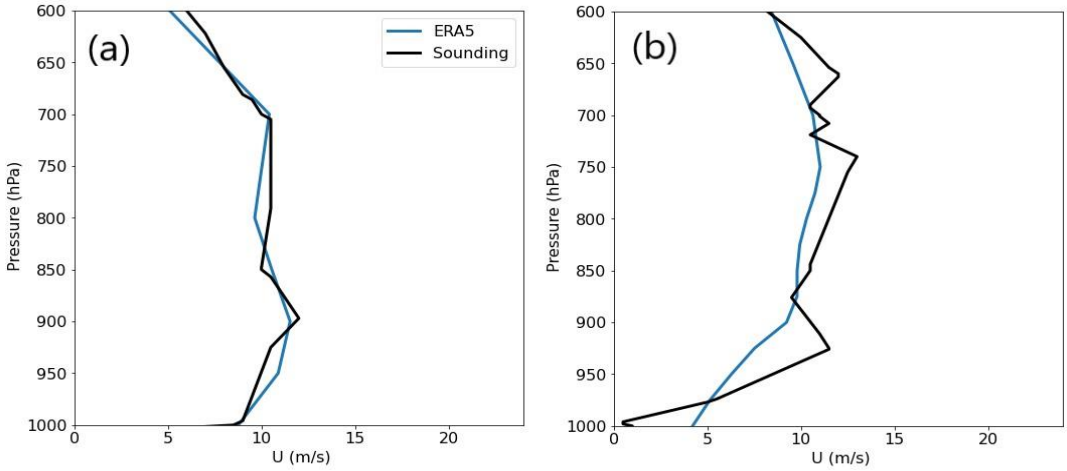

Figure R10. *0000 UTC sounding profiles from (a) Amini Divi and (b) Mangalore on 13 June 2016.*

Is Figure 11 representative of the grid point data from the three simulations? Have you considered the radiosonde track into consideration? Probably averaging over an area corresponding to 12 km may be appropriate.

Figure 11 has been revised to take this into account. The values are averaged over a 12 km box centred over the radiosonde location. The equivalent potential temperature (θ_e) plot is removed from this figure and a θ_e profile is added to Figure 10 in the revised manuscript (also shown in Figure R8 here) as it shows the vertical variations as well.

Regarding Figure 13: it is clear that the onshore is associated with the lows or systems that form over the north BoB and are situated over the central Indian region. The offshore case has only weak circulation. The choice of the period as described above has this type of synoptic feature. More the active and break monsoon in the literature, please give adequate references to compare with typical terminology.

Although the offshore mode has weaker winds along the coast, it does not necessarily imply a monsoon break phase; the offshore trough produces heavy rainfall just off the west coast. The active-break oscillation of the monsoon involves alternate phases of heavy rainfall over the equator and the core monsoon zone of India, and the offshore-onshore oscillation involves variations over the west coast and the Arabian Sea. However, offshore-onshore oscillations can be seen during the break-to-active transition. Shige et al. (2017), Fletcher et al. (2020), and Hunt et al. (2021) suggest that the offshore-onshore oscillation of rainfall over the Indian west coast is associated with the Boreal Summer Intraseasonal Oscillation (BSISO) phases. These studies are cited in the manuscript. The distinction between active-break and offshore-onshore oscillations is discussed in the revised text. Please see Section 3.2.1 [Line no 230-234].

What do you mean by no convection? Is it with the MP scheme alone and no convection scheme is used? These results are interesting that the model produced the rainbands. Is it so that with convection model did a lot of mixing and reduced the clouds and precipitation? I think that two way nesting in D1 will change results. It is probably.

Yes, only the microphysics scheme is used in the *NoCu* simulation. It is possible that the convection scheme is overdoing the entrainment. The New Tiedtke convection scheme which is used by the tropical suite of the WRF model has an increased rate of entrainment compared to the original scheme in order to delay build-up of convection and improve the diurnal cycle of rainfall. In two-way nesting, the output of the 4 km domain overrides the output of the 12 km domain. Therefore, the offshore-onshore oscillation is present in the 12 km domain with two-way nesting.

Justification of D12 without a convection scheme giving better results may be a bit confusing, as per Figure 5, the onshore convection showed no westward propagation with time in D12 simulation. Please check Figure 12d, it appears to be from a high-resolution simulation.

Figure 12d is from D12 with explicit convection – or more precisely, with the convection scheme switched off. Propagation of mesoscale systems depends on features like downdrafts, cold pools, and gravity bores which can be associated with heavily precipitating convective cores. The explicit representation of convection allows the cores to grow stronger and hence propagating mesoscale systems may appear. However, with the increasing size of the grid box, entrainment into the convective core decreases and hence these systems grow unrealistically. With a convection scheme, the convective cores are weak. This could be the reason that propagating

systems are absent when a convection scheme is being employed. This discussion is included in the revised text. Please see Section 4.2 [Line no 372-378].

The schematic needs a description.

A description has been added in the Figure 14 caption.

Please add the keyword: Indian Summer Monsoon

'Indian Summer Monsoon' has been added to the keywords.

References:

Flynn, W.J., Nesbitt, S.W., Anders, A.M. and Garg, P., 2017. Mesoscale precipitation characteristics near the Western Ghats during the Indian Summer Monsoon as simulated by a high-resolution regional model. *Quarterly Journal of the Royal Meteorological Society*, *143*(709), pp.3070-3084.

Pierrehumbert, R.T. and Wyman, B., 1985. Upstream effects of mesoscale mountains. *Journal of the atmospheric sciences*, *42*(10), pp.977-1003.

Phadtare, J., 2018. Role of Eastern Ghats orography and cold pool in an extreme rainfall event over Chennai on 1 December 2015. *Monthly Weather Review*, *146*(4), pp.943-965.

Phadtare, J.A., Fletcher, J.K., Ross, A.N., Turner, A.G. and Schiemann, R.K., 2022. Froude-number-based rainfall regimes over the Western Ghats mountains of India. *Quarterly Journal of the Royal Meteorological Society*, *148*(748), pp.3388-3405.

Shige, S., Nakano, Y. and Yamamoto, M.K., 2017. Role of orography, diurnal cycle, and intraseasonal oscillation in summer monsoon rainfall over the Western Ghats and Myanmar Coast. *Journal of Climate*, *30*(23), pp.9365-9381.

Fletcher, J.K., Parker, D.J., Turner, A.G., Menon, A., Martin, G.M., Birch, C.E., Mitra, A.K., Mrudula, G., Hunt, K.M., Taylor, C.M. and Houze, R.A., 2020. The dynamic and thermodynamic structure of the monsoon over southern India: New observations from the INCOMPASS IOP. *Quarterly Journal of the Royal Meteorological Society*, *146*(731), pp.2867-2890.

Hunt, K.M., Turner, A.G., Stein, T.H., Fletcher, J.K. and Schiemann, R.K., 2021. Modes of coastal precipitation over southwest India and their relationship with intraseasonal variability. *Quarterly Journal of the Royal Meteorological Society*, *147*(734), pp.181-201.

Unravelling the Mechanism of Summer Monsoon Rainfall Modes over the West Coast of India using Model Simulations

Jayesh A. Phadtare | Jennifer K. Fletcher | Andrew N. Ross | Andrew G. Turner| Reinhard K. H. Schiemann | Helen L. Burns

The offshore and onshore rainfall modes are largely a consequence of the large-scale atmospheric variability. During the offshore mode, a trough extends over the Arabian Sea from the Indian peninsula (Fig. a). It provided favourable conditions for offshore convection. During the onshore mode, a ridge moved over the west coast and offshore region (Fig. b), the low-level westerly winds were strong resulting in the direct orographic uplift of winds and hence, heavy rainfall over the Western Ghats and west coast.